AD-A058 889 RCA ASTRO ELECTRONICS PRINCETON NJ F/G 22/2
SPACECRAFT HYDROGEN FREQUENCY STANDARD/CLOCK SYSTEM.(U)
APR 78 N00014-75-C-1148
UNCLASSIFIED AE-R-4258 NL

1 OF 2
ADA
058889

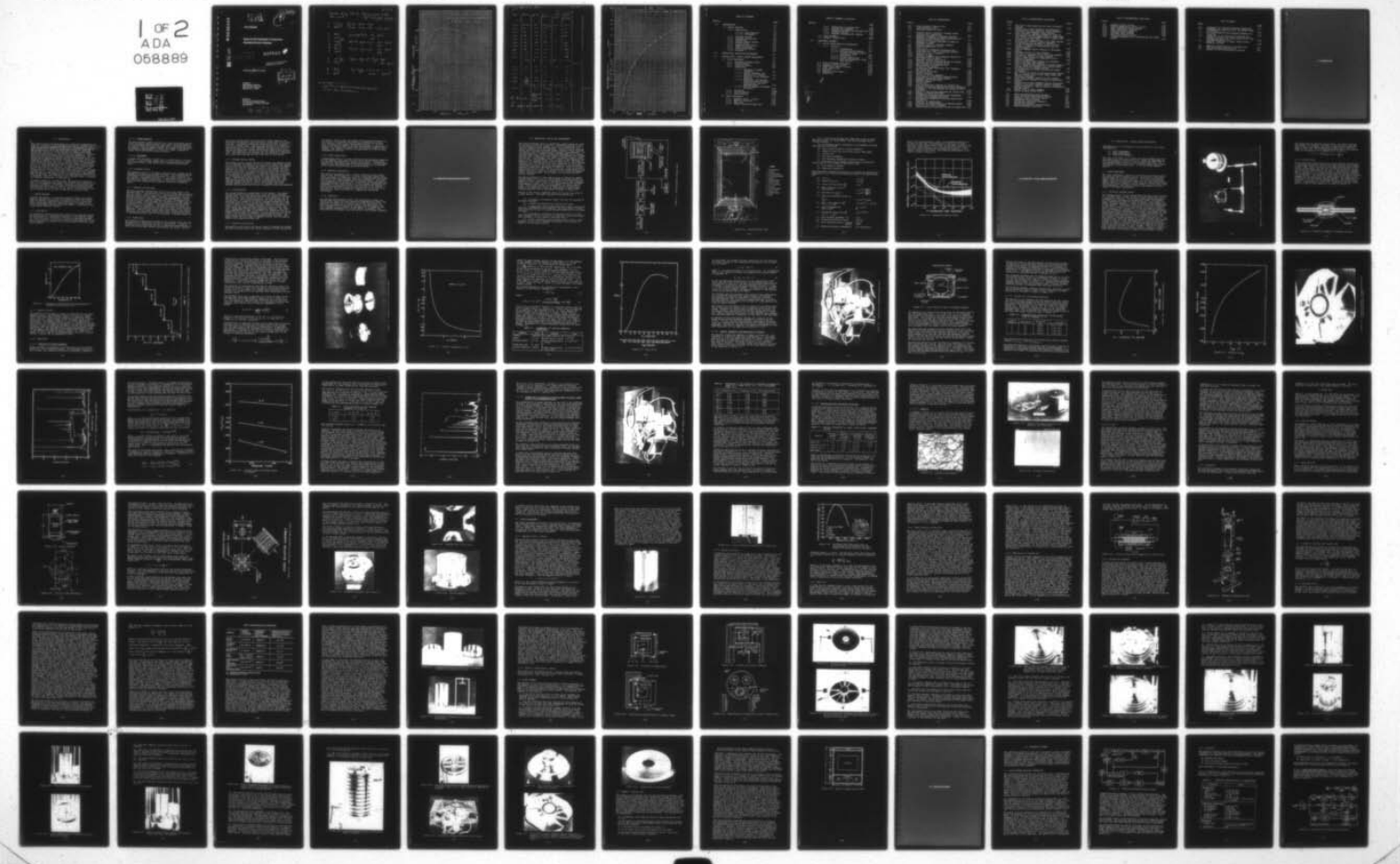

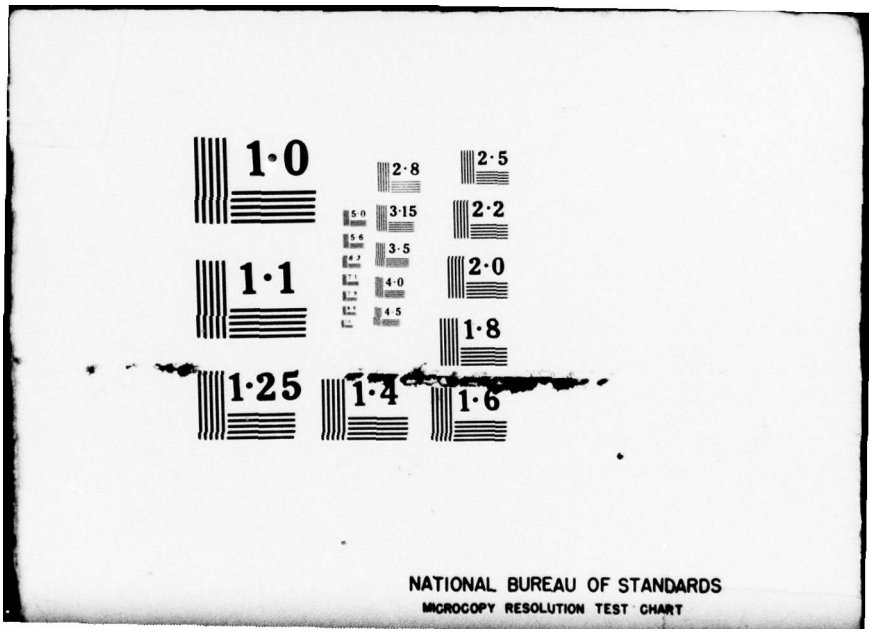
1·0
1·1
1·25
2·8
3·15
3·5
4·0
4·5
5·0
5·6
2·5
2·2
2·0
1·8
1·4
1·6
NATIONAL BUREAU OF STANDARDS
MICROCOPY RESOLUTION TEST CHART

LEVEL II

(14) AE-R-4258
28 April, 1978

(9)

(9) Final Report

(11) 28 Apr 78

(6) Spacecraft Hydrogen Frequency Standard/Clock System

537653

(12) 130p.

(15) Contract No. N00014-75-C-1148

Prepared for
Naval Research Laboratory
4555 Overlook Avenue, N.W.
Washington, D.C. 20375

Prepared by
RCA Government Systems Division
Astro-Electronics, Princeton, New Jersey
April 28, 1978

8-8-77

Connector wiring label for Hydrogen pressure control
Maser unit
(Ref. Sabisky print 10-14-76
rev 10-28-76)

1	red	one cable	Purifier heater - high
2	black		Purifier heater - low (comm. gnd)
3	blue	one cable	pressure gauge heater low (gnd)
4	red		" " " high
7	orange		thermistor pressure sensor low (gnd)
8	green		" " " high
H	brown		thermistor, temp sensor low (gnd)
J	yellow		" " " high
9	red	one cable	Reference voltage set (V_{set}) high
10	black		" " " " low (gnd)
K	blue		Power Supply + 20 V DC
L	grey		" " common (gnd)

~~On DC supply~~

~~high voltage (present is that 3½ V. fuse)?~~

~~Can they safely remove fuse?)~~

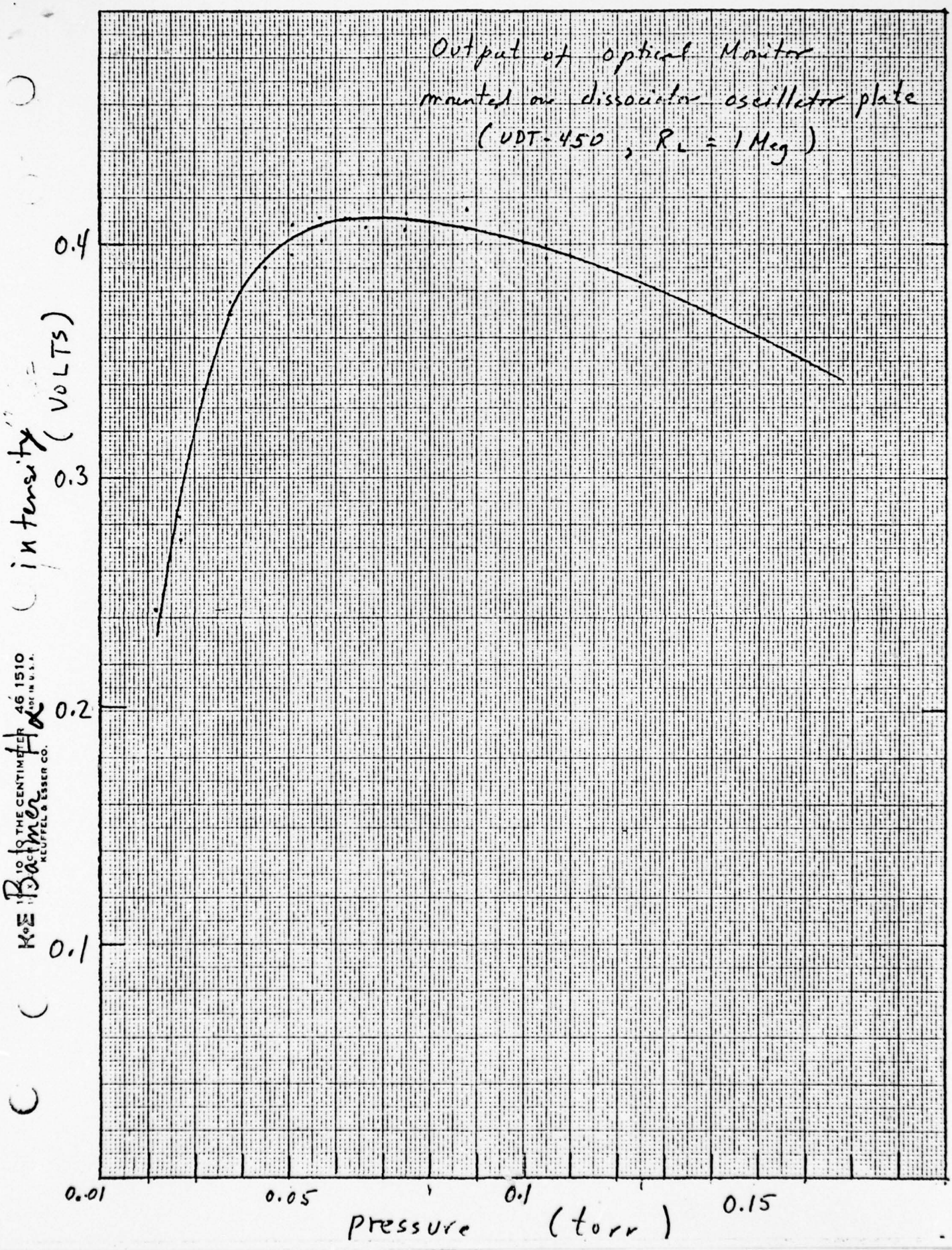
Output of optical Monitor
mounted on dissociator oscillator plate
(UDT-450, R_L = 1 Meg)
intensity (VOLTS)
0.4
0.3
0.2
0.1
0.01
0.05
0.1
0.15
pressure (torr)
KE 10 to the CENTIMETER 46 1510
KEUFFEL & ESSER CO.

Operating data 4-6-78

V_{set}	Pressure	Op. mon.	Vac ion pressure	"C" field current (1)	5751 Hz receiver amplitude (2)		
10.60	.063 torr.	.416	135 μamp.	18 ma	.250 V		
10.50	.056	.417	125 "	"	.100		
10.80	.076	.415	165	18 "	.400		
11.00	.088	.410	195	"	.440		
11.00	.088	.411	195	"			
11.20	.105	.400	230	"	.500		
11.50	.125	.375	280	"	.540		
12.00	.160	.332	370	"	.650		
12.50	.200	.277	455	"	.580		
10.80	.076	.414	165	"	.440		
	change to 10.50, leave overnight,						
						4-7-78	
10.50	.056	.416	125	18 ma	.250		
10.40	.051	.415	110	"	.140		
10.40	"	"	110	"	.130		
10.30	.045	.401	130	"	.06		
10.70	.070 ~~.075~~	.396	155	"	.32		
	8 l/sec	pump only, after purging since 15:00					
10.70		391	700 μamp.	"	.35		at 16 30

(1) Trim coils 4} + {43 mv, 3} + {, current = 1 ma

1} − {38 mv, 2} + {, current = 1 ma

(1)

(2) peak to peak amplitude − best average.

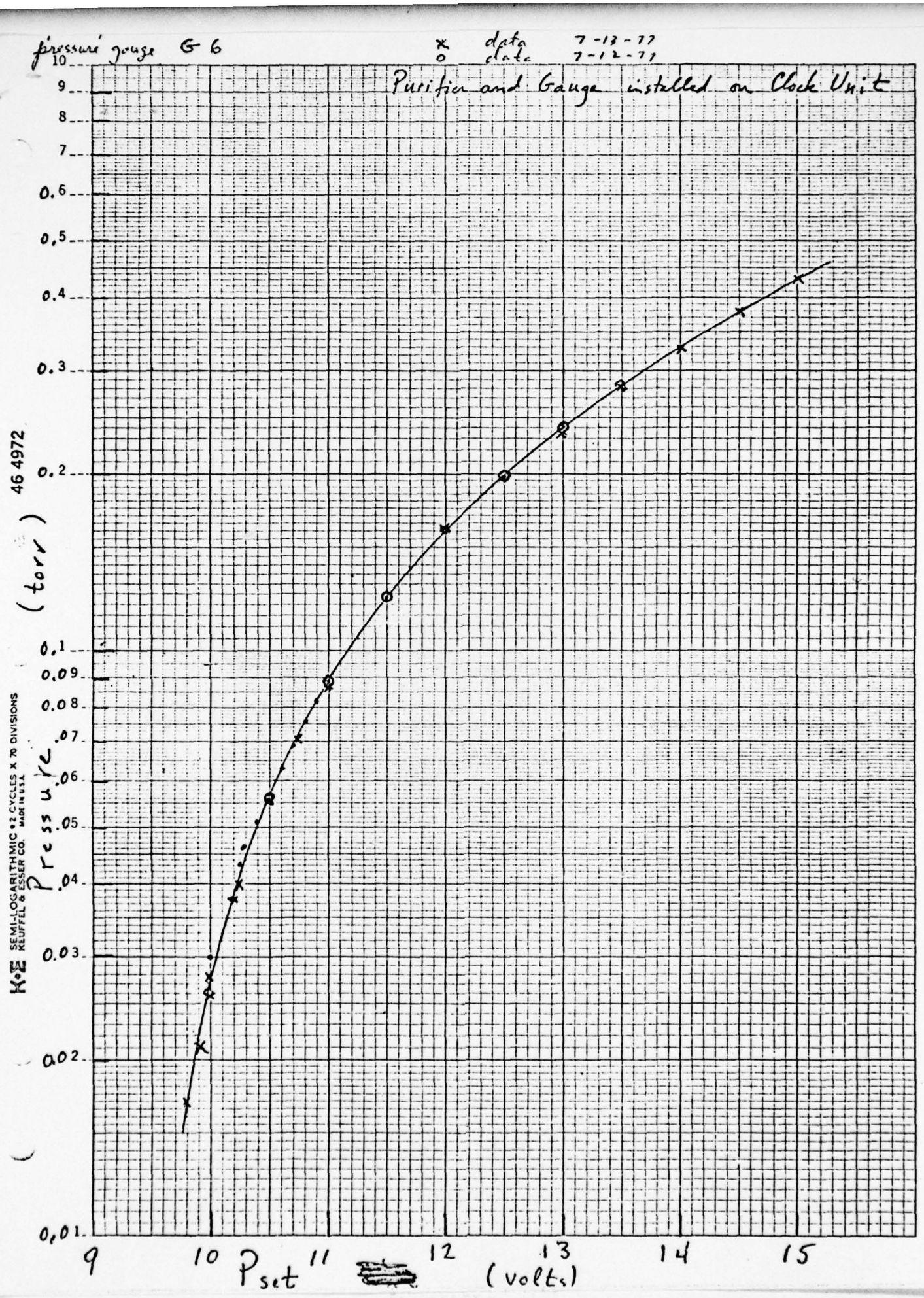
pressure gauge G 6
x data 7-13-77
o data 7-12-77
Purifier and Gauge installed on Clock Unit
10
9
8
7
0.6
0.5
0.4
0.3
0.2
0.1
0.09
0.08
.07
.06
.05
.04
0.03
a02
0.01
Pressure (torr)
46 4972
K&E SEMI-LOGARITHMIC 2 CYCLES X 70 DIVISIONS
KEUFFEL & ESSER CO. MADE IN U.S.A.
9
10
11
12
13
14
15
Pset (volts)

TABLE OF CONTENTS

TABLE OF CONTENTS (Continued)

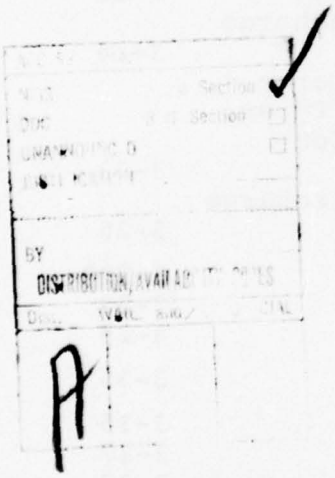

LIST OF ILLUSTRATIONS

LIST OF ILLUSTRATIONS (continued)

LIST OF ILLUSTRATIONS (continued)

LIST OF TABLES

1.0 INTRODUCTION

1.0 INTRODUCTION

This report covers the development of a Feasibility Demonstration Model of a Hydrogen Clock done under Contract No. N00014-75-C-1148 for the Naval Research Laboratories. A proposal for design and production of flight model hydrogen clocks was submitted to NRL in April 1977. A flight model design based on knowledge gained from evaluation of the Feasibility Demonstration Model would have applications as the primary time standard in the NTS-3 satellite and future generations of NAVSTAR Satellites. The design was configured to achieve the best performance within the contractually specified maximum envelope size of 16"N (40.64 cm) diameter by 30"N (76.2 cm) long. A flight model based on the same novel design concepts, but using a shorter cavity of dimensions similar to those successfully used in many masers could be packaged in an envelope 14"N (35.6 cm) in diameter (or slightly less) by 20"N (50.8 cm) long, complete, including electronics. This design uses the proven active mode (maser oscillator), and a TE_{011} unloaded cavity. A very small maser utilizing the novel hydrogen beam optics, a loaded TE_{011} cavity, and operating in the passive mode is feasible. An envelope size of approximately 8"N (20.32 cm) in diameter, 16"N (40.64 cm) long, for a hydrogen clock, including the receiver electronics, is possible.

Successful operation, including maser oscillation and receiver lock, of the demonstration model, was achieved upon completion of the initial assembly. Adjustments required to optimize the performance, and the conduct of tests to establish quantitatively the frequency stability have not yet and will not be done at RCA prior to delivery of the unit to NRL due to a lack of time.

1.1 DESIGN FEATURES

A design philosophy to incorporate promising design innovations enabling reduced size, weight, and production costs for flight model clocks when compared with designs relying on conventional design techniques which have been universally utilized in the large ground-based hydrogen clocks was chosen. Significant innovative design features include:

1.1.1 Beam Optics

The feasibility demonstration model uses a novel beam optics system which enables a considerable reduction in the overall length of the physics unit, reduction in the rate of hydrogen consumption, and a reduction in the size of vac-ion pumps required for hydrogen pumping when compared with systems using conventional beam optics designs.

1.1.1.1 State Selector

The state selector design consists of a small quadrupole device using rare-earth cobalt magnets rather than the large hexapole or large quadrupoles which have been used in conventional hydrogen clocks. This new design enables the length of the maser to be reduced by approximately 8 (20.32 cm) inches, compared to masers using conventional state selectors.

1.1.1.2 Collimator

A single hole collimator (0.005" dia. × 0.040" long) or (0.0127 cm dia. × 0.102 cm long) rather than the multiplicity of capillary tubes normally used significantly reduces manufacturing costs.

1.1.2 Microwave Cavity

The microwave cavity is all metal, consisting of a copper-plated molybdenum cylinder and aluminum end caps. This construction is considerably less expensive than cervit or quartz cavities, is not subject to breakage from shock, is relatively light in weight, has excellent thermal conductivity, a relatively low thermal coefficient when compared with aluminum, and may be "thermally" tuned.

1.1.3 Hydrogen Storage Bulb

The novel hydrogen storage bulb used for the first time in any hydrogen maser is constructed of teflon film rather than of quartz with an internal coating of teflon. Advantages include ability to withstand shock without damage, extremely lightweight, low cost, ease of fabrication, bulb and cavity interchangeability, effect of bulb on cavity frequency reduced from about 60 megahertz for the typical quartz bulb to about 270 kilohertz for a bulb made of 0.0025 cm teflon (a 0.00025 cm teflon bulb would further reduce the effect to 27 kilohertz). This reduction of bulb effect on cavity frequency significantly reduces the effect of slight movements of the bulb position within the cavity upon cavity resonant frequency. The film bulb should have longer storage time characteristics than the teflon coated quartz bulb, which should result in increased Hydrogen Line "Q" and increased frequency stability.

1.1.4 Dissociator

The feasibility demonstration model of the hydrogen clock has been equipped with a dissociator utilizing a pyrex bulb. A similar dissociator was constructed and put in operation approximately two years ago and has been working continuously ever since. RCA has

also built dissociators utilizing quartz bulbs, sapphire, and bulbs made of beryllium oxide internally coated with a thin layer of glass. Successful dissociator operation has been achieved with all of these bulbs. The beryllium oxide bulb is especially attractive for use in a flight designed hydrogen clock since it has an extremely high thermal conductivity enabling heat to be removed by conduction, and may be precisely fabricated dimensionally. The pyrex bulb was selected for the feasibility demonstration model since RCA had the most test data on this design.

1.1.5 Thermal Control System

The thermal control system consists of heaters and sensors on the cavity, heaters and sensors on an inner over, heaters and sensors on an outer oven, and heaters and sensors controlling the temperature of the receiver synthesizer and critical thermal control electronics circuits. The heat transfer rate between the cavity and the inner oven, the inner oven and the outer oven, and the outer oven and the environment is extremely small due to the use of low emissivity surfaces on all ovens and insulation consisting of an extremely high vacuum inside the outer envelope of the maser. The thermal sensors consist of thermistors which have been specially selected and aged for extreme stability. Heat transfer between the cavity, ovens, and outside environment through conductive paths is held to an extremely low value through careful design and the use of selected insulating materials.

1.1.6 Vacuum System

Two vacuum systems are incorporated in the design. One vacuum system evacuates the hydrogen from inside the teflon hydrogen storage bulb. The other system evacuates the balance of the system inside the outer vacuum enclosure. Each system has its own vac-ion pump. The volume evacuated by the inner system pump is essentially the volume of the teflon hydrogen storage bulb, and this pump does not have to handle the outgassing products of the cavity, C-field coil, magnetic shields, ovens, or any metal surfaces inside the outer vacuum enclosure, or any 0 rings. The outer system pump handles these outgassing products. The feasibility demonstration model is equipped with commercial vac-ion pumps mounted outside the nominal 16" x 30" envelope of the clock. A small vac-ion pump was designed, constructed and tested; two of which can be mounted within the above-mentioned envelope. The pumping speed for this pump is somewhat greater than the pumping speed of the commercial pumps used.

1.1.7 Magnetic Field Control

The magnetic field within the cavity region is produced by current through a solenoid which fits inside a magnetic shield surrounding

the cavity. Taps on the coil enable the current distribution to be adjusted for purposes of producing a homogeneous, uniform, axial magnetic field within the microwave cavity. A total of four (4) concentric magnetic shields is employed in the design to magnetically isolate the cavity from the external magnetic environment. The magnetic shields are constructed of 0.064 cm thick molypermalloy material.

1.1.8 Power Conditioner

A brass-board model of a power conditioner which enables operation of the hydrogen clock from a 28 volt dc source was constructed for use with the feasibility demonstration model. A flight design based on the techniques used on the brass-board can be packaged to fit within the previously mentioned envelope.

1.1.9 Receiver Synthesizer

The receiver synthesizer uses a triple conversion phase locked loop to lock the frequency of a voltage controlled crystal oscillator precisely to a frequency equal to a predetermined fractional multiple of the hydrogen maser oscillating frequency. This system is similar to the system used on hydrogen clocks developed at the Goddard Space Flight Center. A novel digital synthesizer was developed for this receiver which is much smaller and simpler in design than synthesizers used in other hydrogen clock designs. The complete receiver synthesizer package fits on the top of the physics unit vacuum enclosure in a temperature controlled environment.

1.1.10 Autotuner

An autotuner was designed, built, and functionally tested, but has not been tested with the feasibility demonstration model. The autotuner is useful for initially fine tuning the cavity, but would not be essential for flight clocks. The model built was not "packaged" to be included in the physics unit assembly; however, compact packaging for a flight design is feasible. The autotuner would thermally tune the cavity to the correct frequency.

2.0 DESCRIPTION, DESIGN AND PERFORMANCE

2.0 DESCRIPTION, DESIGN AND PERFORMANCE

The atomic hydrogen clock is conceptually simple device as shown by the block diagram of Figure 2-1. Molecular hydrogen is purified and enters a glass chamber where it is dissociated into atoms of hydrogen by an RF discharge. Neutral atoms of hydrogen emerge from the glass discharge chamber through a small aperture (collimator) and then pass through a magnetic state selector. In the state selector, undesired atoms are defocused while the des desired atoms (atoms in the two higher energy states) are focused to pass into a confinement cell which is located inside a microwave cavity. The microwave cavity is tuned to the resonance frequency of the hydrogen atoms. Due to maser action, the atoms in decaying to a lower energy state emit radiation at a well defined frequency near 1.4 GHz which is then coupled out of the cavity. This stable frequency can now be processed by various electronic schemes to match the requirements of the user. This is a simplified version of the clock. An actual device incudes magnetic and thermal shielding, means for producing a low, stable DC magnetic field, vacuum enclosure, vacuum pumps, and various electronic control systems.

The design presented in this report is for a feasibility demonstration model of a clock for the NAVSTAR satellitees which will require reliable, long-lived clocks having a long term frequency stability of at least 1 part in 10^{14} while meeting the stringent environmental, weight and size requirements for space applications. The overall design of the model is for the most part based on the experience gained by researchers at NASA Goddard. A cross-sectional view of the design is shown in Figure 2-2.

Details of the various component parts of the clock are given in a later section. The basic features of the design are:

(a) A Standard low pressure vessel (300 psi) for storage of molecular hydrogen;

(b) A simple palladium-silver purifier and valve;

(c) A capacitively RF coupled dissociator using a pyrex bulb having an ion-depleted inside surface; (In later models, a beryllium oxide bulb having its inside surface coated with a thin layer of glass.)

(d) A collimator consisting of a single 0.0127 cm (0.005 inch) diameter hole in a 0.1016 cm (0.040 inch) thick glass wafer; (The collimator is heat fused to the pyrex bulb.)

(e) A small quadrupole state selector which allows a short distance of only 8.25 cm between the selector exit and the entrance to the microwave cavity;

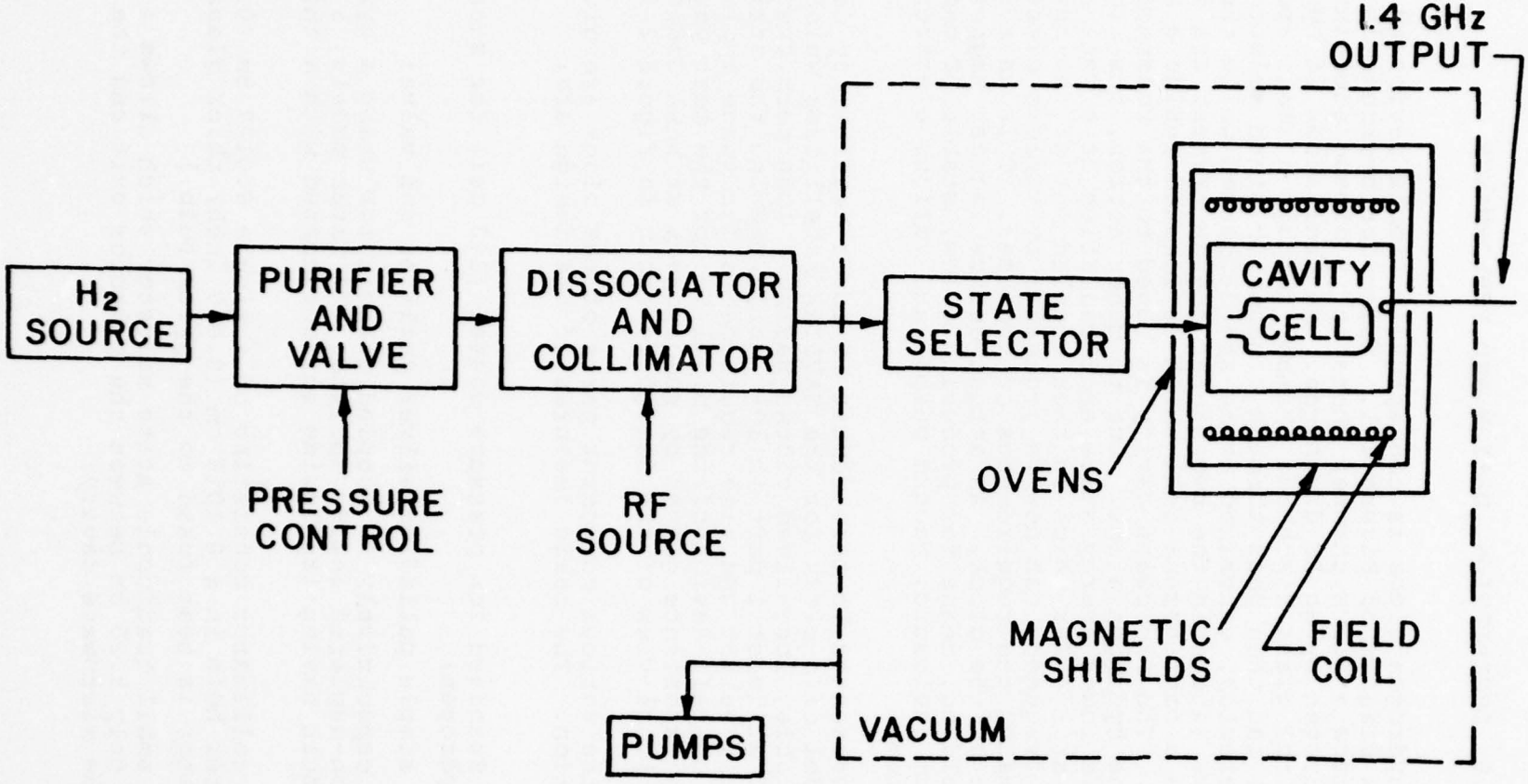

Figure 2-1. Block Diagram of Physics Unit

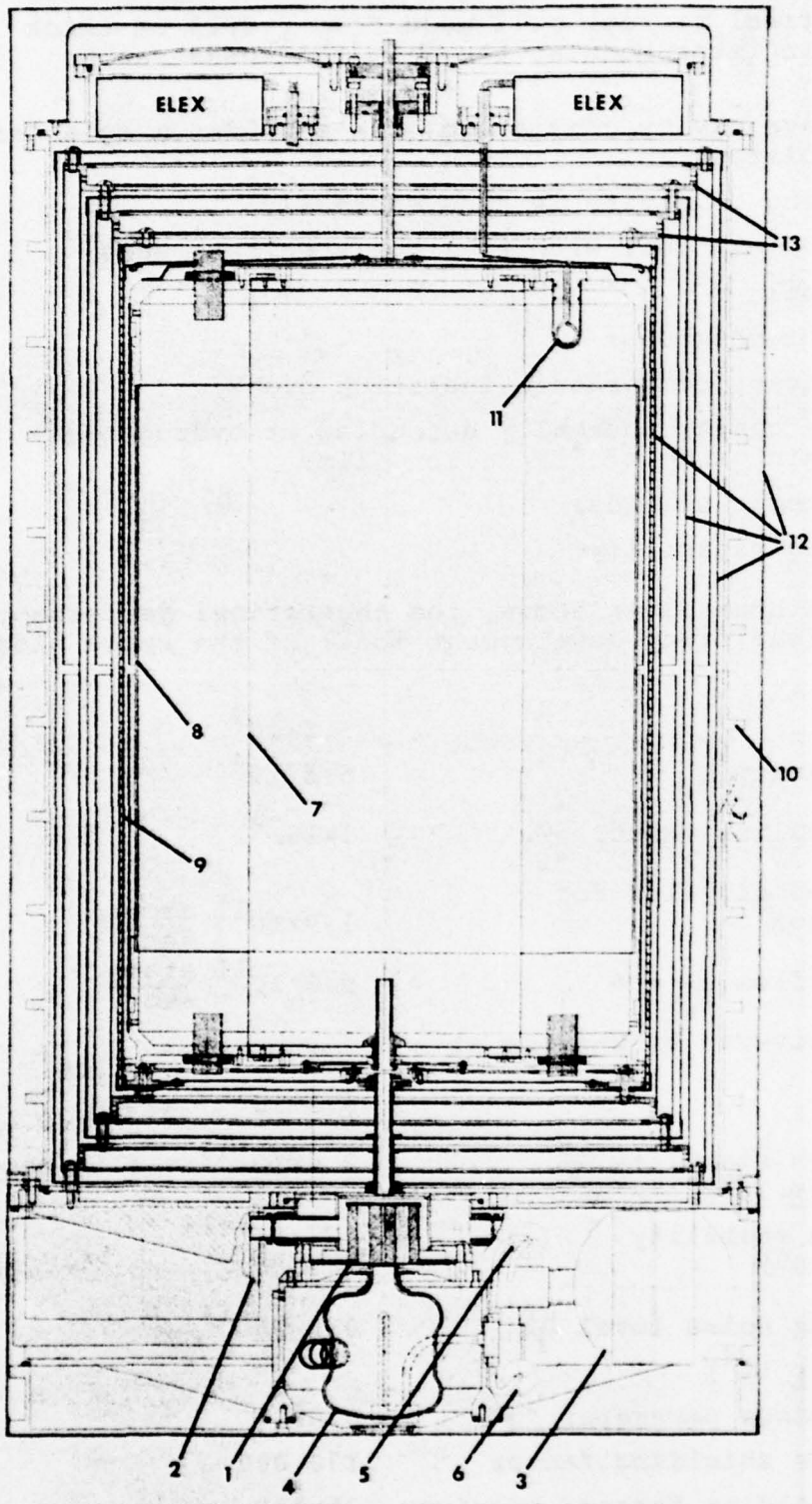

LEGEND

1 – STATE SELECTOR
2 – ION PUMP
3 – H_2 STORAGE VESSEL
4 – RF DISCHARGE CHAMBER
5 – PURIFIER
6 – PRESSURE SENSOR
7 – TEFLON FILM CELL
8 – CAVITY STRUCTURE
9 – FIELD COIL
10 – VACUUM ENCLOSURE
11 – COUPLING LOOP
12 – MAGNETIC SHIELDS
13 – OVENS

Figure 2-2. Cross-Sectional View

(f) A cylindrical storage cell made from 0.0025 cm thick FEP teflon film; (In later models, the film thickness can be further reduced.)

(g) A microwave cavity consisting of a molybdenum cylinder with aluminum end plates;

(h) Fine tuning of cavity is done thermally;

(i) Magnetic field coil with trim coils on both ends;

(j) A neck coil;

(k) Two vacuum chambers;

(l) Two secondary temperature isolation ovens;

(m) Microwave cavity thermally decoupled at hydrogen entrance tube by a thin piece of FEP teflon film;

(n) Four magnetic shields;

(o) Degaussing capability.

With the design features given above, the theoretical performance parameters of the feasibilty development model of the space clock are:

(a)	Line Q_ℓ	5.5×10^{9}
(b)	Loaded cavity Q_c	5.5×10^{4}
(c)	Cavity pulling factor $\frac{Q_c}{Q_\ell}$	1×10^{-5}
(d)	Beam threshold flux for oscillation	1.9×10^{11} $\frac{\text{atoms}}{\text{sec.}}$
(e)	Net beam flux $\frac{I}{I_{th}} = 6$	9.6×10^{11} $\frac{\text{atoms}}{\text{sec}}$
(f)	Power delivered by H-atoms at $\frac{I}{I_{th}} = 6$	5.3×10^{-13} watts
(g)	Short term stability $\frac{\Delta f}{f}$ $(0.1 \leq \tau \leq 10^2)$	$2.0\times10^{-13}/\tau$, τ in sec.
(h)	Long term stability $(10^2 \leq \tau \leq 10^6)$	$\frac{\Delta f}{f} < 10^{-14}$
(i)	Perturbing noise level $\frac{\Delta f}{f}$ $(10^2 \leq \tau \leq 10^4)$	$9.0\times10^{-15}/\sqrt{\tau}$
(j)	Spin exchange parameter "q"	0.05
(k)	Transverse shielding factor	130,000
(l)	Axial shielding factor: passive active	30,000 $>10^5$
(m)	Molecular hydrogen comsumption	0.02 moles/year

Apart from self-explanatory terms, the parameters above are: I is the net beam flux (the difference in the flux of atoms entering in the higher energy state of the maser transition and the lower energy state); I_{th} is the threshold flux for oscillation to occur providing spin exchange is neglected; q is a quality factor of the clock. The predicted performance of the clock is given in Figure 2-3.

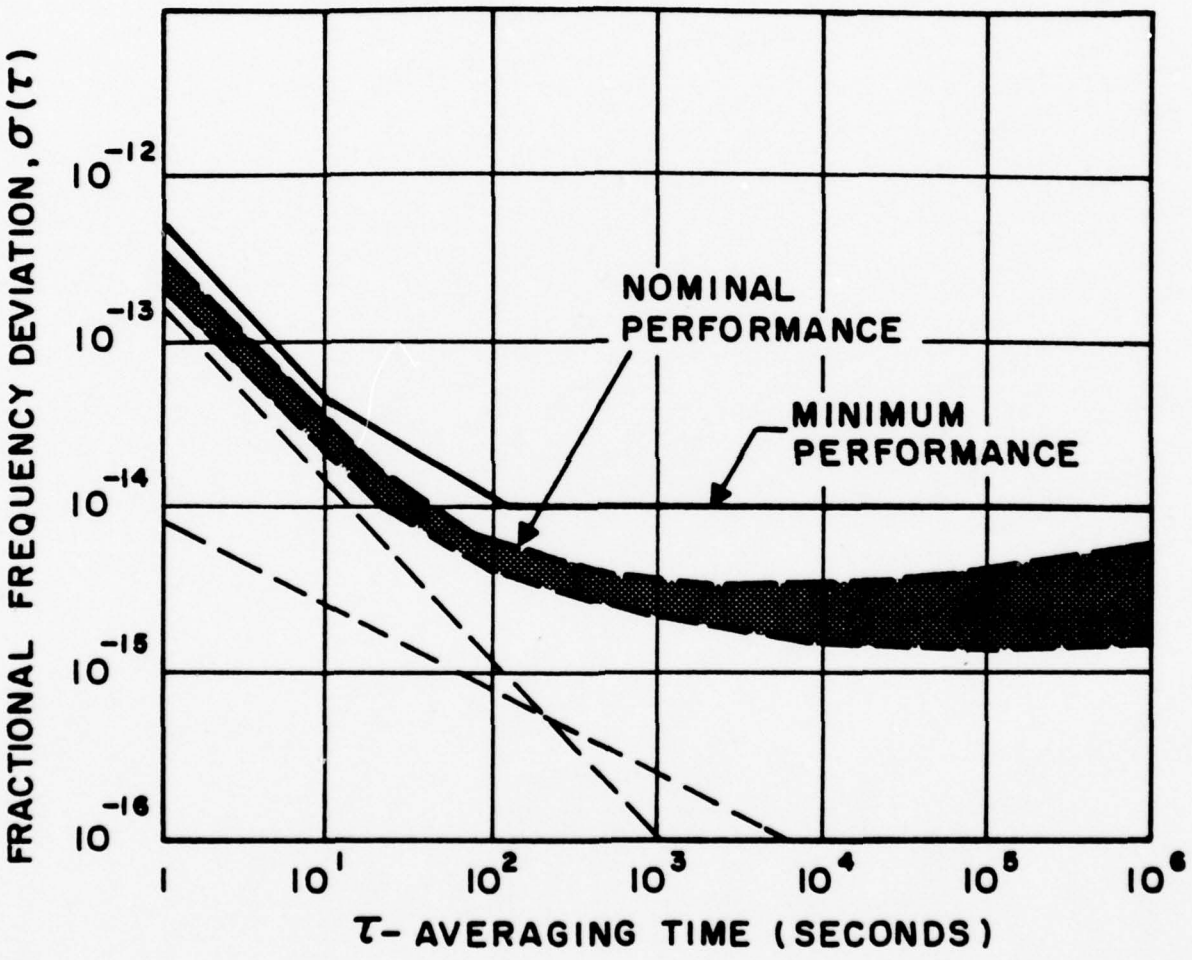

Figure 2-3. Predicted Stability Curve

3.0 PHYSICS UNIT – DETAIL DESIGN DESCRIPTION

3.0 PHYSICS UNIT - DETAIL DESIGN DESCRIPTION

The physics unit of the hydrogen clock consists of three major subassemblies:

(1) Lower Subassembly
(2) Upper Subassembly
(3) Outershield Assembly

The clock is divided into an upper and lower assembly with the main base plate as the dividing line. These two subassemblies will be described in detail in the following sections. The outershield assembly consists of a magnetic shield which covers the outside of the entire clock. It is the fourth magnetic shield.

3.1 LOWER SUBASSEMBLY

The lower subassembly consists of the molecular hydrogen supply, the purifier/valve, pressure control, dissociator, collimator, optical detector and state selector. In a clock designed for space flight, the vacuum pumps would also fit into this subassembly, however the feasibilty model utilizes vacuum pumps placed outside the clock structure to save assembly and test time. From this subassembly, the atomic hydrogen atoms emerge to be processed in the upper subassembly.

3.1.1 Molecular Hydrogen Supply

The hydrogen supply in most ground-based hydrogen clocks consists of a cylinder with a volume of about 1-liter filled with gas at a pressure of 1000 psi. In the space probe maser developed by the Smithsonian Astrophysical Observatory (SAO), the hydrogen supply consisted of about 70 grams of $LiAlH_4$. When heated, the $LiAlH_4$ releases hydrogen at a rate controlled by the temperature of the material. This design (Figure 3-1) consists of pressure vessel with a volume of 0.4 liter filled with gas at 300 psi. This corresponds to a storage of 0.4 mole of molecular hydrogen, and with a hydrogen consumption rate of about 0.02 moles per year, the hydrogen would last 20 years. (In fact, measurements on the dissociator assembly which has been in operation for over one year confirms the calculation on the hydrogen loss rate. The data showed a hydrogen consumption of 0.025 moles per year.) The stainless steel container weighs 453 grams (1 pound) and occupies a space of 500 cm^3. With the exception of size, this type of storage is simple and reliable and does not require any preparation of any special material like the metal hydrides which can store molecular hydrogen in small volumes. There are a number of metal hydrides which may be used if desired, however to make a final selection would require comparative performance testing.

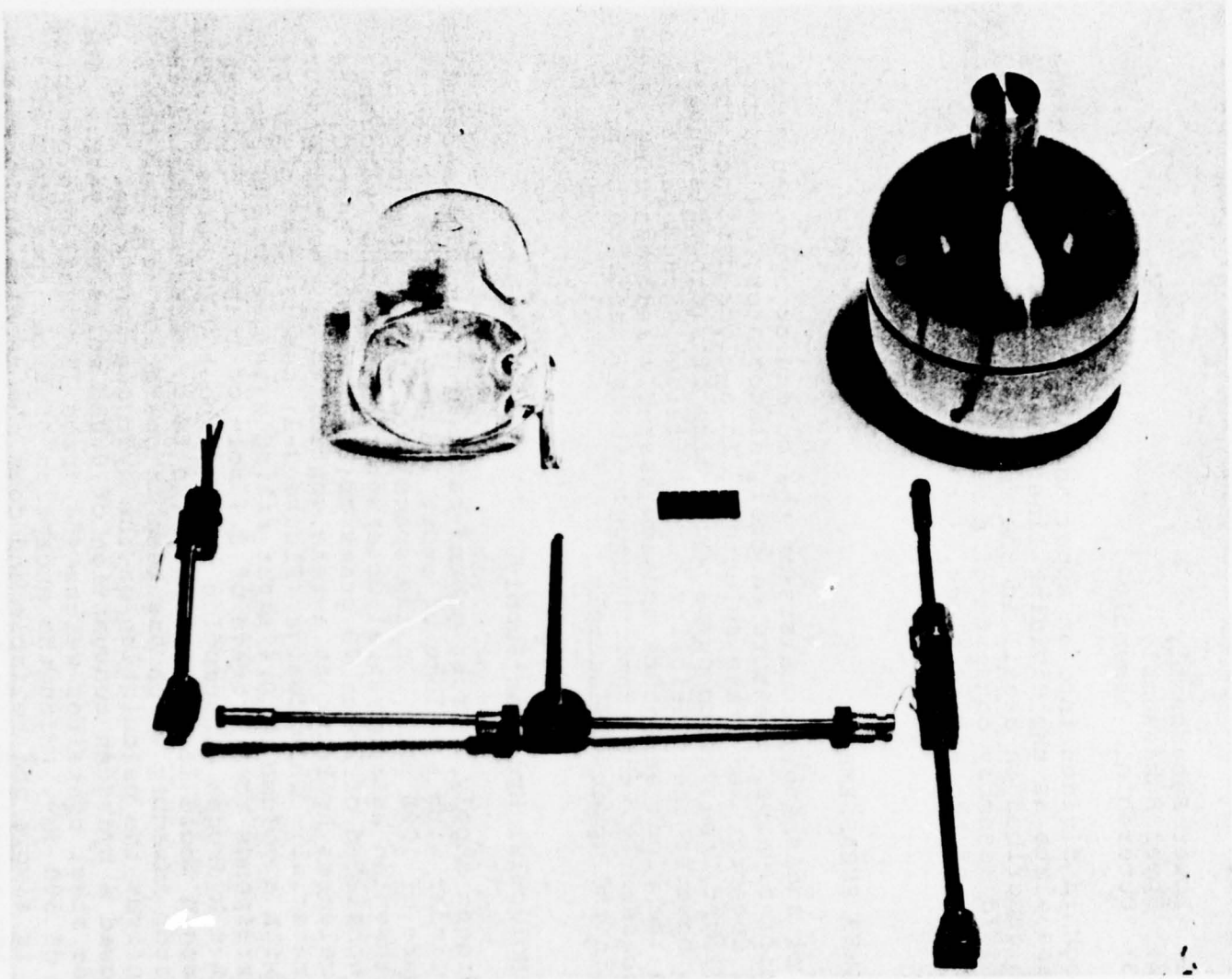

Figure 3-1. Pressure Bottle, Purifier, Pressure Guage, Coupling Tee, Dissociator

The candidates are depleted uranium metal, the $LaNi_5$-H systems and $LiAlH_4$. For example, 100 grams of uranium metal would adequately supply the needed molecular hydrogen while occupying a space of 5-10 cm^3. For the depleted uranium metal, the pressure P(mm) of the hydrogen at a temperature T is given by

$$P = 1.6 \times 10^9 \exp\left[-1.027 \times \frac{10^4}{T}\right].$$

3.1.2 Purifier/Valve

The purifier being used consists of a solid metallic pellet alloy of 75% palladium and 25% silver which restricts gas flow through a small tube. The pellet permits hydrogen diffusion while blocking all other matter, and the rate of hydrogen diffusion is controlled by the temperature of the alloy. The mechanical assembly shown in Figure 3-2 is relatively easy to fabricate and process. The incorporation of the copper sleeve improves thermal conductivity and welding. The copper-stainless steel joints need no special preparation for brazing and the copper-copper and copper-pellet surfaces can be very readily brazed together. The temperature of the pellet is varied by a resistance heater wound on the copper sleeve. A temperature of about 75°C is needed to achieve a pressure of 0.05mm in the dissociator as shown in Figure 3-3.

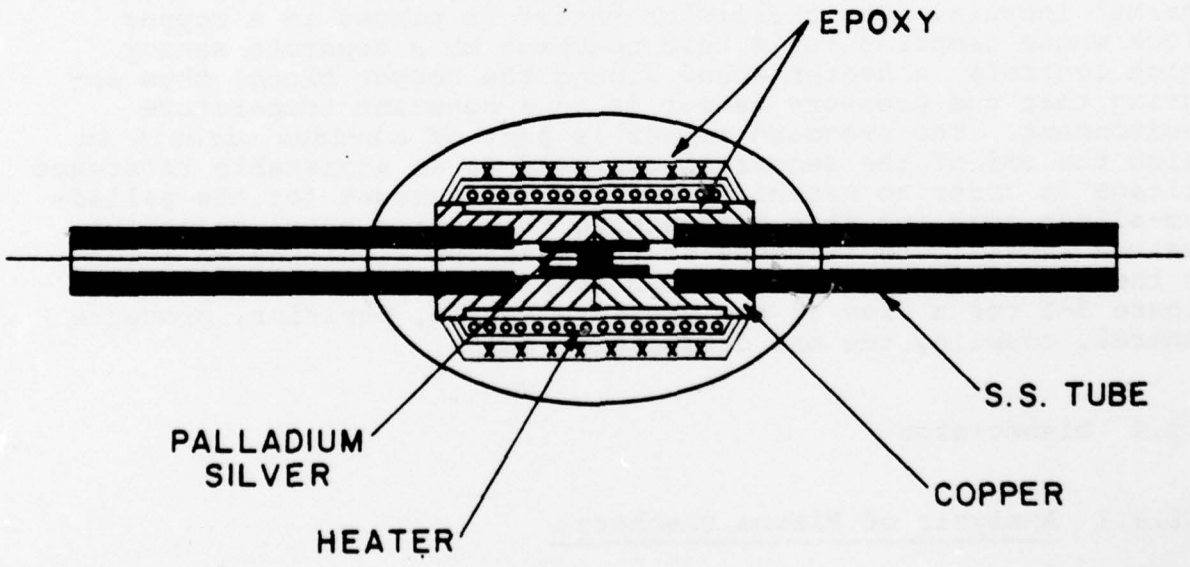

Figure 3-2. Mechanical Assembly of Hydrogen Purifier

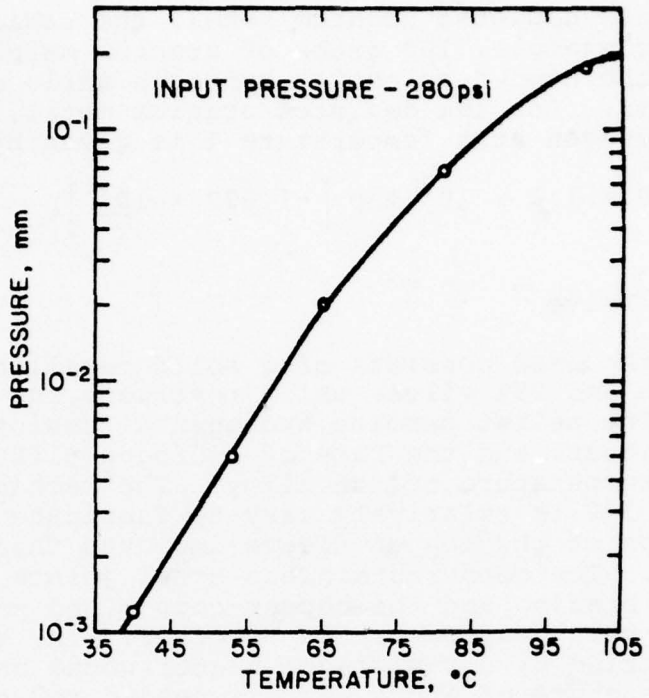

Figure 3-3. Pressure in Dissociator Versus Temperature of Palladium-Silver Purifier No. 2

3.1.3 Pressure Control

The pressure control/gauge is simply a thermistor having a small thermal inertia. The thermistor sensor is placed in a copper block whose temperature is held constant by a separate sensor which controls a heater wound around the copper block, thus ensuring that the pressure sensor is in a constant temperature environment. The pressure sensor is part of a bridge circuit in which the emf of the sensor is compared to an adjustable reference voltage in order to establish the heating current for the palladium-silver leak and thus maintaining the source pressure at the desired level. The response of the pressure regulator to steps in the reference voltage is shown in Figure 3-4. (Refer to Figure 3-1 for a view of the pressure bottle, purifier, pressure control, coupling tee and dissociator bulb.)

3.1.4 Dissociator

3.1.4.1 Analysis of Plasma Discharge

Atomic hydrogen is produced by the dissociation of molecular hydrogen in a "cold" plasma discharge. The discharge is excited by a 120 MHz, two transistor oscillator, described in Section 4.2

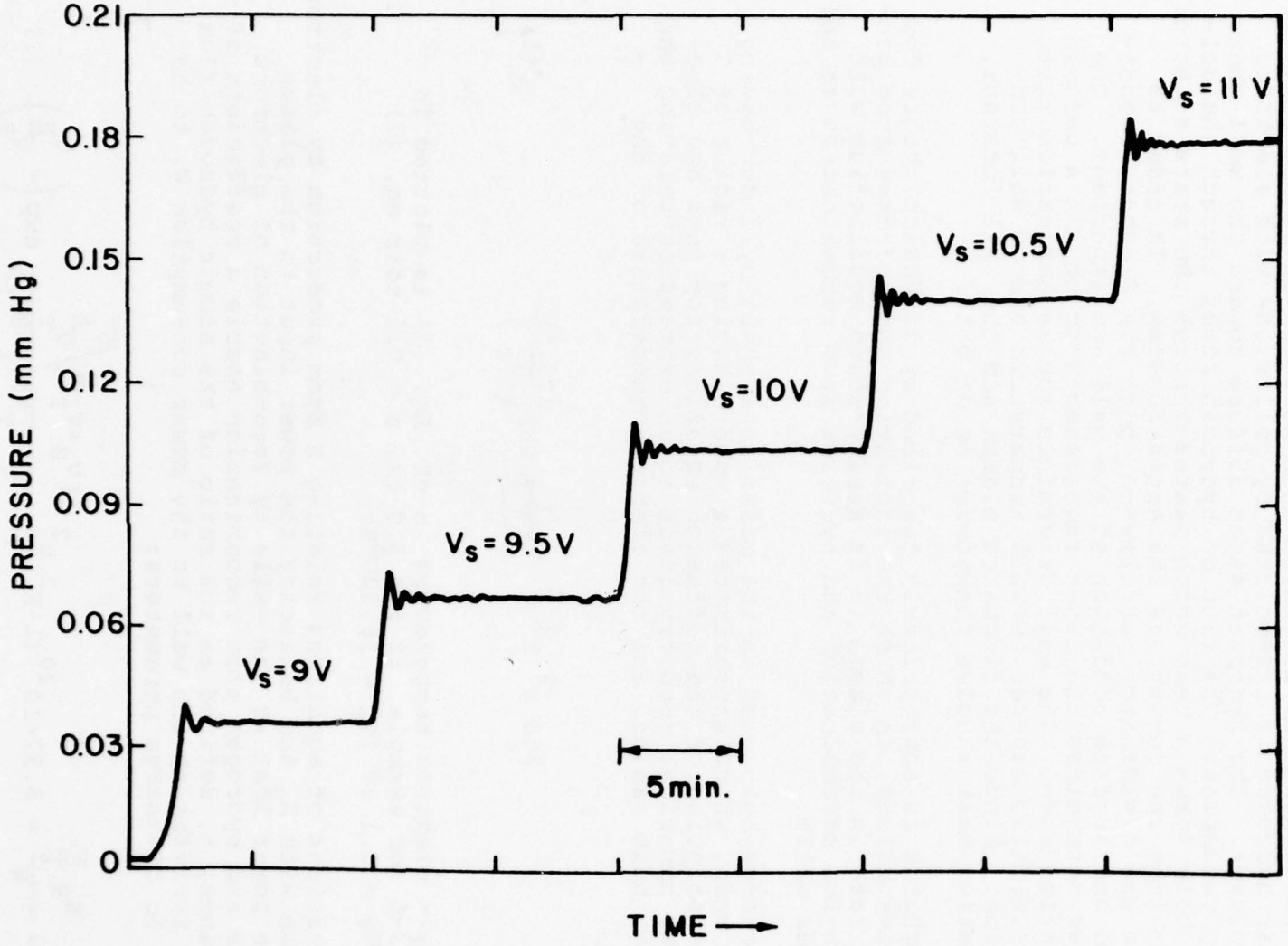

Figure 3-4. Response of Pressure Regulator To Steps In Reference Voltage

capacitively coupled using external electrodes. The oscillator is mounted on a curved plate which is attached to the aluminum housing containing the discharge pulb as shown in Figure 3-5. Molecular hydrogen is dissociated by collisions with electrons in the plasma. The hydrogen atoms diffuse toward the wall where they may recombine. The flux of hydrogen atoms through the collimator hole forms a beam which passes through the state selector and then into the cavity via the entrance stem. In order to optimize the dissociator performance, both the discharge condition and the surface condition of the wall are important. The discharge determines the power requirements to obtain a certain dissociation rate. The wall determines the recombination rate, which critically depends on wall temperature and on wall contamination. Since the discharge plasma and the wall interact, optimization must involve consideration of both.

The discharge is appropriately described by diffusion theory for a positive column, in which the ionization and hydrogen atom production rate in the plasma is in steady state equilibrium with electron-ion recombination and hydrogen atom recombination at the container walls.

The discharge bulb used in the maser is a short cylinder having rounded ends, which approximates a sphere having a radius of 3 cm. The solution of the diffusion equations for ions and electrons for spherical geometry leads to an expression relating the pressure, bulb radius, and the electron temperature of the plasma:

$$750\ p^2\ R^2 = \frac{1}{\sqrt{\frac{15.5}{V_T}}} \exp\left(\frac{15.5}{V_T}\right) \qquad (1)$$

where V_T = electron temperature in eV. Eq. (1) is plotted in Figure 3-6 for example, if R = 3.0 cm, p = 0.1 torr eq. (1) yields V_T = 3.1 eV (T_e = 36,000°K).

Considerations of equations relating H atom production by electron collision with H_2 and balancing the power input to the plasma with the power lost at the walls by recombination of electrons and ions and hydrogen atom recombination enable a coefficient of performance, η, defined as the ratio of the atomic hydrogen flux density arriving at the wall to the power consumption W, to be related to discharge parameters:

$$\eta = \frac{N_H \frac{\bar{C}}{4}}{W} = 5.97\times10^{20}(1-K^2)\frac{p^2}{\gamma} \frac{(V_H+V_T)\sqrt{\frac{V_i}{V_T}}}{(V_i+V_T)(V_i+8V_T)} \exp\left(-\frac{V_H}{V_T}\right) \qquad (2)$$

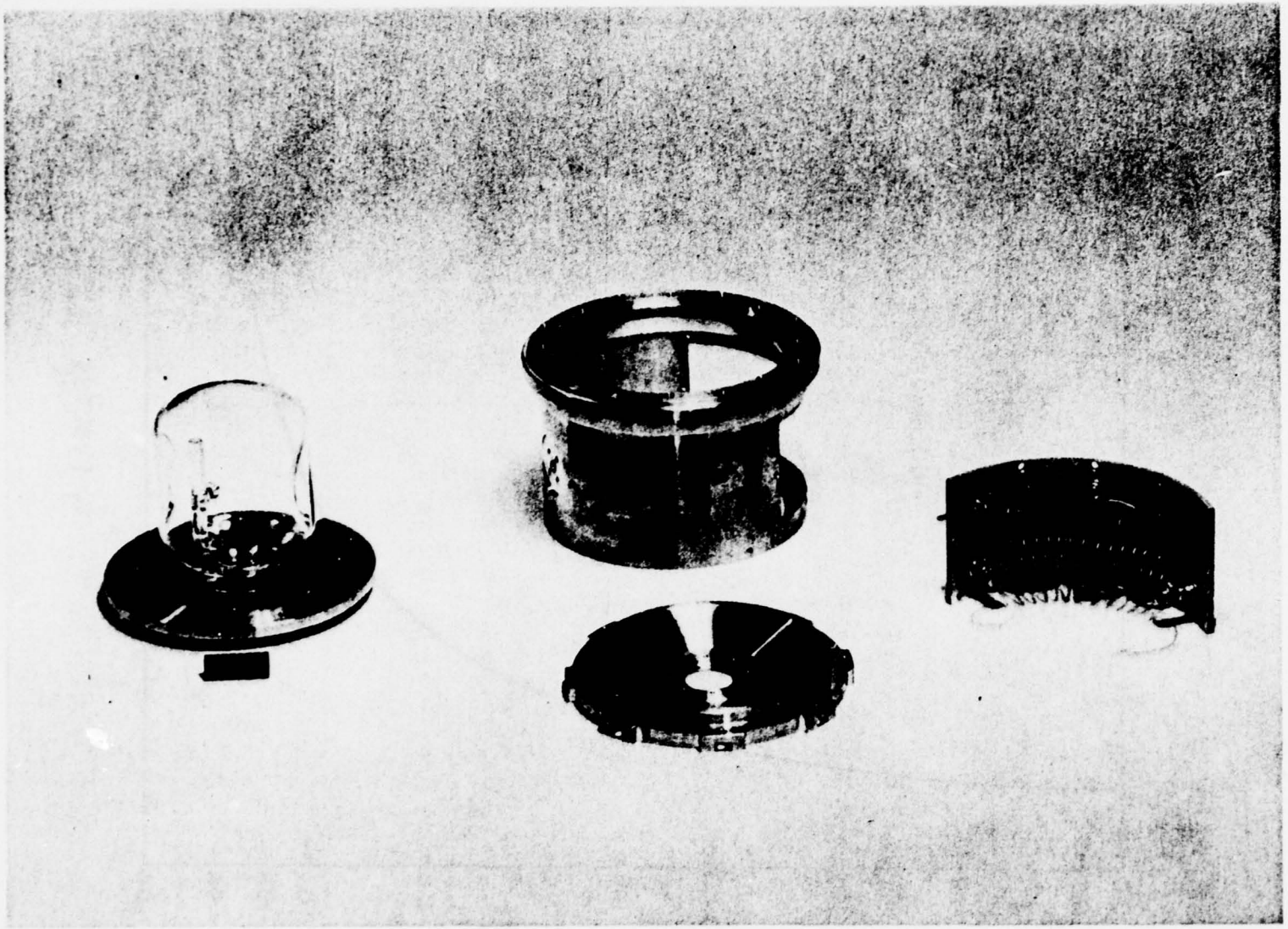

Figure 3-5. Component Parts of Discharge Assembly

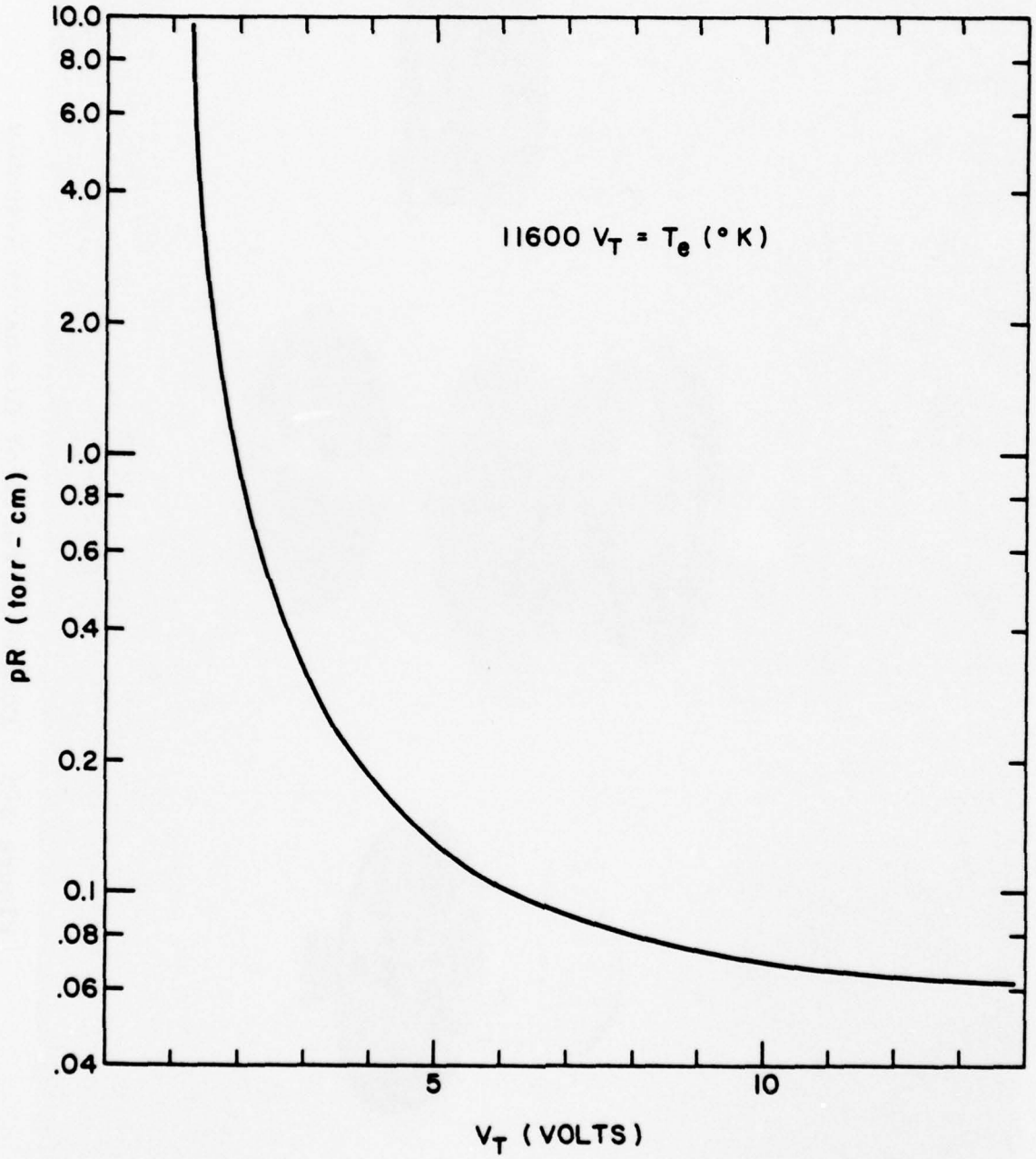

Figure 3-6. Electron Temperature vs p^R

where $\bar{C}$ is mean thermal velocity of the atoms, p is the pressure in the chamber, K is the degree of dissociation, V_i is the ionization potential, V_H is threshold for dissociation, $V_T = \frac{T_e}{11600}$ where T_e is the electron temperature, and γ is probability of recombination at the wall. For example, if $K \ll 1$, $p = 0.1$ torr, $\gamma = 4\times10^{-3}$ (typical number for pyrex), $V_H = 8.8$ volts, $V_T = 3.10$ volts, and $V_i = 15.5$, the above equation yields $\eta = 3.10\times10^{18}$ atoms cm^{-2} sec^{-1} W^{-1}. Typical flux rates for an operating hydrogen dissociator is 10^{15} atom/sec through a 0.005-inch diameter exit aperture, or $\sim 8\times10^{18}$ atoms cm^{-2} sec^{-1}. At a power input of 4 watts, the above equation yields a flux rate of $\sim 1.2\times10^{19}$ atoms cm^{-2} sec^{-1}, which is in good agreement with experimental values.

For a given pressure p, the coefficient of performance η is a function of the electron temperature:

$$\eta = \frac{p^2}{\gamma} F(V_T) \tag{3}$$

where:

$$F(V_T) = 5.97\times10^{20} \frac{(8.8+V_T)\frac{15.5}{V_T}}{(15.5+V_T)(15.5+8V_T)} \exp\left(-\frac{8.8}{V_T}\right) \tag{4}$$

$F(V_T)$ vs V_T is plotted in Figure 3-6, which also shows values for the ion impact energy V_W, assuming $T_D = 1000^{\circ}K$ along the abscissa. It is seen that η has a maximum for V_T 7.5 volts, whereas our typical operating unit has a V_T 3.10 volts. Notice that at $V_T = 7.5$ volts, the corresponding ion-impact energy is about 47 volts (see Figure 3.7) which probably exceeds the threshold for sputtering damage of the wall. This is the reason why smaller size pyrex bulbs have a relatively short life time. In order to increase the efficiency and/or to reduce the unit size, a material must be chosen which has a high threshold for sputtering damage. Parameters of a typical operating dissociator are given in Table 3-1.

TABLE 3-1. PARAMETERS OF A TYPICAL OPERATING DISSOCIATOR

Parameter	Value	Parameter	Value
Geometry	Spherical	Ion impact energy at wall	20 volts
Radius	3.0 cm	Plasma density at center	10^{11} cm^{-3}
Hydrogen pressure	0.1 cm	Atomic hydrogen density at wall	1.3×10^{14} cm^{-3}
Plasma pump power	4 watts		
Electron temperature	$36000^{\circ}K$	Atomic hydrogen arrival rate at wall	1.3×10^{19} $cm^{-2}sec^{-1}$

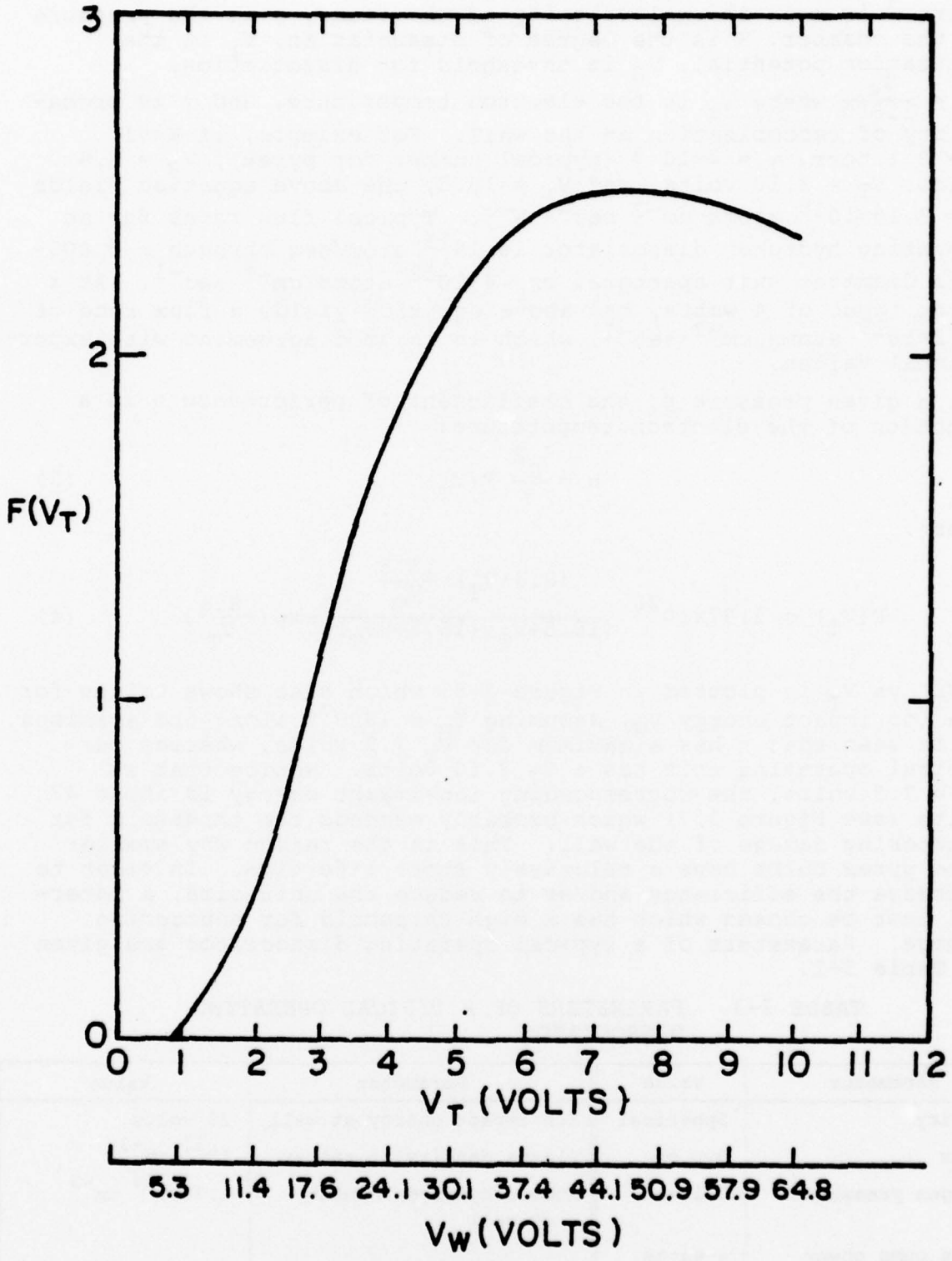

Figure 3-7. $F(V_T)$ vs V_T

In this model, the primary process responsible for the formation of atomic hydrogen is the dissociative excitation of H_2 by electron collision.

$$e + H_2 \rightarrow 2H + e \qquad (5)$$

where H is atomic hydrogen in its ground state. An intermediate step in this reaction involves the production of excited states of hydrogen, H*

$$e + H_2 \rightarrow H + H^* + e \qquad (6)$$

At the low densities characteristic of our experimental conditions, excited atoms in the interior of the plasma relax only by the emission of radiation, and the characteristic color of the discharge is dominated by the Balmer emission series $n \rightarrow 2$ where n is the principal quantum number. In particular, the reddish color of a "good" hydrogen discharge is a result of the emission of the strong Balmer Line H_α at 6563Å.

The emission from the discharge also contains lines characteristic of molecular hydrogen (the second spectrum of hydrogen). This spectrum consists of thousands of lines and contains no regular features. The transition probabilities are, in general, not known but are estimated to be at least 10^4 times smaller than those of atomic hydrogen.

The intensity of the Balmer α line is taken as a convenient measure of the relative concentration of hydrogen atoms in the discharge. However, the relationship between the H_α intensity and the ground state concentration of H is not necessarily a linear one. The H_α intensity data should be used together with pressure and discharge power as a descriptor of the state of the discharge.

An analysis of the relationship between the intensity of the Balmer lines and the discharge parameters is given in Section 3.1.4.3. In this section other spectral measurements characterizing the discharge and the identification of impurities is also discussed. The design, assembly, and operating parameters of the maser discharge unit are described in Section 3.1.4.2.

3.1.4.2 Design, Assembly, and Operation of H Source

The hydrogen dissociator assembly is shown in Figure 3-8. The container is a short cylinder with rounded ends, 2.5 inch diameter and 2.8 inch long, made from Pyrex 7740 glass 1.5 mm thick. The collimator is attached to the end of a 0.50 in. long 0.50 dia. neck of the bulb. The bulb is sealed to the stainless steel vacuum flange by a Torr-Seal epoxy joint between the Pyrex and a flared Kovar sleeve as shown in the cross section sketch of the assembly in Figure 3-9.

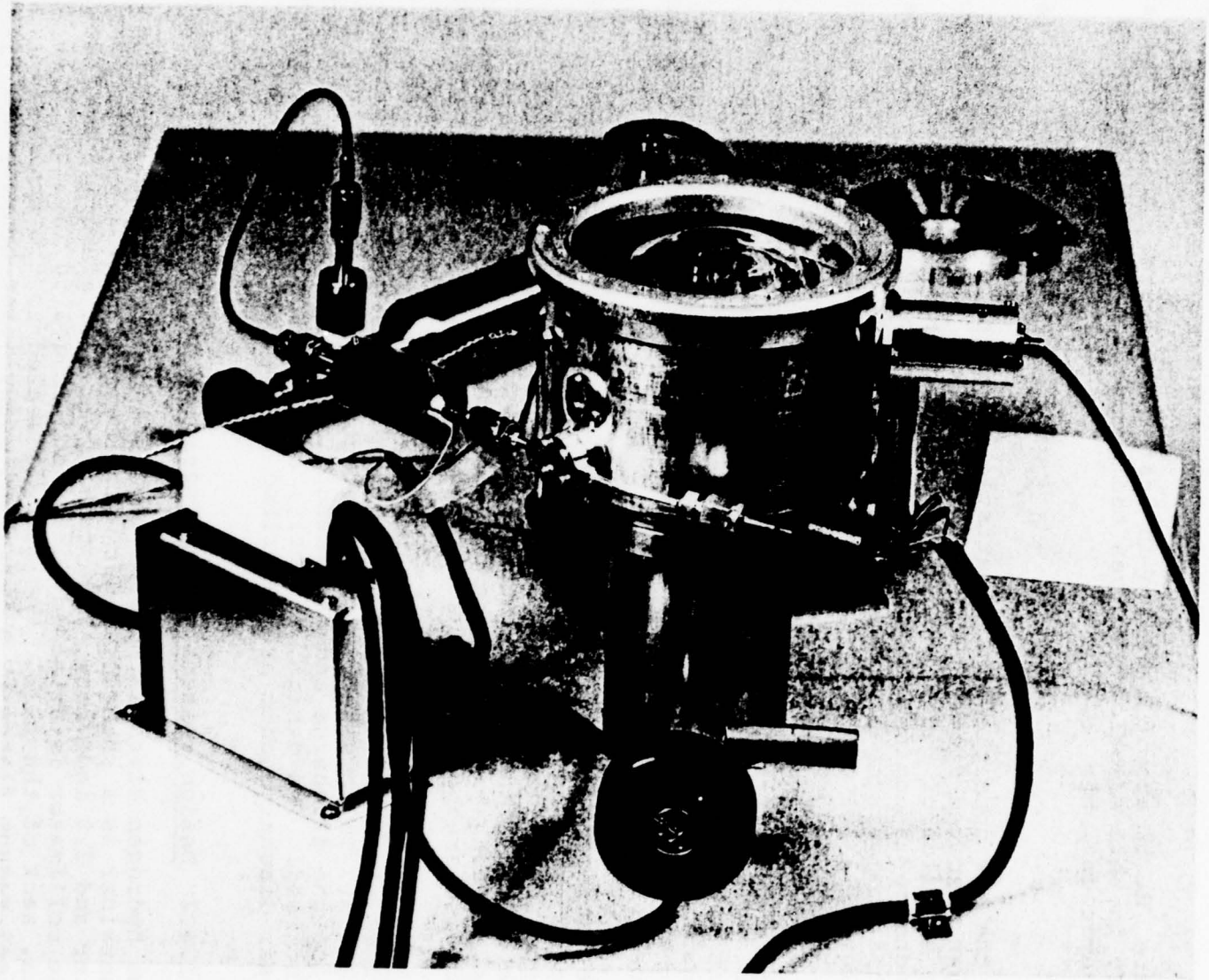

Figure 3-8. Photograph of Assembled Discharge Unit

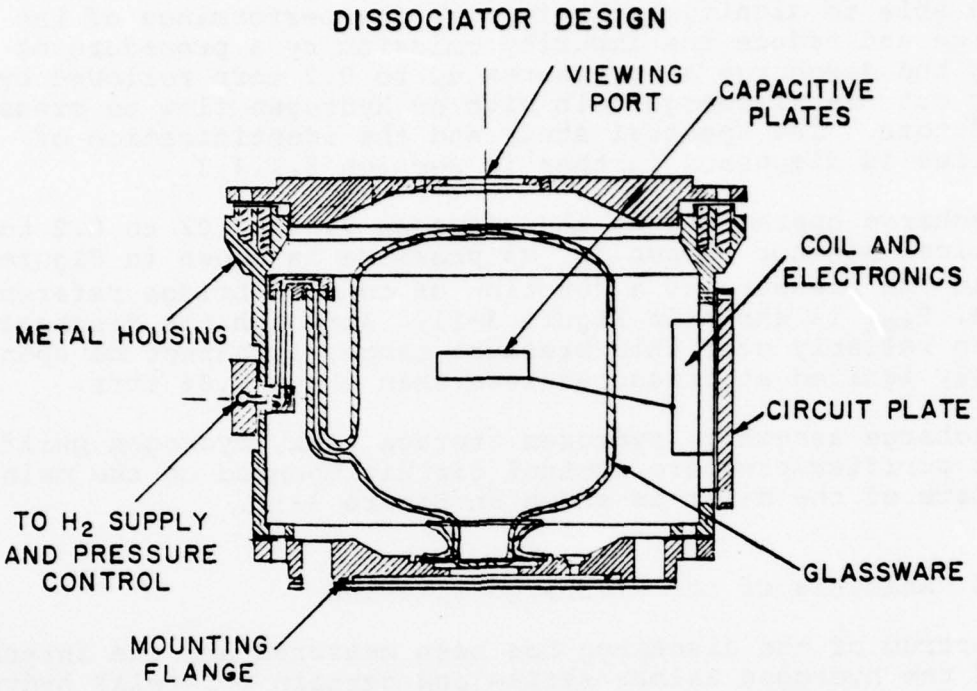

Figure 3-9. Cross Sectional View of Discharge Assembly

The hydrogen inlet tubing from the purifier and pressure gauge is all stainless steel with a 1 in. long, 0.25 in. O.D. flexible bellows section attached to the Pyrex inlet capillary with Torr-Seal epoxy. The collimator hole was approximately centered with the aid of a microscope and a mounting jig served to hold the bulb in place until the epoxy seal was cured. Provision was made on the state selector mounting flange to allow approximately 0.010 inch adjustment in order to obtain the final alignment of the collimator with the center line of the state selector.

The Pyrex bulb was cleaned by rinsing several times with a 50% methanol-50% distilled water mixture followed by a pure distilled water rinse, and finally the container was dried in a vacuum. After assembly on a test bed, the bulb was evacuated using an $8\ell sec^{-1}$ Vac-Ion pump for 48 hours and the bulb was heated to about $80^{o}C$ by a hot air flow for the last several hours before a hydrogen discharge was ignited.

Hydrogen was admitted to the container to a pressure of 0.05 torr and a discharge was ignited. The oscillator was tuned to give the maximum intensity of the Balmer H_α line, as measured by the optical monitor (described in Section VI). Initially, the color of the discharge was pale blue-pink with I_{H_α} = 0.020 V, but within one hour the discharge became distinctly redder and I_{H_α} = 0.30 V for P = 0.05 torr.

During the course of the spectroscopic study of the discharge, we were able to significantly improve the performance of the discharge and reduce the impurity emission by a procedure of running the discharge at pressures up to 0.2 torr followed by pumping out the discharge bulb with no hydrogen flow to pressure of 10^{-8} torr. The spectral study and the identification of impurities is discussed further in Section 3.1.4.3.

The discharge operates over the pressure range 0.02 to 0.2 torr. The optical monitor output $I_{H\alpha}$ vs pressure is shown in Figure 3-10 and the pressure as a function of control bridge reference voltage, P_{set} is shown in Figure 3-11. Although the discharge operates reliably over this pressure range, it cannot be spontaneously ignited at pressures less than about 0.04 torr.

The discharge assembly, hydrogen storage tank, hydrogen purifier, and the purifier/pressure control circuit mounted on the main base plate of the maser is shown in Figure 3-12.

3.1.4.3 Analysis of the Discharge Spectrum

The spectrum of the discharge has been measured and the intensities of the hydrogen Balmer series and certain molecular hydrogen lines have been measured as functions of various discharge conditions. The spectrum in the range 4000-7000 Å is shown in Figure 3-13. The Balmer lines H_α, H_β, H_γ, and H_δ are evident, the remaining lines in this spectral range are all molecular hydrogen lines. The wavelengths and transition probabilities of the first four Balmer lines are given in Table 3-2.

TABLE 3-2. WAVELENGTH AND INTENSITIES FOR THE BALMER LINES OF HYDROGEN, $n \rightarrow 2$

Initial State, n	Designation	Wavelength (A)	$J_{n,2}$ (ergs/sec)
3	H_α	6562.9	11.8×10^{-4}
4	H_β	4861.3	5.38×10^{-4}
5	H_γ	4340.5	2.87×10^{-4}
6	H_δ	4101.8	1.50×10^{-4}

The intensities are sums over the excited state orbital quantum numbers, $J_{n,2} = \sum_{\ell\ell'} (2\ell+1) h\nu_{n,2} A_{n\ell,2\ell'}$.

The measured intensity of the Balmer lines provides a qualitative indication of the atomic hydrogen density in the discharge. A quantitative relationship has not been deduced yet because of the complexity and number of processes which populate and de-populate

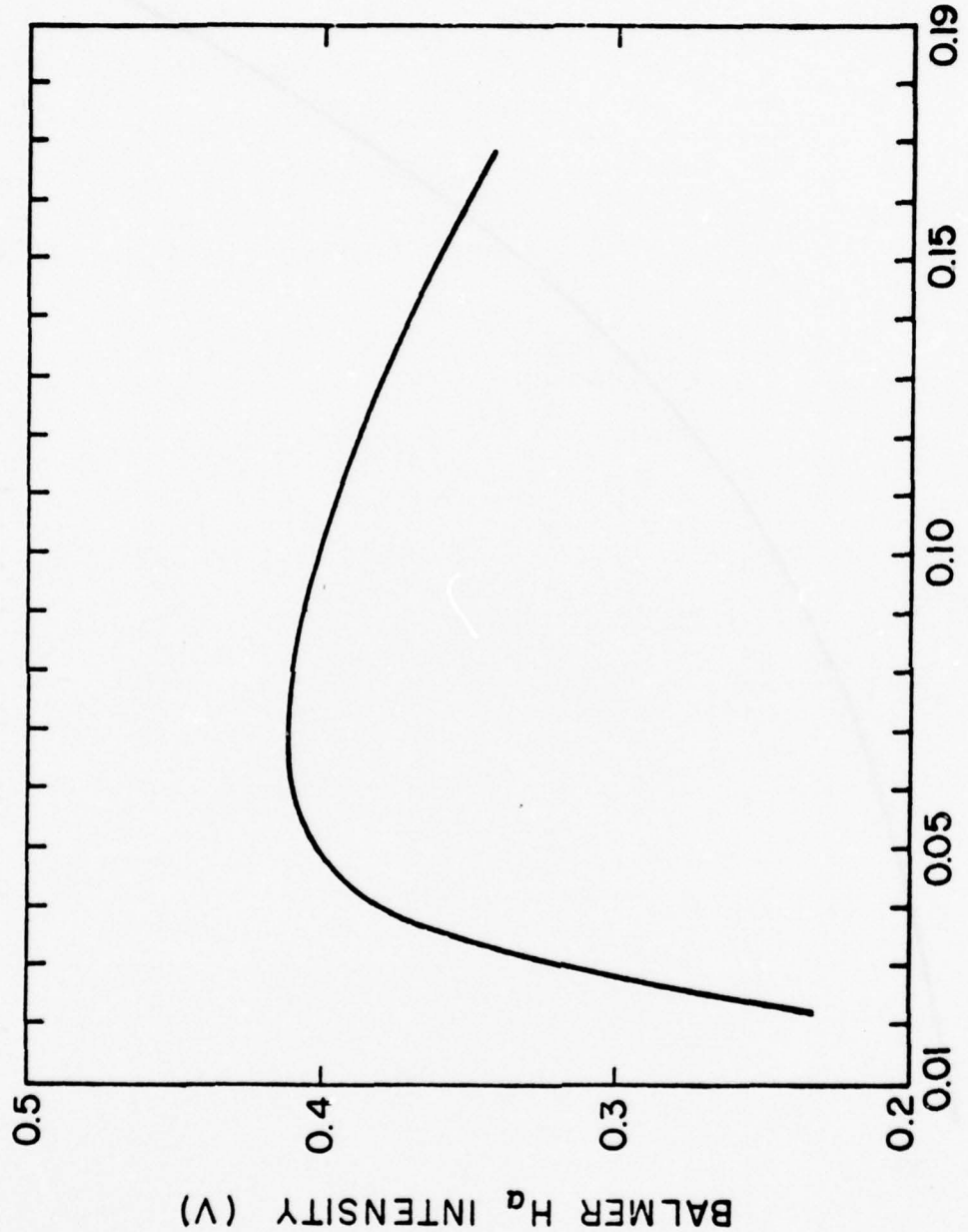

Figure 3-10. Intensity of H_α vs Pressure

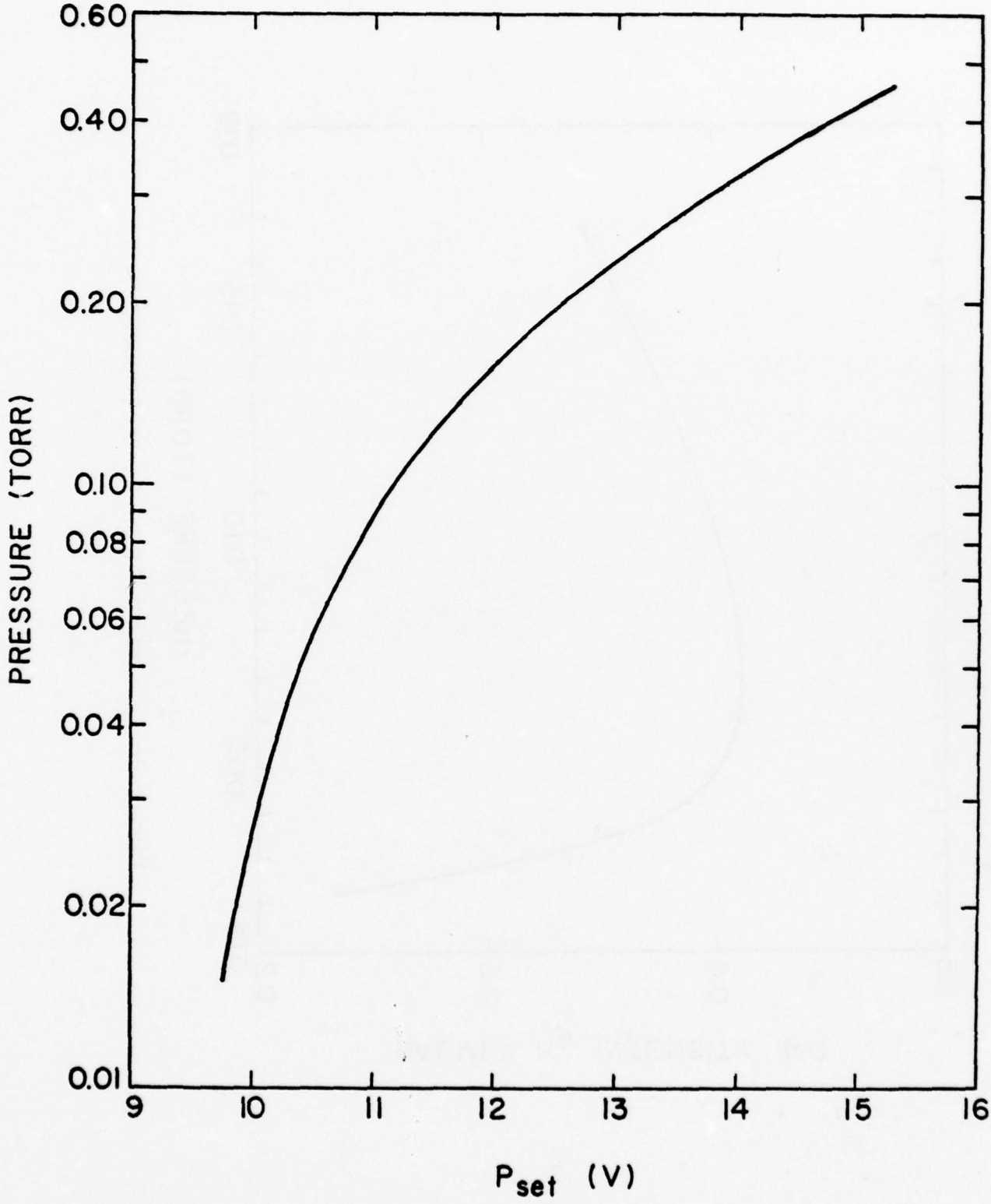

Figure 3-11. Pressure vs P_{SET}

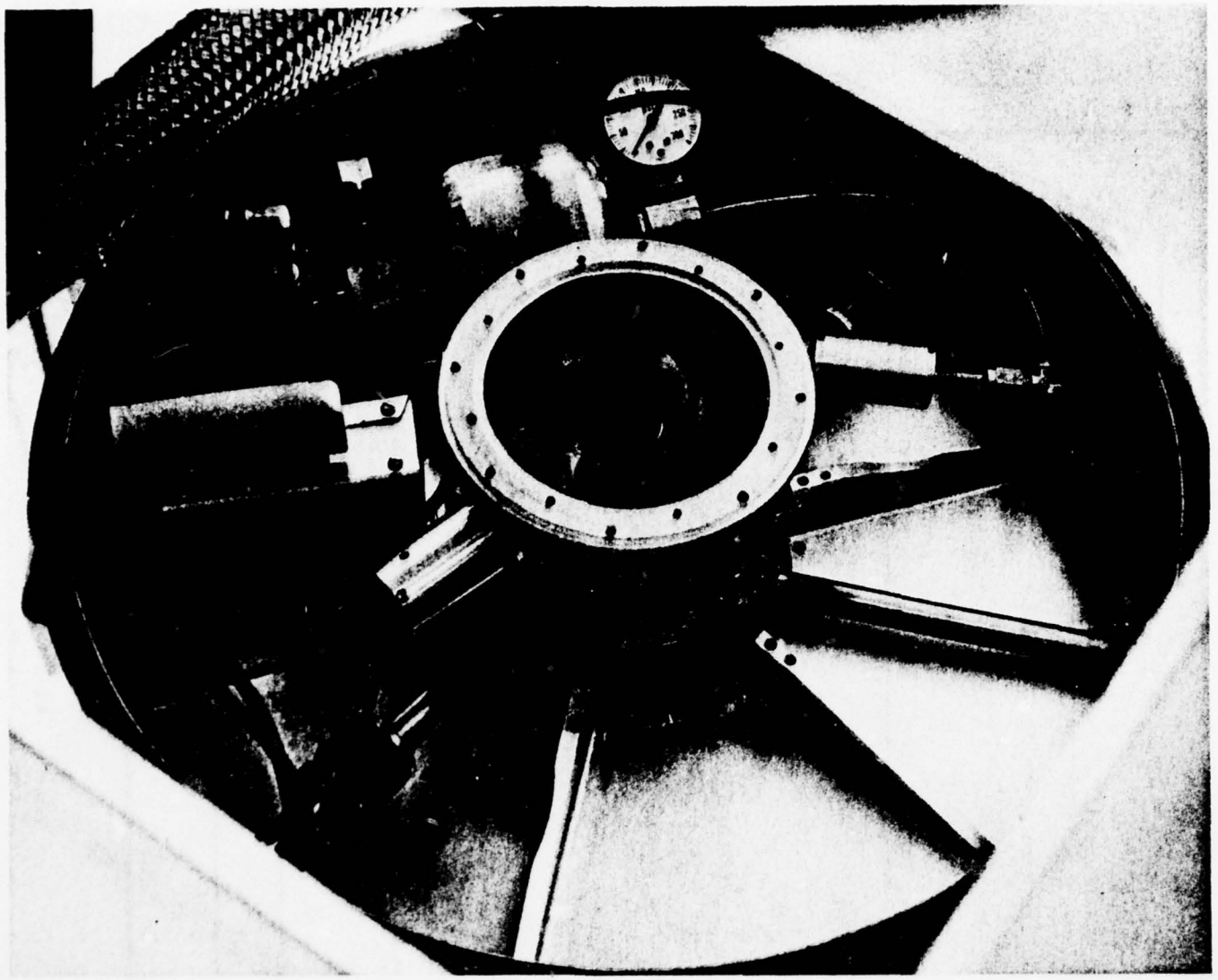

Figure 3-12. Discharge Assembly and Components Mounted on Main Base Plate of Maser

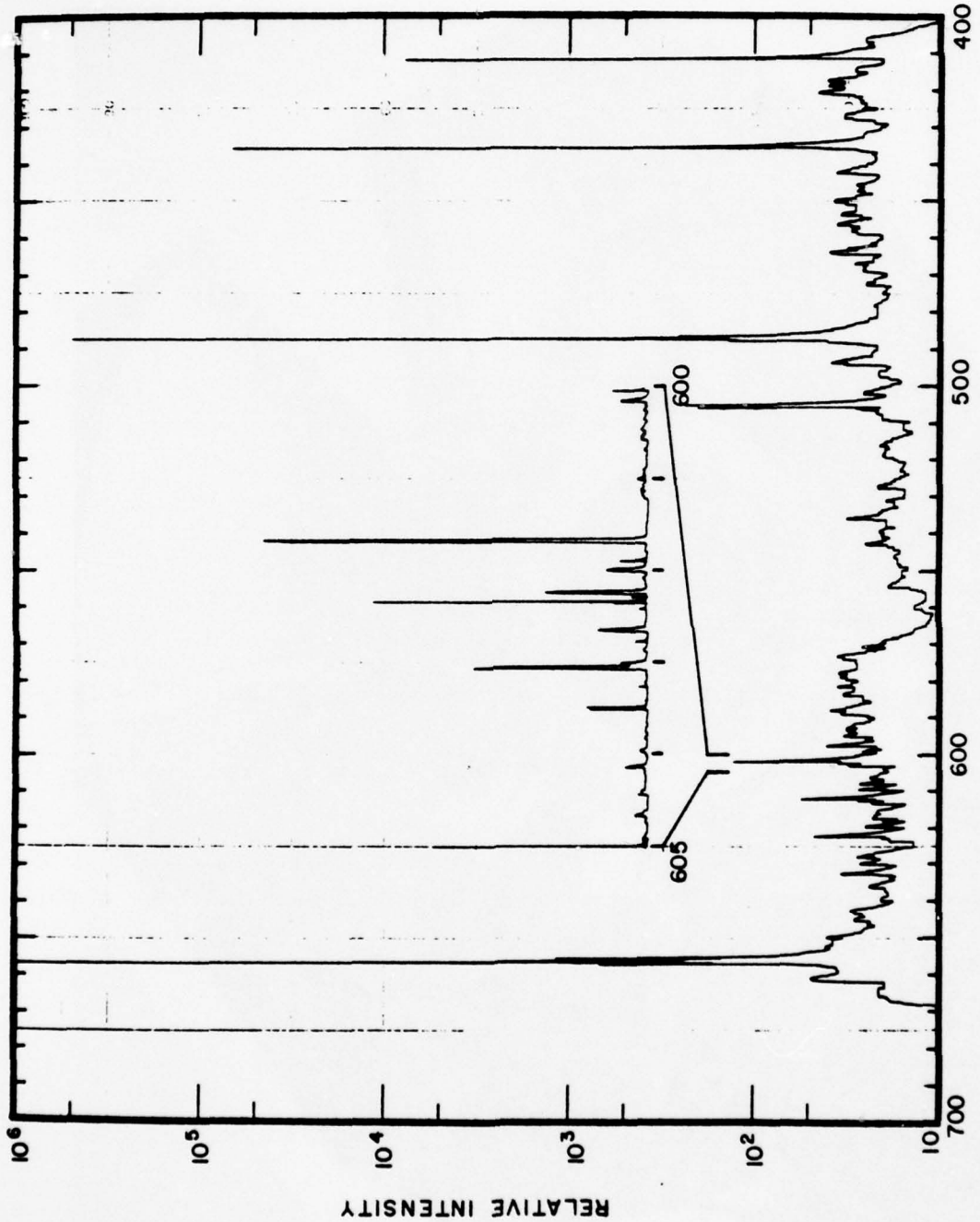

Figure 3-13. Spectrum in Range 4000-7000 Å

the excited states. The atoms are not in thermal equilibrium in the gas; although the effective ion temperature is a few hundred degrees according to the discharge analysis of 3.1.4.1 and confirmed by line width measurements; the excited state populations are much larger than predicted by equilibrium statistics. This is a result of the low atomic density and the fact that the rate of atom production is much greater than the atom collision rate.

The excited atomic states are formed by electron collision with ground state hydrogen and dissociative electron excitation of H_2. The excitation cross sections for H atoms are approximately 10 to 100 times larger than the dissociative excitation cross sections for H_2; therefore, both processes contribute significantly to populating excited states of H, even for a small degree of dissociation.

The intensity of a transition p → 2 is given by

$$I_{p,2} = K\, n_p\, J_{p,2} \tag{1}$$

where n_p is the excited state population and K includes geometrical and collection efficiency factors. The problem is to deduce the values of n_p, and in the non-thermal equilibrium situation applicable here, they are given by solution of the rate equations for the steady state, i.e. $\frac{dn_p}{dt} = 0$ for all P. If we neglect the effect of cascade transitions and wall collisions

$$n_p = \tau_p \left[n_e n_o \langle \nu_e Q_p \rangle + n_e N \langle \nu_e Q_p^{diss} \rangle \right] \tag{2}$$

where τ_p is the radiative lifetime of the level p, n_e is the electron density, n_o the ground state hydrogen atom density, N the molecular hydrogen density, ν_e the electron velocity, Q_p the excitation cross section of the p^{th} level from the atomic ground state, Q_p^{diss} the dissociative excitation to the p^{th} atomic level, and $\langle \cdots \rangle$ represents the average over the electron distribution.

The ratio of the intensities H_β/H_α, H_γ/H_α, and H_δ/H_α as a function of pressure is shown in Figure3-14. The ratios increase as pressure decreases (electron temperature increases). According to (2) above the intensity ratio becomes

$$\frac{I_{p,2}}{I_{3,2}} = \frac{\tau_p J_{p,2} \left\{ n_o \langle \nu Q_p \rangle + N \langle \nu_e Q_p^{diss} \rangle \right\}}{\tau_3 J_{3,2} \left\{ n_o \langle \nu Q_3 \rangle + N \langle \nu_e Q_3^{diss} \rangle \right\}} \tag{3}$$

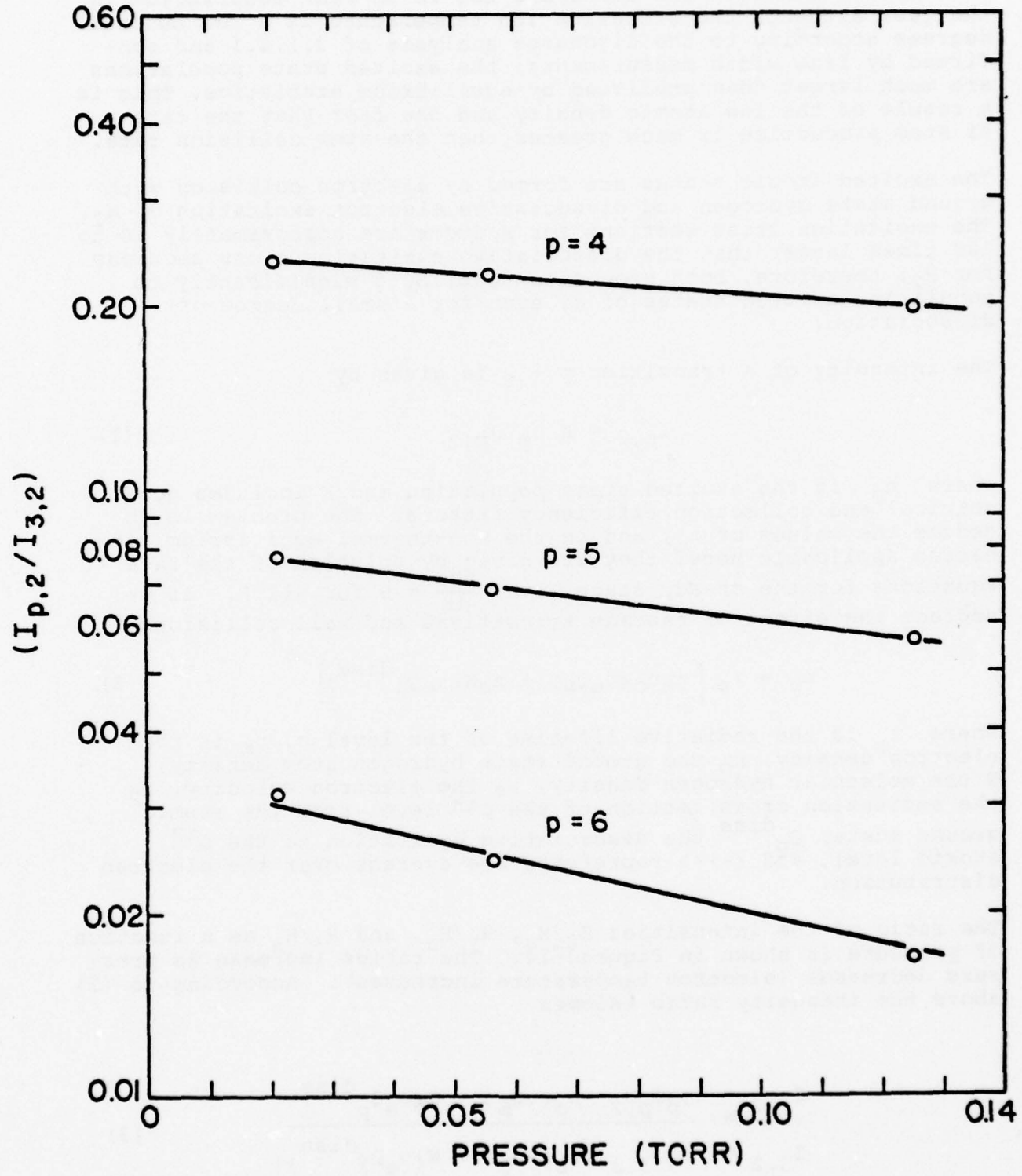

Figure 3-14. Intensity Ratios of Balmer Series vs Pressure

If the average over the cross sections could be evaluated, from measurement of the intensity ratio, n_o/N (equal to the degree of dissociation for small dissociation) could be evaluated.

The relative intensities of the molecular hydrogen singlet $3d'\Sigma \rightarrow 2p'\Sigma$ at 4634 Å and the triplet $4p\ ^3\pi \rightarrow 2s\ ^3\Sigma$ at 4617 have also been measured as a function of pressure. The singlet/triplet intensity ratio increases as pressure increases and the singlet 4634/Balmer H_α intensity ratio decreases from 3×10^{-5} at p = 0.022 torr to 8.8×10^{-6} at p = 0.125 torr. A high resolution spectrograph (resolving power of 60,000) was used to measure the line widths of H_α and H_β at p = 0.056 and p = 0.20 torr. The data, corrected for the instrumental width, are shown in Table 3-3.

TABLE 3-3. FULL LINE WIDTHS AT HALF MAXIMUM INTENSITY OF H_α AND H_β

p (torr)	H_α, W_F (Å)	H_β, W_F (Å)
0.056	0.14	0.06
0.20	0.10	0.04

The calculated Doppler width at T = 1000°K is 0.15 Å for H_α and 0.11 for H_β.

Finally, we consider the impurity species identified in the spectrum. We have found OH by the presence of the distinctive 3064 Å system, NH by the presence of the strong triplet system at 3360, N_2 was seen by identification of the second positive spectrum, primarily the 2814, 2960, 3160, and 3370 groups, and CN was detected by the identification of the 3884 group. These spectra, shown in Figure 3-15, were weaker than the molecular hydrogen lines and we found a method of reducing their intensity to near the detectable limit. This sequence involved running the discharge at high pressure, where their intensity was initially enhanced, extinguishing the discharge and pumping for 24 hours in the absence of a hydrogen flow. Two cycles of this procedure reduced the intensities of OH and NH by a factor of 10 and re-reduced the N_2 and CN lines below our detection limit. Measurement of the intensity ratio of the Balmer lines to the intensity of the NH and OH groups, together with the known oscillator strengths, enables an estimate of the concentration ratios $[NH]/[H] \approx [OH]/[H] \approx 10^{-7} - 10^{-8}$ to be made.

A careful search was made to identify CH by examination of 4300 and 3900 Å regions where this species has characteristic strong spectra, but it was not found. We conclude that our bulbs were quite clean intially and were further cleaned by the procedure outlined above. The presence of OH and NH can occur by chemical reaction of H with the wall. Nitrogen is a common impurity in glass and oxygen is, of course, part of the wall composition.

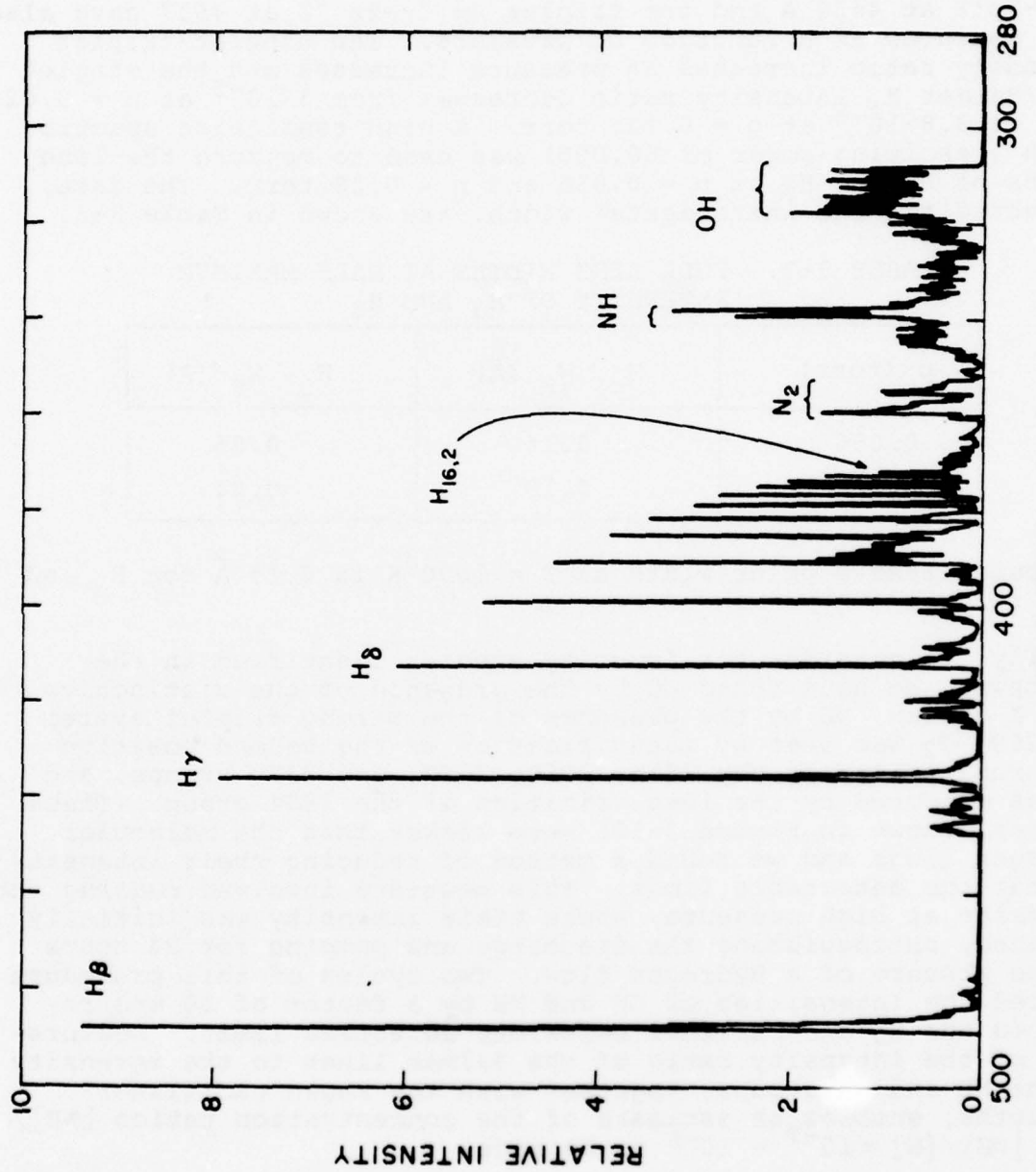

Figure 3-15. Spectral Region Showing OH and NH

We did not find a significant increase in the intensity of OH, nor was Si or SiO detected at the lowest operating pressure (highest electron temperature). Apparently we do not exceed the voltage at which sputtering damage occurs for pressures as low as 0.02 torr, although the calculated electron temperature is 15 eV, according to eq. (1), Section IV-A

3.1.4.4 Comparison of Discharge Containers made of Pyrex, Fused Silica, and Ion-Depleted Pyrex

The recombination of atomic hydrogen at the wall of the discharge container is of paramount importance for the efficient production of H by a plasma discharge. Much effort has gone into development of methods to treat glass surfaces in order to decrease the catalytic activity of the wall, but these efforts have had only limited success. Results obtained from earlier hydrogen maser studies suggest that mobile sodium ions in Pyrex 7740 increase the recombination coefficient, γ, and can shorten the operating lifetime of a discharge container. It has been suggested that fused silica, which is pure SiO_2, may be a better hydrogen discharge container.

We have evaluated three different glass containers for hydrogen discharges by studying the operating characteristics of three physically similar units: D-1 made from Pyrex 7740; D-2 made from fused silica; and D-3 made from Pyrex 7740 whose inside surface was ion-depleted to a depth of 2.5 μm. The shape and dimensions of the bulbs are identical, being short cylinders 2.5 inch diameter, having rounded ends with an overall length of 2.8 inches. Each bulb has a collimator attached which consists of a single 0.005 inch diameter hole in a 0.040 inch thick pyrex disc. Each bulb was attached to a separate test bed having its own hydrogen purifier, pressure gauge, and Vac-Ion pump as shown in Figure 3-16.

The operating characteristics of all three discharge units are quite similar, and although some differences exist, we conclude that these three glasses all have effectively the same recombination coefficient.

In each case, the discharge initially obtained was pale blue-white with very weak Balmer series intensity; however the discharge gradually became redder in color and the Balmer intensity increased and stabilized after a few days of operation. There has been little change in color and in the intensity of H_α, as measured with a standard photodiode-interference filter detector, after the initial stabilization period until the present time (for a given pressure, bulb wall temperture, and oscillator power input). D-1 (Pyrex 7740) has been operating since August 1976 while both D-2 (fused silica) and D-3 (ion-depleted Pyrex) have been operating since February 1977. Typical operating characteristics are summarized in Table 3-4.

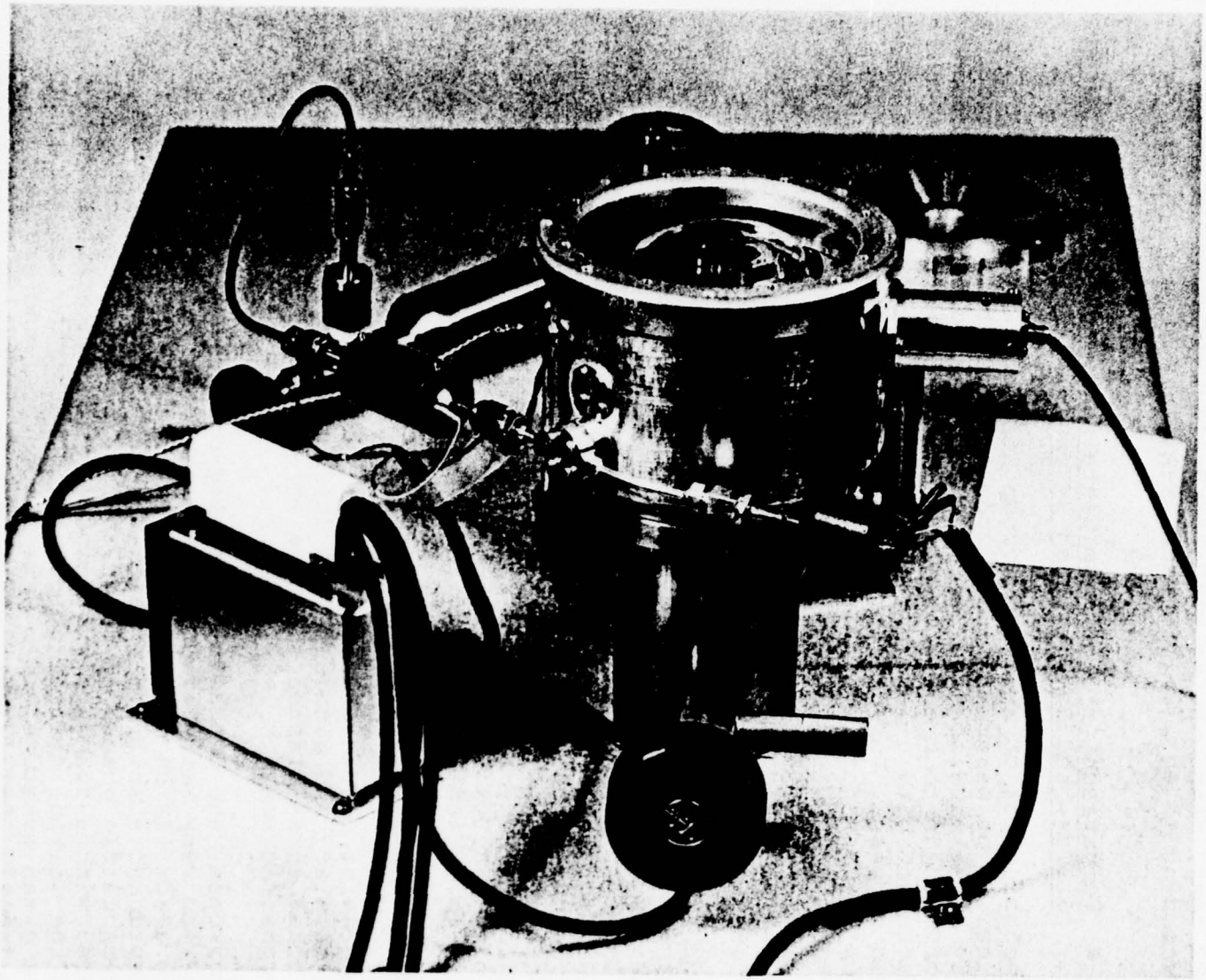

Figure 3-16. Test Assembly for Discharge Unit

TABLE3-4. COMPARISON OF THE OPERATION OF HYDROGEN DISCHARGES IN PYREX (D-1), FUSED SILICA (D-2), AND ION-DEPLETED PYREX (D-3).

Unit	Pressure (torr)	Intensity of H_α	Wall Temperature
D-1	0.03	0.60	86°C
D-1	0.05	0.99	86°C
	0.08	1.04	
D-1	0.12	0.92	86°C
D-2	0.02	0.75	90°C
D-2	0.045	1.18	90°C
D-2	0.07	1.22	90°C
D-2	0.14	0.86	
D-3	0.044	1.26	88°C
D-3	0.056	1.15	88°C

The data shown in Table 1 were all taken with the oscillator operating at 24V DC input and with a DC current of 0.56 - 0.62 amp. An accurate comparison of the discharges is not possible in the absence of measurements of the actual current through the discharge, which is itself affected by the pressure and wall temperature.

In general, the emission spectra from all three discharges were quite similar, consisting primarily of the Balmer lines of H and the second spectrum H_2. The only impurities present in the discharge are oxygen and nitrogen. We have detected OH, NH, CH, and N_2 spectra in trace quantities, but have not found either Si or SiO, although they should be readily detectable. Si has a strong emission line at 2880 Å, a wavelength at which fused quartz is transparent. We have searched for this line at the lowest pressure possible to operate the discharge ($p \sim 0.02$ torr) in a uniform mode. Apparently we have not exceeded the threshold for sputtering, although we estimate that the electron temperature may be as high as 10-15 eV.

Carbon has been detected at CN in the case of Pyrex, although it was made to disappear in 3.1.4.3. Neither CH nor CO were detected although they have prominent spectral signatures. Recently, Auger electron spectroscopy studies at NRL of surfaces from hydrogen discharge bulbs which had failed, showed a correlation between yellow-brown discoloration and carbon deposits. The carbon appears to be a prime cause of failure. Since we do not see carbon in the discharge and have observed no discoloration in our bulb surfaces, it is apparent that carbon is not an intrinsic impurity in Pyrex or fused silica.

The intensity of the H_α line is found to increase 10-20% for a fixed pressure when the temperature of the wall is lowered to 30°C by forced air cooling. This observation is in accord with

an increase in the degree of dissociation resulting from a decrease of γ. It is known that γ increases as T increases for $T > -150^{o}C$.

Finally, we note that the dependence of H_{α} intensity as a function of pressure is similar to that shown in Figure 3-10. The position of the maximum and the exact shape depends on the particular unit. We also find that the discharge tends to become non-uniform at low pressure, resembling a dumb-bell with the more intense red ball in the vicinity of each external electrode.

3.1.4.5 BeO and Sapphire Discharge Containers

A hydrogen discharge container fabricated from a material having a high thermal conductivity and a low value of recombination coefficient, γ, offers several advantages over glass containers. Glass bulbs are fragile and are not amenable to precision alignment. Furthermore, the low thermal conductivity of glass causes the wall to run hot, since the energy in the plasma discharge is ultimately dissipated at the wall, and the usual method of cooling by air circulation is not desirable in a spacecraft environment. Sapphire and BeO have been suggested as suitable materials for discharge containers. Relevant physical properties of BeO, sapphire, and glass are summarized in Table 3-5 below.

TABLE 3-5. PHYSICAL PROPERTIES OF PYREX, FUSED SILICA, SAPPHIRE, AND BeO

Material	Dielectric Constant at $25^{o}C$ 25 GHz	Thermal Conductivity (cal-cm)/ (sec-cm^2-^{o}C) at $25^{o}C$	Lines Expansion Coefficient (in/in/^{o}C) $T<1000^{o}C$	Hydrogen recombination Coefficient, γ ($25^{o}C$)
Pyrex 7740	5.0	0.0023	3.3×10^{-6}	3×10^{-3}
Fused Silica (SiO_2)	3.78	0.0033	0.55×10^{-6}	3×10^{-3}
Sapphire (Al_2O_3)	9.30	0.060	8.2×10^{-6}	?
BeO Ceramic	6.0	0.52	8.6×10^{-6}	?

There is considerable uncertainty concerning the values of γ for glass and the literature value of $\gamma = 0.4$ for Al_2O_3 coated on glass may not be appropriate for sapphire. The value of γ for BeO is not known.

The surface of a discharge container should be very smooth in order to minimize the surface area and thus reduce the catalytic activity of the wall for hydrogen recombination. Surfaces of ceramics are rough compared with glass and single crystal surfaces and it is not possible to polish a ceramic to a smooth finish. The surface of BeO ceramic having a standard finish is

shown in Figure 3-17. We found that the surface could be glazed, providing a smooth, adherent thin glass coating. The glass may also be used to join pieces of BeO giving a rugged hermetic seal. A patent application has been filed on the construction and use of such a container. The same technique was also used to seal pieces of single crystal sapphire and we constructed a container fabricated from glazed BeO and one from single crystal sapphire and a hydrogen discharge was obtained and studied in both cases. The finished containers are shown together with a Pyrex bulb for comparison in Figure 3-18. While the results are not conclusive, sapphire appears to be a poor choice, whereas glazed BeO should make an excellent discharge container.

3.1.4.5.1 Sapphire

A cylinder 1 inch OD and 1.5 inches long was fabricated by sealing sapphire windows to the ends of the cylinder using a technique of pre-glazing mating pieces and then firing them to 1200°C in close contact. The windows are 0.040 inches thick and one contains a 0.050 inch hole in the center for an exit port while a short capillary is sealed into the opposite window with the glass sealing material. The capillary is connected to the hydrogen inlet tubing with an epoxy seal. The cylinder is a one inch OD, 0.030 inch wall thickness EFG (edge defined film fed growth technique) sapphire piece manufactured by Tyco Laboratories, Waltham, Mass.

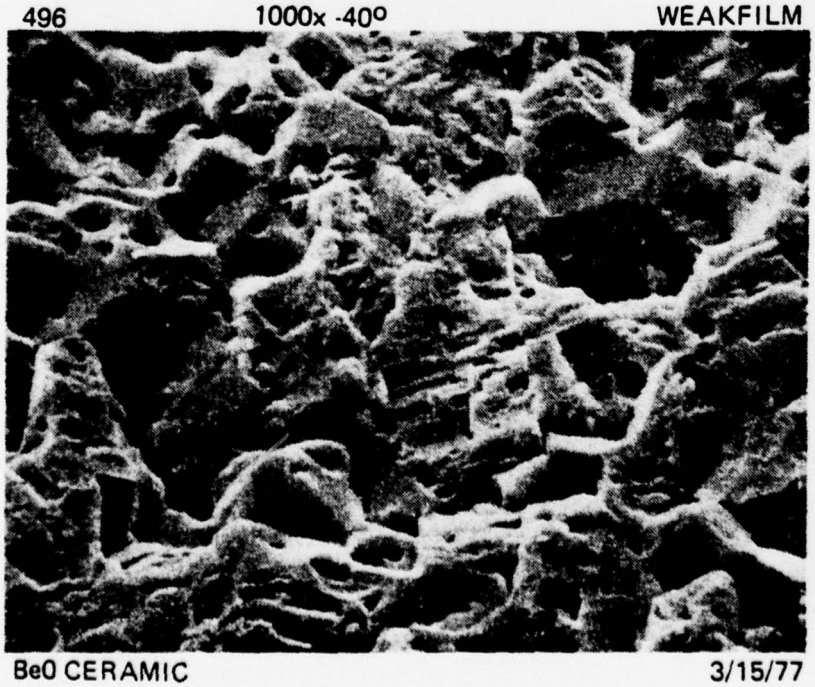

Figure 3-17. Surface of BeO Ceramic

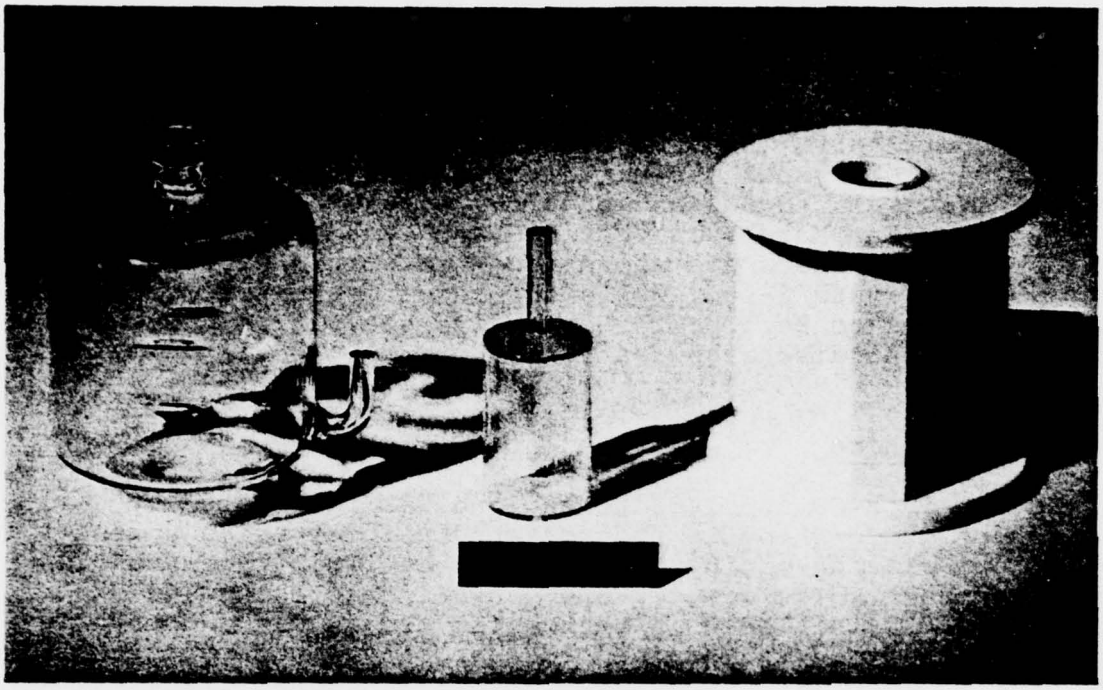

Figure 3-18. Dissociators Made from Pyrex 7740, Sapphire, and Glazed BeO

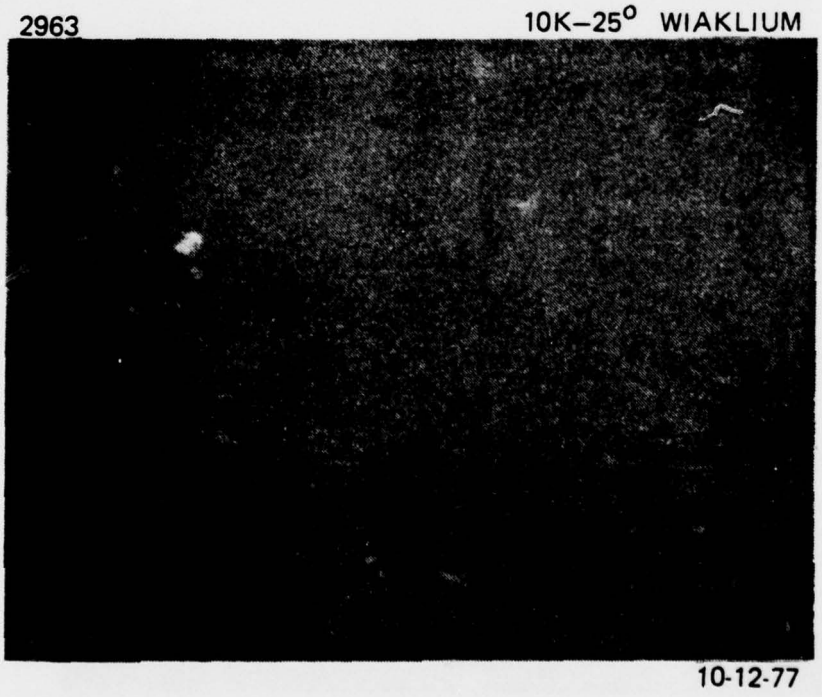

Figure 3-19. Surface of Glazed BeO

The sapphire pieces were all annealed to 1700°C before assembly with the glass seal. This step is necessary to avoid the development of cracks in the cylinder which appear near the joint and which are attributed to twinning stress planes.

A discharge was excited using the same 110 MHz oscillator described in Section 4.2. The discharge color was blue with a slight pink cast. The intensity ratio of H_α to the molecular H_2 singlet transition at 4634A was 20, compared with a ratio of 10^4 -10^5 for a good discharge in Pyrex or fused silica. The spectrum covering the range 3000-7000 A reveals the Balmer series up to n = 9 or 10; intense molecular hydrogen lines; a broad continuum with a maximum near 3600 Å, and a series of bands identified as CO. The discharge was run for 48 hours, but no improvement was seen and the assembly cracked during an attempt to check for leaks. We believe the crack was caused by excessive external stress transmitted to the sapphire and was not a failure of the glass seal. These initial results indicate that the recombination coefficient for sapphire is relatively large and thus we think that a sapphire discharge container offers no advantage over glass. This conclusion is, of course, not definitive because of the brevity of the test and because of the presence of CO impurity, whose source is unknown.

3.1.4.5.2 BeO

The finished BeO discharge assembly is shown in Figure 3-18. The BeO pieces were fabricated by Consolidated Ceramics, Hampton, N.J. The central cylinder is 2 inch ID and is 2.5 inches long. A short BeO tube attached to the side wall by glassing technique serves as the H_2 inlet. The top piece has a sapphire window attached with glass to serve as a viewing port, and the bottom piece contains a 0.050 inch diameter exit hole. The inside surface was first glazed by coating with a suspension of the glass material and firing to 1200°C. A bead of the glass was then formed by application of the glass frit to adjoining surfaces and the final assembly was again fired. The composition of the glass is 50 mole % BeO, 20 mole % Al_2O_3, 50 mole % B_2O_3 chosen because: 1) the thermal expansion coefficient is close to that of BeO; 2) the glass does not crystallize after repeated high temperature treatment; 3) it adheres well to BeO; 4) is free of mobile alkali metal atoms. The glass on the finished piece is approximately 0.0015 inches thick and it is very smooth as shown by SEM photograph in Figure 3-19.

The assembly was attached to the test apparatus and no leaks were found. After pumping for 48 hours with the 8 ℓ/sec Vac-Ion pump, hydrogen gas was admitted and a discharge was excited using the same oscillator used for the sapphire container described above. The initial discharge was pink and spectral measurements showed an intensity ratio of Balmer H_α to the 4634 H_2 singlet line of 1000 at p = 0.025 torr. The spectrum shows a Balmer series

extending to n = 13, molecular hydrogen lines, OH bands, and some weak CO bands.

We found that the discharge was improved considerably (2-3 times increase in the ratio of atomic to molecular hydrogen) after allowing the discharge to run with the flow of hydrogen stopped. The discharge gradually became pale blue-violet and contained OH, CO, and an unidentified continuum and was maintained down to pressure of 5×10^{-7} torr. After re-establishing a hydrogen discharge, $I_{H_\alpha}/I_{4634} = 5000$; however, although the intensity of the OH and CO bands had decreased, they were still present. The intensity of H_α has a strong dependence on pressure, having a maximum near $p = 0.020$ torr. The intensity of the discharge is rather sensitive to the position of the external electrodes and to the oscillator settings indicating that the coupling of the RF energy to the discharge is poor and uncontrolled.

The discharge has been running almost continuously since November 22, 1977 and has become noticeably weaker since mid-January 1978. All attempts to increase the intensity of the hydrogen Balmer lines has been unsuccessful and the spectrum recorded on February 1, 1978 shows only weak Balmer lines, and molecular hydrogen, weak OH lines and a very strong continuum having a maximum intensity near 3200 Å. No other specific impurity lines have been identified.

The reasons for the degraded discharge performance are not known, however we think that the glass surface may have cracked or peeled, thus exposing the underlying BeO surface which has a large effective area (Figure 3-17), and which may be a source of impurities. The recombination coefficient of the glass composition used apparently is larger than that of SiO_2, because the discharges initially obtained was not as rich in H as in Pyrex. The glazed BeO wall does operate at a lower temperature than a discharge in glass, as expected.

We believe that a BeO container, glazed with SiO_2 would be an excellent choice for a discharge container. It would combine the desirable properties of low value of γ for SiO_2 with the high thermal conductivity of BeO enabling efficient cooling by attachment to a heat sink. The difference between the thermal expansion coefficients of SiO_2 and BeO may result in poor adherence; however, a glass composition close to Pyrex would be an acceptable substitute. Further experiments are needed to determine the optimum values for glass composition, and thickness of glass and BeO.

3.1.5 Collimator

The collimator attached to the hydrogen dissociator determines the size and spatial distribution of the hydrogen atom beam emerging from the dissociator. A single hole having 0.005 inch

diameter in a 0.040 inch thick Pyrex disc was used. The total flow rate through such a long narrow channel is given by

$$Q = \frac{2}{3} \left(\frac{r}{\ell}\right) n\bar{v}A,$$

where r is the radius and ℓ is the length of the channel, n is the density of molecules per unit volume in the source, $\bar{v}$ is the mean velocity, and A is the area of the channel opening. The beam is strongly focused in the forward direction. Taking p = 0.1 torr, $\bar{v} = 5\times10^5$ cm/sec, and assuming 1% dissociation, we estimate a total flow of 4×10^{14} atoms/sec from the collimator.

It is difficult to produce uniform holes as small as 0.005 inch in Pyrex. We have developed a technique to produce small diameter holes by pulling and fusing a stack of glass tubes around a Mo wire having the required diameter. The resulting rod is cut into discs and after the Mo is dissolved out by an acid etch, the discs may be polished. A patent application has been filed on this process.

3.1.6 Optical Monitor

The presence of atomic hydrogen in the RF discharge is monitored by a small optical detector designed to detect the Balmer H_α line at 6562 A. The detector shown in Figure 3-20 is contained in an aluminum housing mounted on the plate holding the oscillator. The overall dimensions are 1 inch diameter by 1.75 inches long. The sensor has an unobstructed view of discharge in the center of the bulb with an aperture f/4. The aperture was machined from Vespel, a thermally stable plastic material manufactured by duPont, Inc.

The sensor is a photodiode/amplifier combination in a TO-5 package designated VDT-450 and manufactured by United Detector Technology. The circuit diagram is shown in Figure 3-21. The output voltage is given by $E_o = i_s R_f$, where i_s is the signal current from the photodiode, and R_f is the feedback resistor. A narrow band pass filter centered near 6565 Å, with a bandwidth of 100 Å at the 50% transmission point was used. The detector operates at an elevated temperature because the housing wall is near 60°C for an operating unit. A red shift of 0.17 Å/°C was measured for the interference filter and it was found that the optical monitor output at 6563 is unaffected by temperature up to at least 80°C.

3.1.7 State Selector

Maser operation requires a greater population in the excited (F = 1, m_F = 0) state than the lower energy (F = 0, m_F = 0) final state of the transition. The hydrogen atoms emerging from the dissociator collimater have normal Boltzman distribution of atoms among

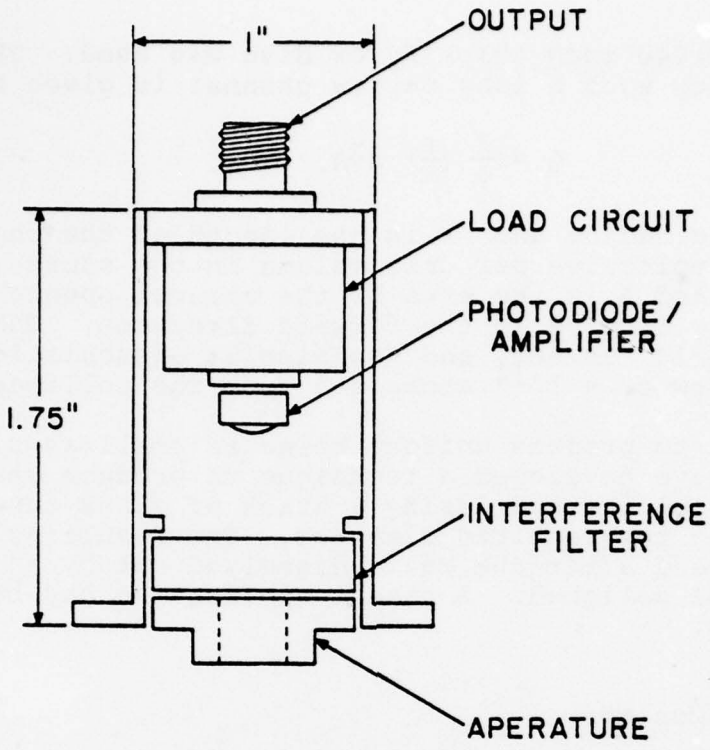

Figure 3-20. Optical Detector

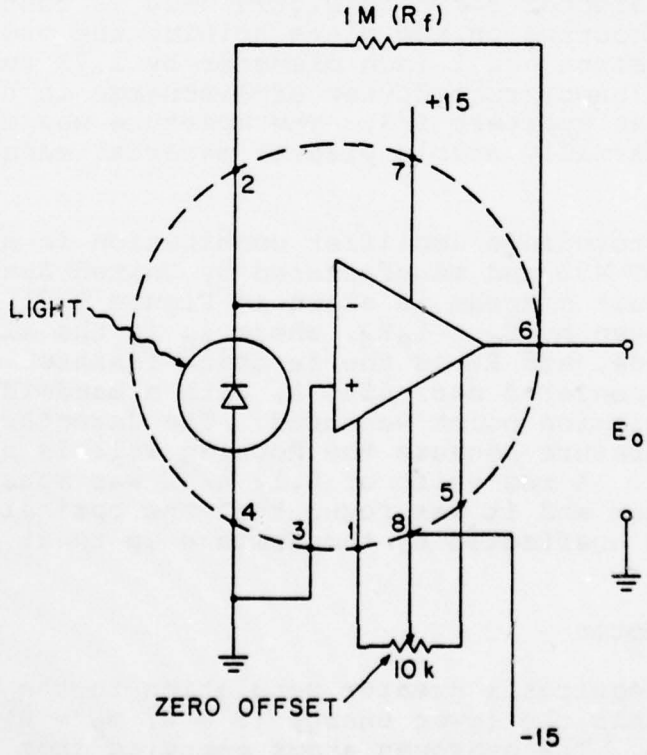

Figure 3-21. Circuit of VDT 450 Detector

the states $n(F,m_F) = \eta_o \exp - [E(F, m_F)/kT]$. A magnet having an inhomogeneous field is used to spatially separate the beam, allowing the excited states to enter the cavity while deflecting the undesired lower energy states away from the cavity entrance.

State selectors using both a hexapole and a quadrupole design have been employed previously in ground based masers. Numerous experiments by H. Peters at NASA/GFSC using both designs and having different lengths, bore diameters, field strengths, with and without central stops, have shown that the quadrupole possesses several advantages over the hexapole design. No stop is required, the distance between the end of the state selector and the cavity entrance is less, the pumping speed is higher because of the more open structure, and the fabrication is easier - four vs. six pole pieces.

The transverse field of a hexapole magnet has a quadratic radial dependence, and a monoenergetic beam having axial velocity v_z is focused a distance $\pi(m/D)^{1/2} v_z$ from the source, where $H = D/2\mu (x^2+y^2)$ and μ is the magnetic dipole moment of the spin 1/2 hydrogen atom. Since the force vanishes on the axis, r=0, there is no deflection for on axis atoms having zero transverse velocity and a stop must be used to exclude these unselected atoms from entering the cavity.

The quadrupole magnet has a linear transverse field dependence, $\vec{H} = \frac{A}{\mu}(\vec{x}i-\vec{y}j)$ and the force is a constant $\vec{F} = \mp A \vec{r}/|r|$, where the upper sign is for the $m_s=1/2$ state and the lower sign is for the $m_s=-1/2$ state. The force is independent of distance and is directed away from the axis for the lower $m_s=-1/2$ spin state.

The beam is not focused, but the lower energy state atoms are always deflected away from the axis and no stop is required. The radial equation of motion is $m\frac{d^2r}{dt^2} = \pm 1/2$ spin states. The general solution is

$$r = r_o + v_{o,r} t \pm \frac{A}{2m} t^2$$

where r_o is the initial position and $v_{o,r}$ the initial transverse velocity. The beam separation is given by $A/m\ t^2$; and if the axial velocity is v_z, at a distance ℓ from the origin the separation Δr is given by $\frac{A}{m}(\frac{\ell}{v_z})^2$.

A small quadrupole state selector was designated using soft iron for the outer cylinder and the pole tips and is shown in Figure 3-22. The permanent magnets are rare-earth cobalt rods having square cross section. The energy BH product is 1.2×10^7 and by scaling the results of H. Peters' earlier work, we expect a field strength of 10 kgauss at the positions of maximum field. The state selector is 1.5 inches outside diameter, 1.25 inches long and has a distance of 0.020 inches between opposite pole tips.

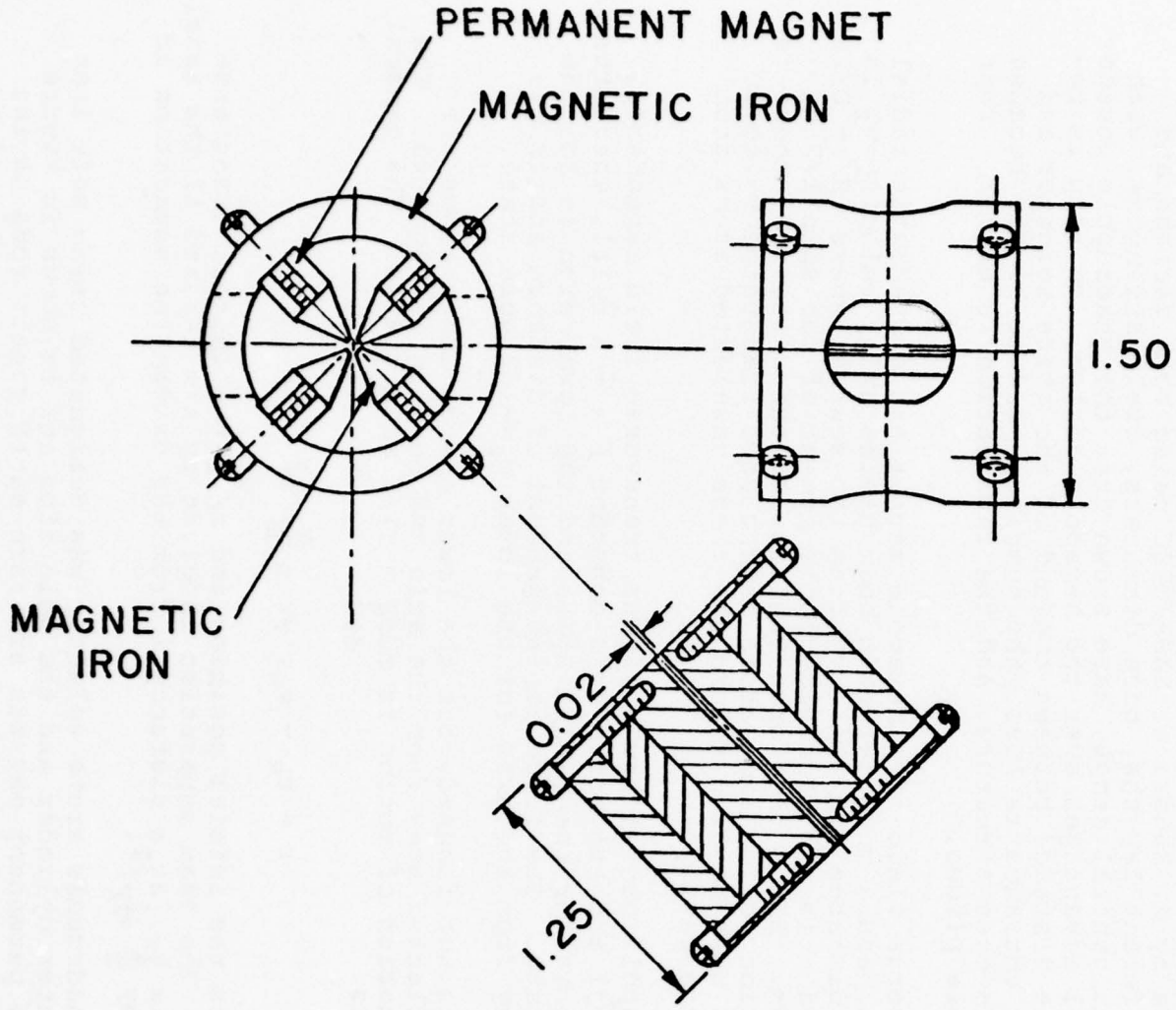

Figure 3-22. Cross Section of Quadrapole Magnet Design

The unit weights 362 grams and occupies a volume of 36 cm^3. The design permits a distance of 2.85 inches between the end of state selector and the entrance of the teflon entrance stem of the cavity.

The tapered pole pieces were carefully polished and protected by a thin (<0.0005 inch) coating of nickel. The pieces were assembled with the aid of a microscope in order to achieve the quadrupole symmetry and to make the gap distances equal. The assembled unit is shown in Figure 3 23 and an enlarged view of the pole tips is shown in Figure 3-24. Note the large slotted holes in the sides of the housing, shown in Figure 3-23, which aids in pumping unwanted H_2 away from the central axis.

The magnet is held in a mounting flange having slotted holes which allows slight transverse adjustment in order to align the collimator hole with the central axis of the state selector. The distance between the face of the collimator and the state selector is 0.002 ± 0.005 inches.

If the hydrogen beam is modulated between a high and a low flux rate, the resulting change in the cavity resonance frequency may be used by an autotuner to adjust the maser oscillation frequency to lie at the center of the atomic resonance line. A shutter has been designed for this purpose and it is actuated by a coil and armature from a G.E. 3SBC1394A2 (13.5-20 volt) relay mounted on the side of the state selector housing as shown in Figure 3-25.

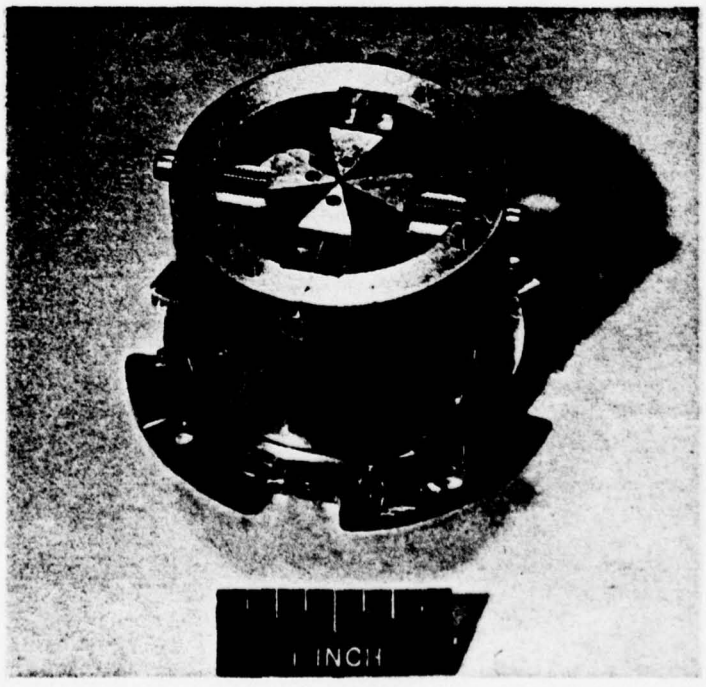

Figure 3-23. Assembled Quadrapole State Selector

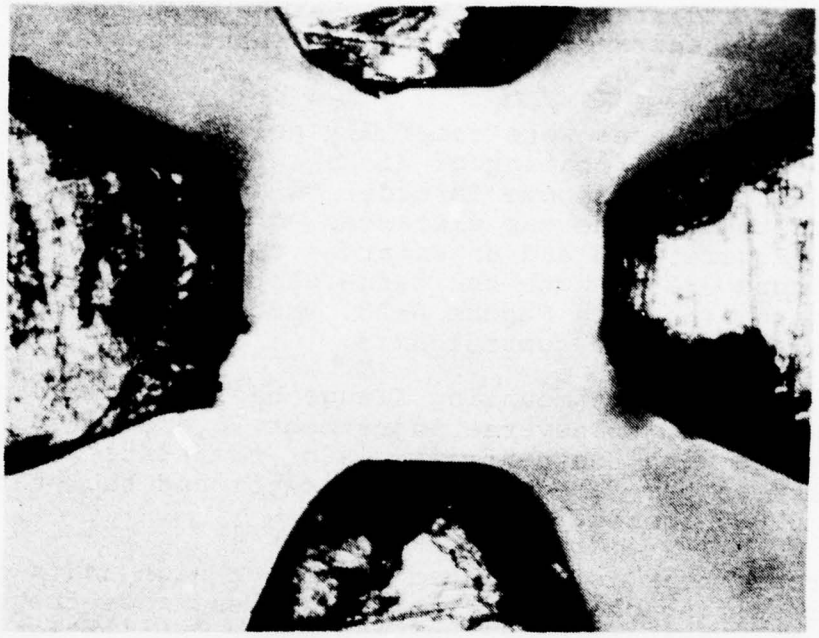

Figure 3-24. Expanded View of Pole Tips

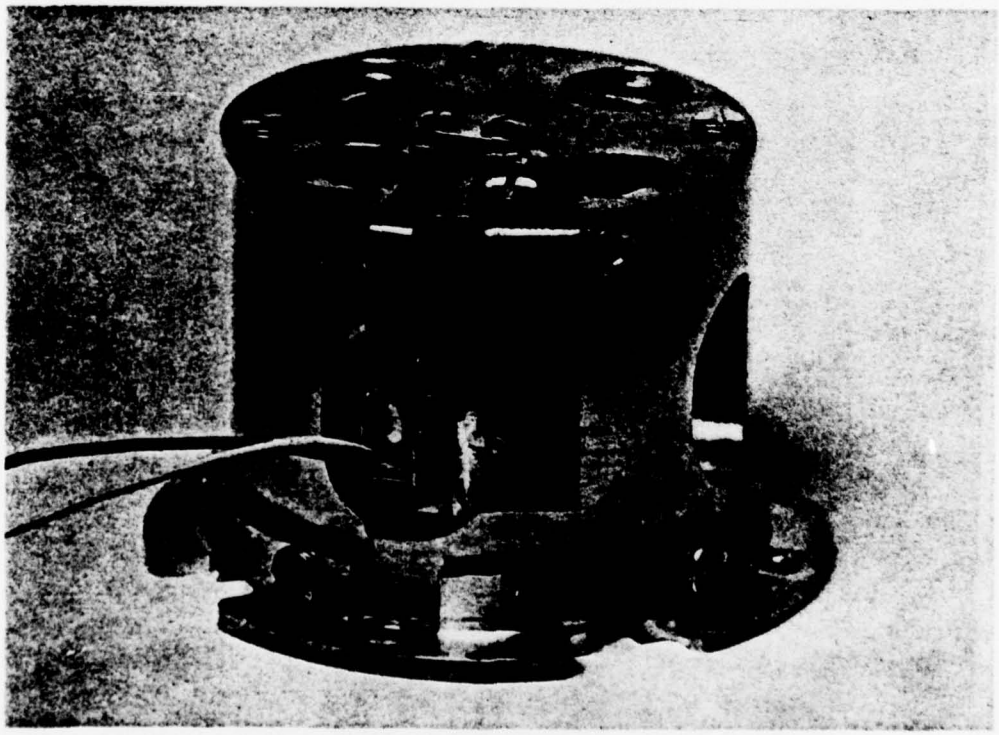

Figure 3-25. Shutter Assembly

A phosphor bronze leaf spring was cemented to the armature and bent to slide over the 0.020 inch diameter orifice in the cover plate. When the coil is energized, the leaf spring covers half of the exit orifice and this condition provides the low flux condition. The shutter has not been extensively evaluated and was not installed on the maser.

3.2 UPPER SUBASSEMBLY

The upper subassembly consists of the C-field coil, 3-nested magnetic shields, neck coil, atomic hydrogen storage cell, microwave cavity, 2-secondary temperature isolation ovens, degaussing circuit, RF output, and vacuum enclosure. The upper assembly is divided into two separate vacuum chambers. The vacuum enclosure encompasses all of the above components.

3.2.1 Magnetic Field: C-Field

The ground state energy levels of atomic hydrogen are such that the two lowest energy states characterized by the quantum lavels F-1 and F-0 are not degenerated even at zero magnetic field. The ground state energy levels have a zero field splitting. It is possible therefore to theoretically operate a hydrogen maser in zero magnetic field. This raises the practical problem of achieving essentially zero field which is exceedingly more difficuly than operating at some finite magnetic field. Therefore, masers operate with applied magnetic fields which are somewhat larger than the background noise level. Practical operating masers have an applied field of 0.5 to 1.0 milligauss. The applied field is generated by passing current through a solenoid whose axis coincides with that of a TE_{011} cylindrical cavity. The stability requirements of the current source is a function of the applied field strength. For example for a stability of 1 part in 10^{15} at a field of 10^{-3}G, the required current stability is 0.025% while at an operating field of 10^{-4}G the required stability is only 2.5%. Thus the stability of the current supply for the solenoidis not a problem. Furthermore, the lower the applied field, the smaller is the effect of the field (current) fluctuations on the clock frequency. This is seen from the relationship between the maser frequency f, and the magnetic field H, given by

$$f = f_o + 2.7 \times 10^3 H^2$$

where f_o = zero field hyperfine splitting frequency in Hz and H is the applied magnetic field in Gauss.

The design of the C-field coil for this clock consists of an aluminum cylinder 0.0508 cm (0.20") thick with 28 gauge wire (diameter = 0.032 cm) wound on the cylinder. The field coil was constructed by forming a cylinder from aluminum sheet and spot welding a one-inch wide aluminum strip on the inside of the cylinder to hold the cylinder round. In addition, a metal ring

made of aluminum was spot-welded to the upper end of the cylinder. This metal ring positions the field coil to the top of the microwave cavity. A sheet of plastic (Kapton) with a thickness of 0.00254 cm (0.001") is made to cover the outside of the cylinder. The plastic was epoxyed to the aluminum at a few places. The plastic is a good electrical insulator between the wire and the metal cylinder, and thereby eliminates the possibility of shorts. Four pieces of berryllium copper strip 0.0076 cm (0.003") thick and 0.254 cm (0.10") wide were placed on the plastic and epoxyed in place (Figures 3-26 and 3-27). A strip of plastic (Kapton) is now placed over the metal strips and epoxyed in place. Holes are cut in the plastic to allow electrical contact with the wire at the desired locations. The wire before being wrapped onto the plastic covered cylinder goes through a container of epoxy and the wire emerges from the container with a thin coating of epoxy. The epoxy coated wire is wrapped onto the cylinder at the desired spacing. The wire spacing was chosen to be 0.317 cm (0.125") and 140 turns were required to cover the length of the cylinder. Two taps, one near each end of the cylinder, were incorporated in the design. The relationship between the current and magnetic field was measured to be H = 3.0I where H is the magnetic field and I is current in amps.

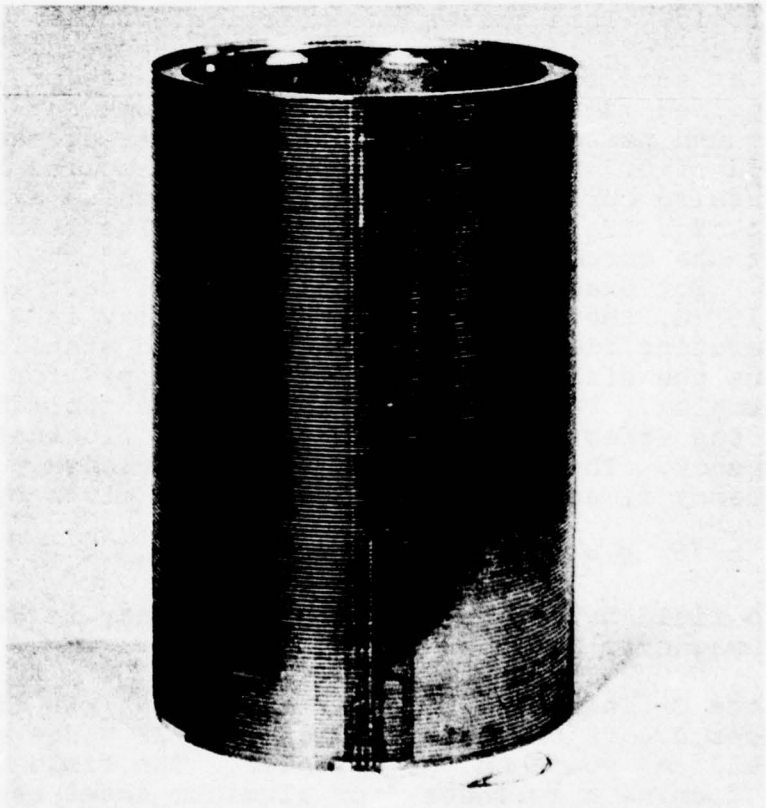

Figure 3-26. C-Field Coil

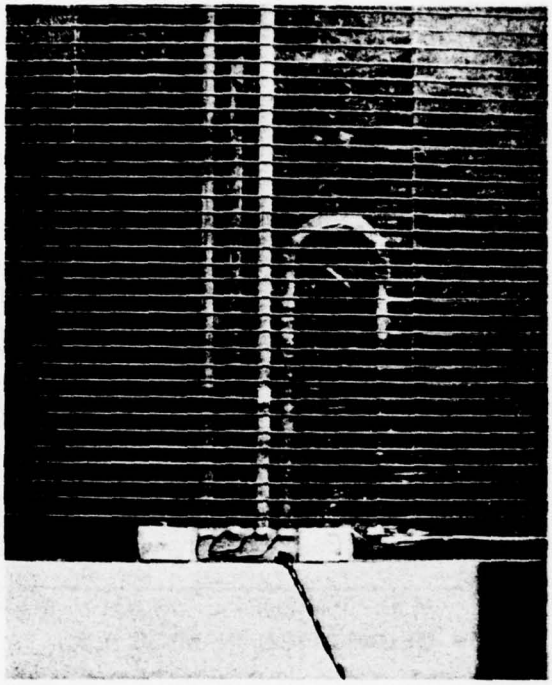

Figure 3-27. View of Electrical Coupling to C-Field Coil

3.2.2 Magnetic Shielding

A problem in clock stability arises due to the fluctuations of the ambient magnetic field if not properly shielded. The earth's field is typically 0.5 gauss and urban magnetic noise in the frequency range of 0.1 to 100 Hz is typically 10^{-2} gauss. There are stray magnetic fields from components such as Vac-Ion pumps, and some external electrical equipments are also sources of magnetic field fluctuation. On ground based clocks, magnetic shielding has been accomplished by using static ferromagnetic shielding. Three, four, five and six nested shields have been used. Shields of various thicknesses and shape factors have also been employed. The processing of the material is very important and there always remains some remnant magnetization in certain parts of the material. Although the magnetic shielding-problem is difficult for ground-based clocks, it is grossly magnified in clocks for space application because of the weight factor. The weight of the magnetic shields may constitute about 35% of the weight of the space maser.

In the analysis of the magnetic shielding of the advanced development model of the space clock, it was clear that a trade-off between weight and shielding is necessary. Calculations have been made on a number of different configurations of shields. The feasibility Demonstration Model shielding design consists of four shields with each shield having a thickness of 0.063 cm (a standard thickness) and the material is 4-79 moly-permalloy. The transverse shielding factor is 130,000 as shown in Figure 3-28 and the axial

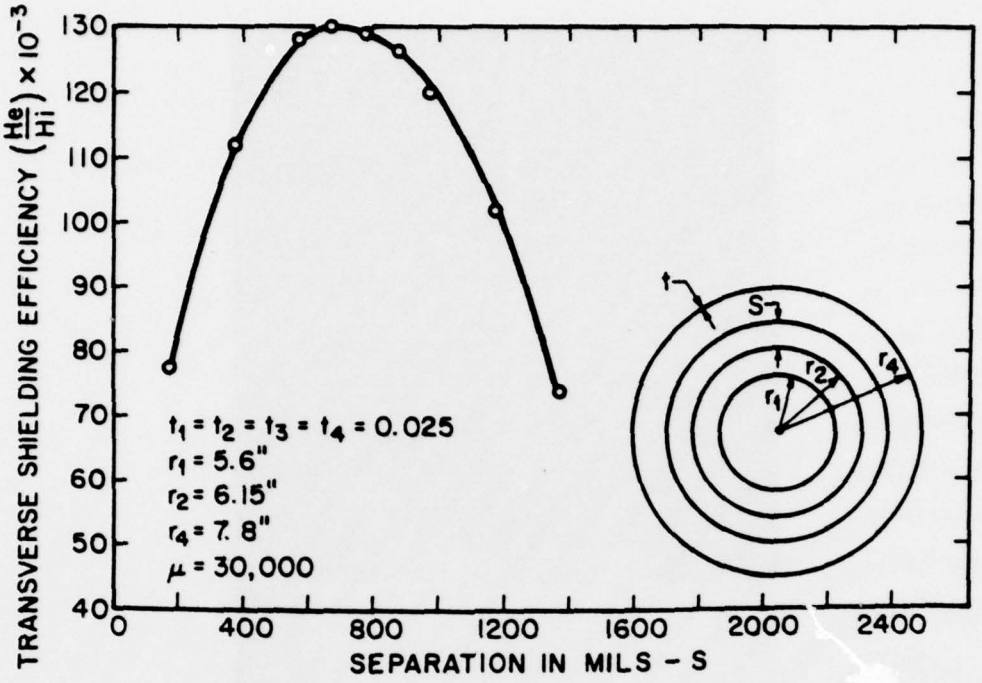

Figure 3-28. Transverse Shielding Efficiency of Four Concentric Cylinders vs Air Gap Between the Second and Third Cylinders

shielding factor is 30,000. The operating maser would then have a calculated sensitivity to external magnetic field fluctuations of

$$\frac{\Delta f}{f_o} = \frac{5500}{f_o} \frac{H_z}{S_A} \Delta H_{ext}$$

where f_o is the maser frequency; H_z is the applied magnetic field, S_A is the axial shielding factor, and ΔH_{ext} is the change in the external field. For H_z = 0.5 milligauss and S_A = 30,000, the sensitivity is 6.5×10^{-14} Gauss^{-1}. Thus static shielding alone without adding appreciably more shields (weight) would be adequate for variations of 0.1 gauss or less. Further improvement of the shielding and/or to reduce weight requires investigation of methods using a combination of static and dynamic shielding.

3.2.3 Neck Coil

In order for the hydrogen atoms to travel from the exit of the state selector to the entrance of the cell inside the microwave cavity, the hydrogen atoms must pass through holes that are drilled in the magnetic shields. Because of the holes in the shields, the hydrogen atoms pass through a region of magnetic field intensity which tend to reduce the number of H-atoms in the desired

magnetic state. It has been found by experiment that a small axial field generated in this region tends to eliminate the deleterious effect of the magnetic field covered by holes in magnetic shields. In this design, a small solenoid was placed between the second and third magnetic shields where the holes were located in the shields. The solenoid was made from plastic and it is in the shape of a bobbin. The length of the coil is 1.016 cm, the diameter is 1.09 cm and 50 turns of insulated copper wire with a diameter of 0.032 cm was placed on the bobbin. From measurements the relationship between current and field was found to be H = 45 I. Typically the magnetic field needed is in the range of 0.01 to 0.1 gauss.

3.2.4 Atomic Hydrogen Storage Cell

The basic reason for the inherent higher frequency stability of the hydrogen clock over the cesium beam clock is that the line Q (frequency divided by resonance width) for the hydrogen clock is typically 100 times higher than that of the cesium clock. A typical resonance width of 250 Hz is obtained for the cesium beam while a one Hz width is usual for the hydrogen atoms. The high line Q or the narrow resonance line for hydrogen is due to the long interaction time of the hydrogen atoms with the microwave field. In this model of the clock, the storage cell has a volume of 6.6 liters. The atom enters the bulb with a velocity of 2.6×10^5 cm per second, bounces around approximately 20,000 times and after about a second departs. The average distance traveled between wall collisions is 12 cm and the hydrogen atom travels about a mile even though it is contained within the volume of a single mode microwave cavity. In order to achieve a narrow resonance width or long lifetime for the hydrogen atoms, any perturbations of the atoms must be kept to a minimum. There are a number of effects which can be considered and the most inportant is that of the effect of wall collisions. The wall collisions can be divided into two categories: adiabatic and nonadiabetic. In an adiabatic collision the hydrogen atoms interact elastically with the walls and a small change in the energy levels (or frequency) always occurs. In the nonadiabatic, the atom is effectively lost either by a change of state or by chemical reaction with the surface of the wall. Thus the surface of the storage cell is of primary importance to the stability, accuracy and reproducibility of the atomic hydrogen clock.

In just about all of the present operational clocks, the storage cells are fabricated by making a cylindrical or a spherical container from fused quartz and then coating the inside surface with an appropriate coating. Measurements of the quality of the wall coatings are very difficult to make but it has been established by experiment that teflon-like materials provide the best coatings. In this design, the storage cell was fabricated from pure teflon film with a thickness of 0.0025 cm. The film bulb storage cell has a number of significant advantages over the teflon coated

quartz cell. 1) The teflon film is homogeneous and does not contain holes in the coating as one usually obtains when coating a quartz cell. The hydrogen atoms interacting with the quartz surface significantly reduces the lifetime. 2) From measurements made at NASA-GSFC, the hydrogen atoms are affected less by the film surface than by the coating deposited on the quartz. This means a smaller frequency shift or correction due to the reaction with the walls. 3) The cells made from the film should be very reproducible. 4) The film cell has a much smaller perturbation on the cavity frequency than the coated-quartz cell. The shift of the cavity frequency by a 0.0025 cm thick film has been measured to be 270 kHz compared to 60 MHz for a typical quartz cell. We have made film bulbs with a wall thickness of 0.0012 cm and it appreas that a film bulb is possible with a wall thickness of only 0.00025 cm (0.0001 inch). This should mean a shift in the cavity frequency of only 27 kHz. This means that the cavity, and therefore the clock frequency, is much less susceptible to changes in the cell caused by mechanical or temperature effects. 5) The Teflon-film cell is naturally less susceptible to breakage than a quartz cell. 6) Since the frequency perturbation on the cavity is much smaller for the film-cell, the cavity need not be fabricated for each cell as is done for quartz cells. 7) The cost of the film cell is much cheaper and can be readily made without special glass blowing techniques. 8) The difficult step of uniformly coating the inside surface of a quartz cell is eliminated by using the film-cell.

3.2.5 Fabrication of Storage Cell

"Teflon" is the registered trademark of the DuPont Company for its fluorocarbon resins. FEP "Teflon" resins are tetrafluoroethylene-hexafluoropropylene copolymers, usually fabricated by melt extrusion or injection molding. FEP type "A" film of 0.0025 and 0.0051 cm thickness was purchased from a DuPont Company distributor. The premium grade type "1" film is not available in thickness less than 0.0127 cm. An open-ended cylinder was made using an overlap heat seal in the arrangement shown in Figure 3-29. In this fixture, the Teflon film is held between two pieces of fused quartz plates. Two nichrome heating strips are placed on the quartz plates and the strips are held in place by two aluminum plates which have one side bonded with synthetic mica 0.05 cm thick. Two weights of 24 lbs. each are used to apply pressure to the unit with a pressure of about one psi on the Teflon. A thermocouple (Chromel-Alumel) is placed midway in the fixture and about 0.6 cm from one of the heating strips. The thermocouple is used to monitor and establish the conditions necessary for a good seal. A simple procedure for obtaining good seals was developed. With the Teflon in place, the variac is turned up until the current meter reads 50 amperes and after about 50 seconds or more accurately when the voltage from the thermocouple read 3.1 mV ($\sim$70°C) the variac is turned down. In a separate experiment, it was established that the temperature at the Teflon joint was 257°C at the time the variac was turned down. If the temperature at the bond was lower,

the seal was poor and easily came apart. If the temperature is too high, bubbles formed and the Teflon stuck to the quartz. The conditions for sealing were similar for films of thickness 0.0012, 0.0025 and 0.0051 cm.

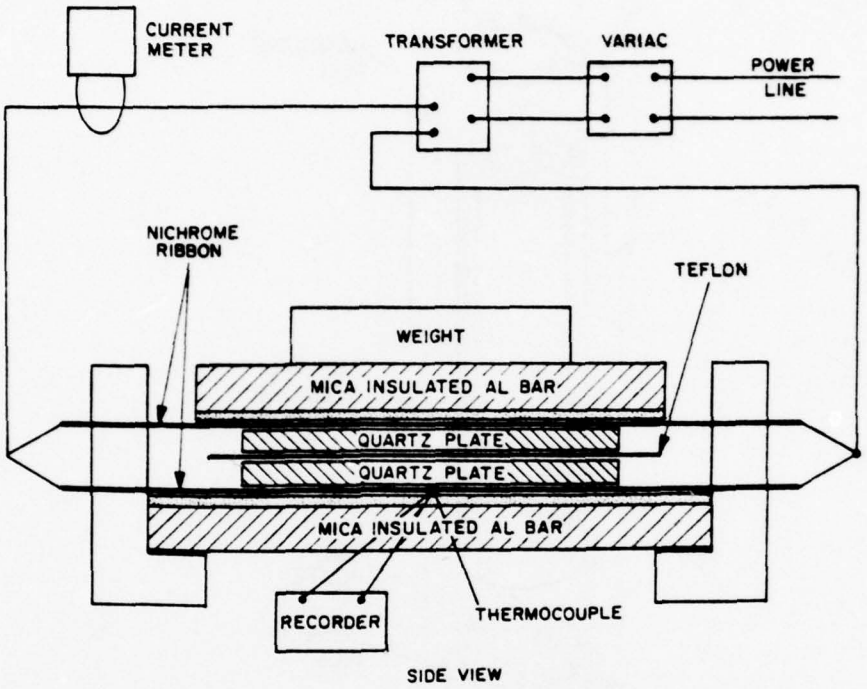

Figure 3-29. Sketch of Heat Sealing Apparatus for Teflon Film

3.2.6 Storage Cell Assembly

A simple aluminum frame (see Figure 3-30) is made consisting of two aluminum rods and two aluminum plates. The inside dimensions of the frame should be large enough to enclose the cell and also to allow working space at both ends. Two aluminum end plates are fabricated which hold the Teflon film and eventually become part of the microwave cavity. A round aluminum rod is attached to each end plate to hold the cell to the frame. These rods are removed when the cell is attached to the cavity. Teflon film of 0.0012 cm thickness is placed over one side of the end plates and the film is brought to the opposite side, stretched and held in place by a metal ring. The open-ended cylinder of Teflon film is now placed over the end plates and both ends of the cylinder are worked carefully until the shape of the cylinder is satisfactory. The Teflon film at the cylinder ends is now clamped to the metal end plates by another metal ring. The first metal ring that was attached to hold the film covering the face of the end plates can now be removed and excess Teflon removed. The length of the cell should be some predetermined distance less than the final length to be used in the cavity. To maintain a rigid cylinder, the film-cylinder should always be in tension.

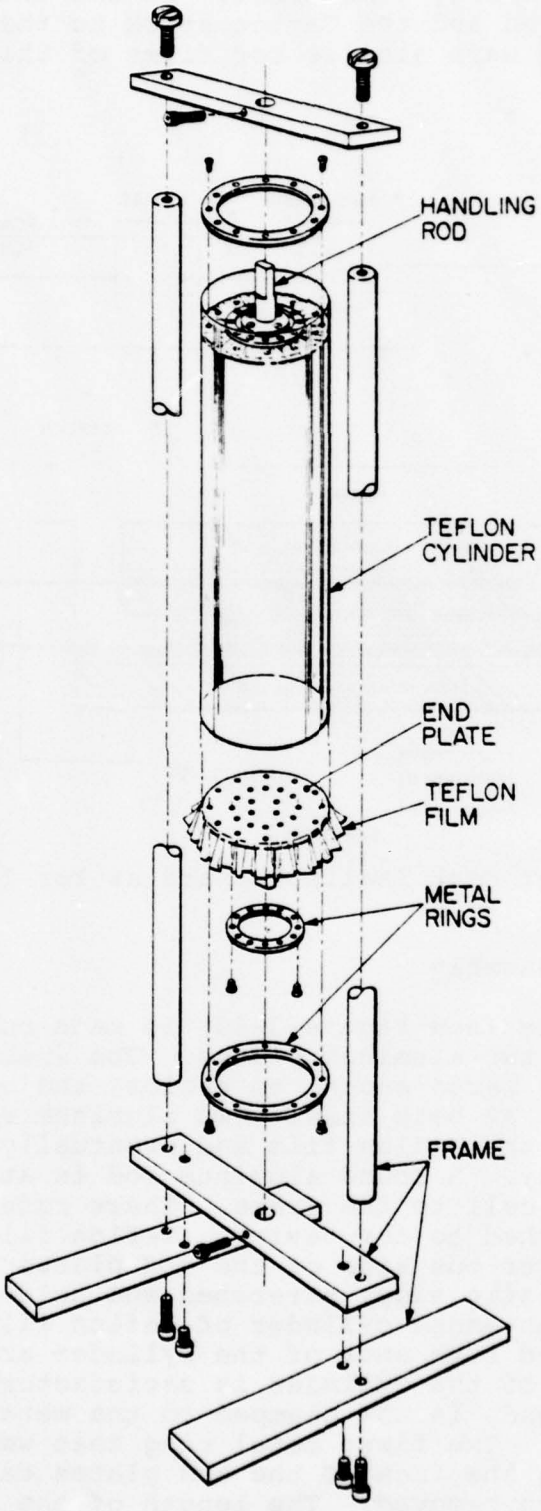

Figure 3-30. Assembly of Teflon-Film Cell

The Teflon cylinder for this clock was made to be 38.7 cm (15.25 inches) in length between the two end plates. The cylinder was vacuum baked at 200°C for 6 hours in an unstretched condition. The cylinder was then stretched to 40 cm (15.75 inches), held in place and vacuum baked at 90°C for 15 hours. The cylinder was placed inside the microwave cavity, stretched to 40.64 cm (16 inches) and clamped to the two end caps of the microwave cavity. The length of the microwave cavity is 40.64 cm (16 inches).

The baking of the cylinder is necessary for annealing of the Teflon film. It was found that if a teflon cylinder was fixed in position and heated the cylinder would develop spiral ridges. If the cylinder was held at only one end and heated, the bottom end of the cylinder would rotate with respect to the top end. This rotation or twisting of the cylinder is caused to stresses in the material which are different in two perpendicular directions. This problem can be eliminated by cutting the material before making the cylinder so that the one stress direction is along the axial direction of the cylinder. In the cylinder used in this clock, the effect of the twisting was circumvented by heating the cylinder in an unstretched state. That is, the cylinder was stretched after the cylinder reached its equilibrium state.

3.2.7 Escape of Hydrogen From Storage Cell

The stem (entrance collimator to storage cell) determines the lifetime of the atoms due to the probability of the atoms escaping from the cell. The escape rate of atoms from the cell γ_o is found by equating the incident beam flux with the emergent flux $NKvA_e/4$ where N is the density, v is the mean velocity, A_e is the area of the stem and K is a factor depending on the geometry of the stem. If the volume of the storage cell is V_b, then the storage time T_b is determined by

$$T_b = \frac{4V_b}{vA_eK}$$

For a cell size V_b of 6.69 liters, $v = 2.6 \times 10^5$ cm per sec, $K = 0.1367$ and the diameter of the exit hole of 0.635 cm, $T_b = 2.4$ seconds. Therefore if all other relaxation mechanisms were not important, the lifetime of the hydrogen atoms in the cell would be limited by the exit aperture and length of the stem (5.08 cm) and the lifetime for this design is 2.4 seconds. In which case, the maximum $Q_\ell = f\pi\tau_\ell = 10^{10}$.

3.2.8 Microwave Cavity

The microwave cavity design is a critical component in the clock because: (1) the cavity must have a sufficiently high Q (low losses) in order to achieve maser operation; (2) the stability of the clock, particularly the long-term stability, is strongly

coupled to the frequency stability of the microwave cavity-storage cell combination; (3) for spacecraft systems where size and weight are important factors, the size and weight of the clock is to a large extent determined by the size of the cavity.

There are two different modes of operation of the clock; namely, active and passive modes. Since the cavity requirements are very different for the two modes, and this design uses the active mode, this discussion on cavities will only be directed to the active mode. In this mode of operation, two different electrical designs of the cavity have been proposed and used. (1) A cylindrical cavity using the TE_{011} mode and (2) a cavity using the TE_{111} mode. The cavities designed for the TE_{011} mode have the higher Q (the unloaded Q for a copper surface is 80,000 for the TE_{011} compared to 33,000 for the TE_{111}). The TE_{111} mode cavity in this application requires that a septum made from a material like Teflon be positioned to divide the cavity into two parts. The septum is necessary because of the RF magnetic field configuration which makes it necessary that the hydrogen atoms in one-half of the cavity do not travel in the other half of the cavity. For an ideal system, the hydrogen atoms should be located in the cavity where the RF magnetic field direction is parallel to the applied DC magnetic field direction. The RF magnetic field configuration for the TE_{011} is more suited to the above requirement than the magnetic field configuration for the TE_{111}. The spin exchange parameter "q" of the clock is typically $q \simeq 0.05$ for masers using the TE_{011} mode cavity while a $q \simeq 0.16$ is expected for masers using the TE_{111} mode cavity. The closer the value of "q" is to zero the better the design. Since maser threshold requires a $q < 0.172$, the masers using the TE_{111} mode cavities are not far from threshold and thus become very susceptible to ageing of material and environment changes. The singular advantage of the TE_{111} mode cavity is its size which is inherently smaller than for the TE_{011} mode cavity. A typical size cavity for the TE_{111} mode is 15 cm in diameter by 15 cm long while for the TE_{011} mode the length is 28 cm and the diameter 28 cm. However, a smaller cavity means a smaller storage cell which means a larger wall shift and a lower line Q and therefore a reduced stability of the clock. For these reasons and particularly because of the many years of experience using the TE_{011} cavity compared with only very recent laboratory operation of a single clock with a TE_{111} mode cavity, the cavity design using the TE_{111} mode was not being seriously considered at this time. In addition, we feel that reducing the cavity size of the TE_{011} mode cavity by various techniques is more promising than the use of the TE_{111} mode cavity.

The long term stability of the clock is strongly correlated with the stability of the cavity-storage cell system. The problem is summarized by noting that the fraction of the atomic resonance linewidth by which the maser is "pulled" by a mistuned cavity is identical to the fraction of the cavity linewidth by which the cavity is mistuned. The shift of the oscillation frequency f

from the true resonance frequency f_o by a cavity tuned to a frequency f_c is

$$\frac{f-f_o}{f_o} = \frac{f_c-f_o}{f_o}\,\frac{Q_c}{Q_\ell}$$

where Q_c is the cavity Q and Q_ℓ if the line Q of the atomic hydrogen. The smaller the ratio $\frac{Q_c}{Q_\ell}$, the less sensitive is the oscillator frequency to changes in the cavity frequency. Typically for a TE_{011} mode cavity $Q_c \approx 50{,}000$ and $Q_\ell \approx 5\times10^9$ or $\frac{Q_c}{Q_\ell} = 1\times10^{-5}$. Also, a shift in the cavity frequency of 1.4 Hz results in $\frac{\Delta f}{f_o} = 1\times10^{-14}$ for $\frac{Q_c}{Q_\ell} = 1\times10^{-5}$.

Two configurations of cavity design have been used and tested in the past. In one design, the cavity is made using a dielectric like Cer-vit which has a very small thermal coefficient of expansion and the inside surface is copper or silver plated. In the other design, the cavity is made from a metal such as aluminum which has a rather large thermal coefficient of expansion. The large coefficient of expansion is utilized for fine tuning of the cavity. Table 3-6 gives the properties of the cavity and the storage cell as they relate to the temperature stability requirements of the cavity structure to achieve a clock stability of at least 1×10^{-14}. Based only on this criterion, one should use a cavity made from a material with a small thermal coefficient of expansion such as Cer-vit combined with a very thin Teflon storage cell. However, the stability of the cavity due to temperature changes is only one of a number of factors to be considered and evaluated. The mechanical design is very important and a difficult to measure parameter like the dimensional stability of the material being used must be evaluated.

There are a number of factors relating to the use of dielectric cavities which can be identified. (1) Copper or silver plating of about 0.0025 cm thick is required on dielectric cavities and thin spots and/or holes in the plating can occur. Thin areas of plating or holes permit electromagnetic coupling between the cavity and the external environment. (2) The low thermal conductivity of suitable dielectrics can result in temperature gradients along the cavity. (3) The low tensile strength of most dielectrics makes the cavity susceptible to breakage during fabrication and processing. (4) The material is expensive as is the cost of fabrication. (5) The fine tuning must be done by adding an additional coupling loop to the cavity.

CAVITY AND STORAGE CELL PROPERTIES

COMPONENT	THERMAL COEFFICIENT OF EXPANSION	TEMPERATURE DEPENDENCE OF SHIFT IN CAVITY FREQUENCY	TEMPERATURE STABILITY, ΔT, REQUIRED FOR FREQUENCY STABILITY(2) OF CLOCK OF 1 PART IN 10^{14}
CER-VIT CAVITY	1.5×10^{-7}/°C	180 Hz/°C	7.9×10^{-3}
ALUMINUM CAVITY	25×10^{-6}/°C	29,900 Hz/°C	4.7×10^{-5}
MOLYBDENUM CAVITY	5×10^{-6}/°C	5,980 Hz/°C	2.4×10^{-4}
GFEC CAVITY	DIA: 1×10^{-6}/°C LONG: 1×10^{-6}/°C	1200 Hz/°C	1.2×10^{-3}
FUSED QUARTZ CELL 1 MM THICK	0.5×10^{-4}/°C(1)	400 Hz/°C	3.5×10^{-3}
TEFLON FILM CELL 0.001 INCH THICK	6.4×10^{-4}/°C(1)	48 Hz/°C	2.9×10^{-2}

(1) Temperature dependence of dielectric constant.
(2) Assumed $Qc/Ql = 1 \times 10^{-5}$.

The factors relating to the use of metal cavities can also be identified. (1) The plating is not critical and a sufficiently high Q can be achieved without plating. (2) A metal such as aluminum or molybdenum has a high thermal conductivity and relieves the problem of temperature gradients. (3) The strength of the metal cavities is very high and breakage due to handling or shock is not a problem. In fact, the metal cavity for a given cavity design lends itself to a lightweight structure. (4) The cost of fabrication is considerably cheaper than a corresponding dielectric cavity. (5) Thermal tuning can be used to fine tune the cavity and control the cavity resonance. (6) The relatively high thermal expansion coefficient for aluminum or molybdenum compared to the dielectric requires a higher temperature stability for the metal cavity structure. It has been demonstrated for an aluminum cavity that the average untuned linear drift rate of the clock, due to the cavity drift, among the NASA-GSFC NP masers is only 5×10^{-15} per day. Thus for applications of a few weeks or less, which is one of the specifications for the GPS system, autotuning isn't required for metal cavities except perhaps to help in the initial frequency setting.

Thus, for data acquisition up to a few weeks, the stability of a cavity design using aluminum has been experimentally verified by the hydrogen clocks built by NASA/GSFC without the use of auto tuning. Taking into account the other parameters important for space applications like shock, vibrations and strength, the all metal cavities have a distinct advantage over dielectric cavities. The only advantage of dielectric cavities is in their very small thermal coefficient of expansion. This advantage however is somewhat offset by the poor thermal conductivity of the dielectric. The replacement of aluminum, which was used in past applications, by molybdenum which is used in this application reduces the requirements on the temperature stability of the cavity by a factor of 5. The thermal coefficient of expansion for molybdenum is a factor of 5 smaller than that for aluminum. In fact molybdenum whose thermal conductivity is only slightly below that of aluminum has a thermal expansion coefficient of $5 \times 10^{-6}/^{\circ}C$ which is only a factor of 5 larger than that of GFEC (Graphite Fiber Epoxy Composite) if the GFEC is manufactured to give equal values for both the longitudinal and diametric directions.

In this model of the clock, the microwave cavity is made using molybdenum for the cylinder and aluminum for the end caps. The cavity was assembled by heat shrinking the aluminum end caps onto the molybdenum cylinder (Figures 3-31 and 3-32) photographs of the disassembled and assembled cavity). The two aluminum end caps have large holes in their centers to permit the assembled Teflon-film storage cell to be placed inside the microwave cavity. The present cavity design is 40.6 cm (16 inches) long by 26.7 cm (10.5 inches) in diameter. The wall thickness of the molybedenum cylinder is only 0.127 cm (.050 inch). With this wall thickness, the circularity of the cylinder was very good which means the wall thickness can be reduced to save weight. The present cavity assembly weighs 15 pounds (6.8 kilograms) while the cavity for the space clock would weigh about 10 pounds because it would be much smaller in length. The cost of the molybdenum cylinders used in this design was $2200 each. This is much less than the cost of approximately $10,000 for a dielectric cylinder. The measured unloaded cavity Q for the cavity structure without plating is 42,000. The measured unloaded cavity Q for a similar all aluminumstructure unplated is 50,000. A technique was developed for copper plating the molybdenum. The copper plated molybdenum cylinder with unplated aluminum end plates had a measured unloaded Q of 60,000. The insertion of the 0.0025 cm thick film bulb has a negligible effect of the cavity Q. The Q of the dielectric film bulb is 800,000. The fine tuning of the cavity frequency is done by thermal expansion and the experimental results for this cavity structure is 8.7 $kHz/^{\circ}C$. Gross tuning of the cavity frequency is done by 8 metal tuning rods which are located on both ends of the aluminum end caps. The 8 metal tuning rods are made from aluminum and are 1.90 cm (.75 inch) in diameter and have a frequency tuning range of 130 kHz/cm.

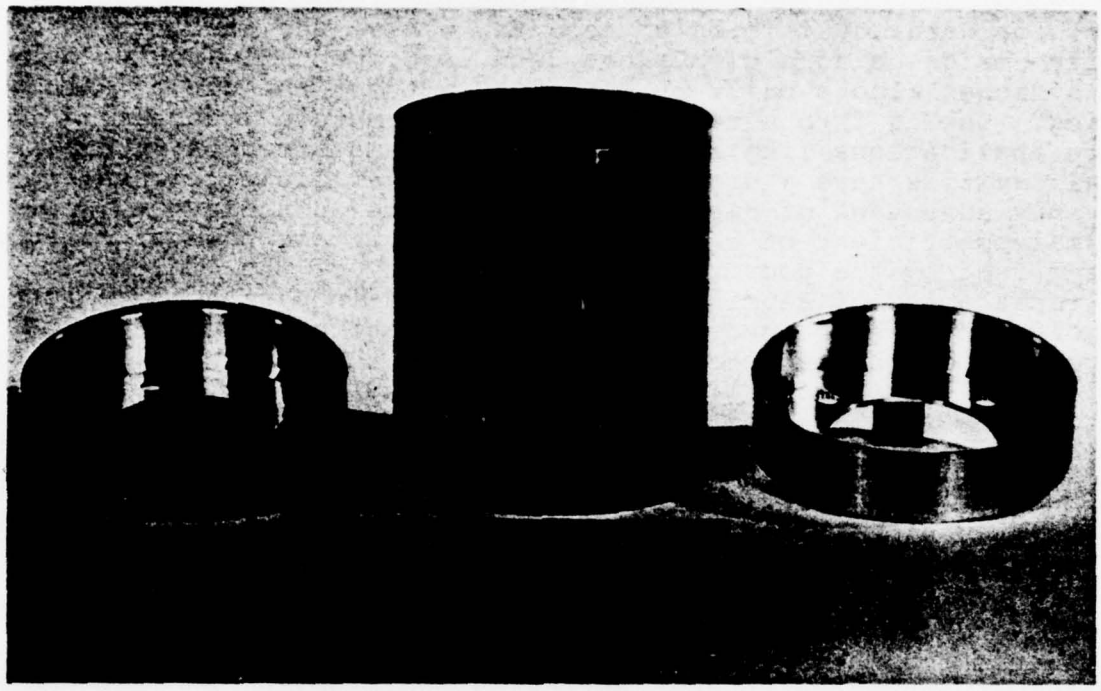

Figure 3-31. Disassembled Microwave Cavity With Molybdenum Cylinder and Aluminum End Plates

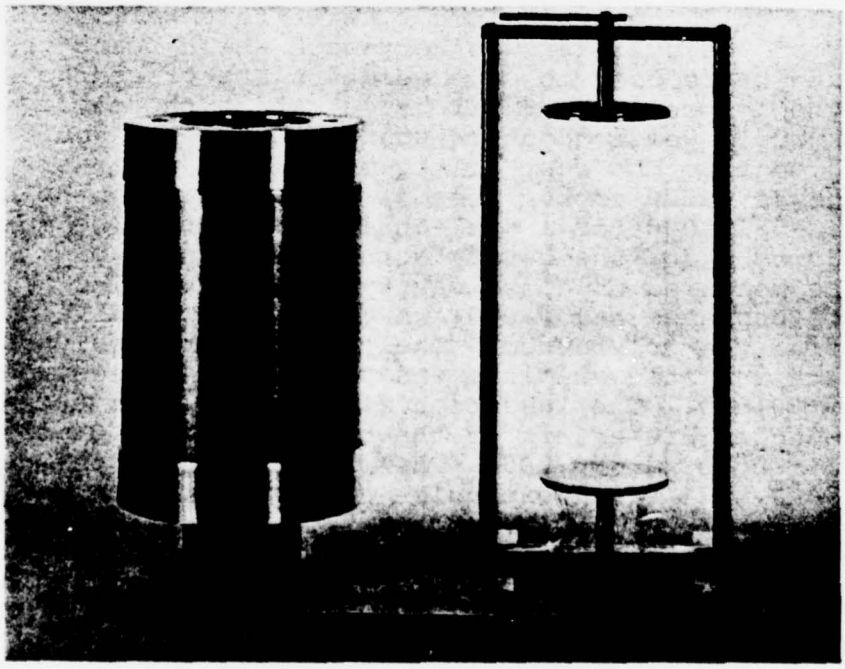

Figure 3-32. Photograph of Assembled Cavity and Teflon-Film Storage Cell.

The large L/D (length to diameter ratio) of 1.6 is desirable for clocks in which the highest performance is the goal. The long cavities can accommodate a large storage cell and the wall contribution to the relaxation time of the hydrogen atoms is reduced by a factor 1.7 for the large cells when compared with that for more conventional shorter cells. The long cavity was used in this model of the clock in order to reduce the effect on clock performance of changes in the microwave cavity so that other critical components necessary for space clocks can more readily be evaluated. In this model of the clock, the cavity with the large L/D ratio results in a clock which is 40.64 cm (16 inches) in diameter and 71.1 cm (28 inches) in length. In the model for the space clock, the cavity would be reduced in length to 20.3 cm (8 inches) and thereby resulting in a clock which is only 50.8 cm (20 inches) long. This reduction in the overall length of the clock can be done by simply reducing the length of the cavity in the present design from 40.6 cm to 20.3 cm. Microwave cavities having a length of 20.3 cm have been used in a number of operating ground based clocks and thus the shorter microwave cavity will not require any new innovations. The smaller size cavity which is responsible for the smaller size clock also means a reduction in weight for the spacecraft clock.

3.2.9 Sensors, Thermocouples, Heaters

The location of the thermal sensors, thermocouples and heaters, along with their identification at the output connector, is shown in Figures 3-33, 3-34, 3-35 and 3-36.

3.3 CLOCK ASSEMBLY

The specific activities conducted and their relative sequence in the assembly of this clock are described. It is assumed that the individual components are complete and ready for installation. That is, the cavity assembly includes the film bulb and the heaters, sensors and thermocouples have been attached. The sequence for assembly of the clock is:

1. A fixture to hold the clock in place during assembly was designed, built and mounted on top of a table. This fixture permits the partially assembled clock to be positioned for ease of assembly.

2. The main baseplate made from aluminum and which separates the clock into an upper and lower subassembly is fixed by screws to the holding fixture (see Figure 3-37).

3. A rather intricate mechanical assembly referred to as the state selector housing and output coupling ports is attached to the bottom face of the main baseplate using screws. (See Figure 3-38 for a picture of the mechanical assembly [center of picture], main baseplate, output coupling plumbing, lower assembly cover cylinder and the holding fixture.) A rubber O'ring

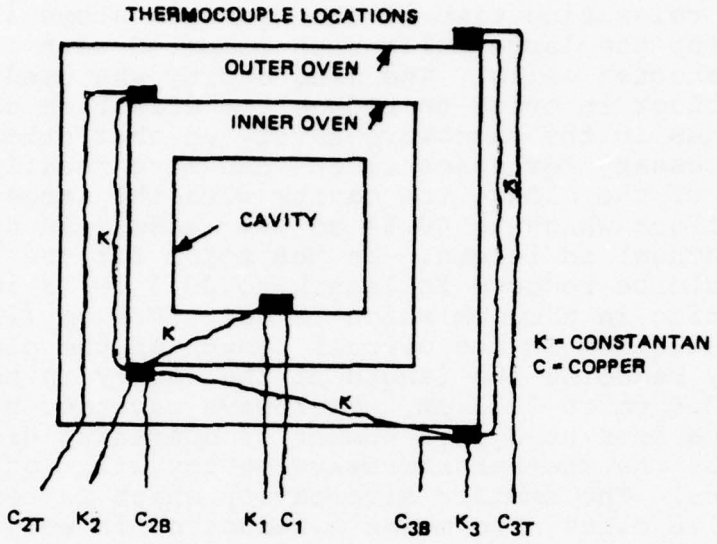

Figure 3-33. Locations of Thermocouple

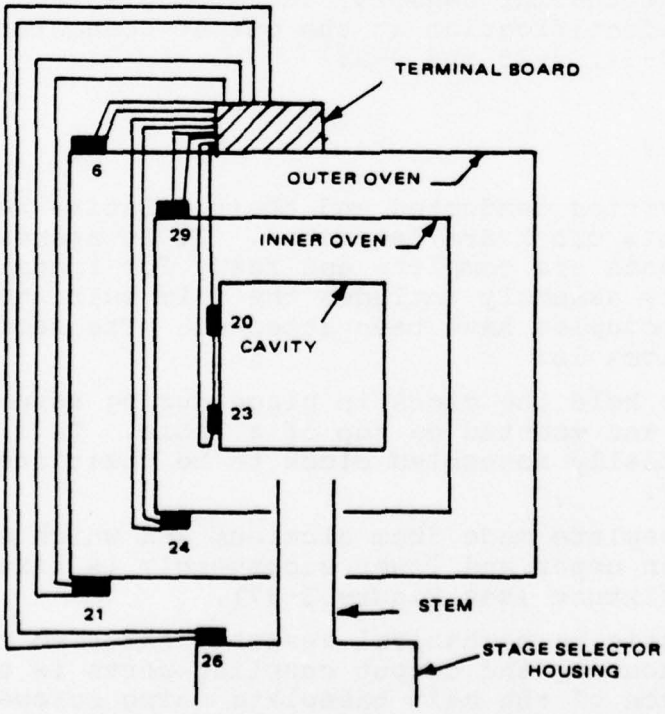

Figure 3-34. Locations and Identification of Thermal Sensor

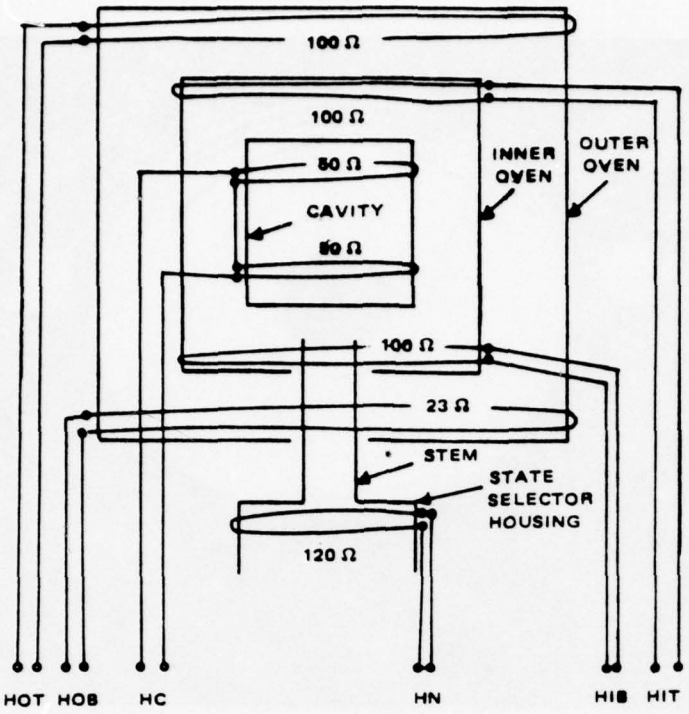

Figure 3-35. Location and Values of Heaters

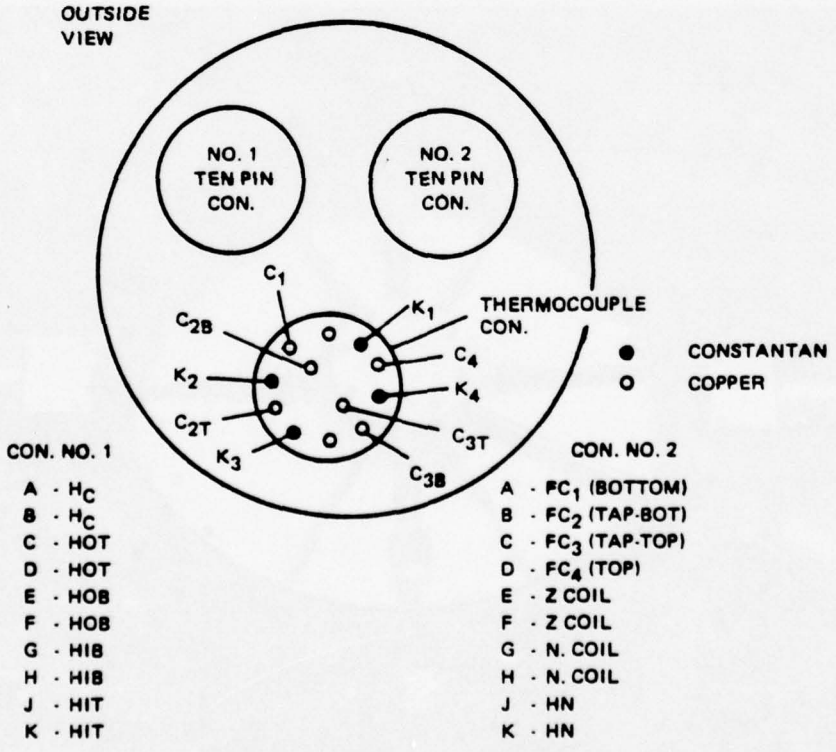

Figure 3-36. Identification of Electrical Wiring at Output Port

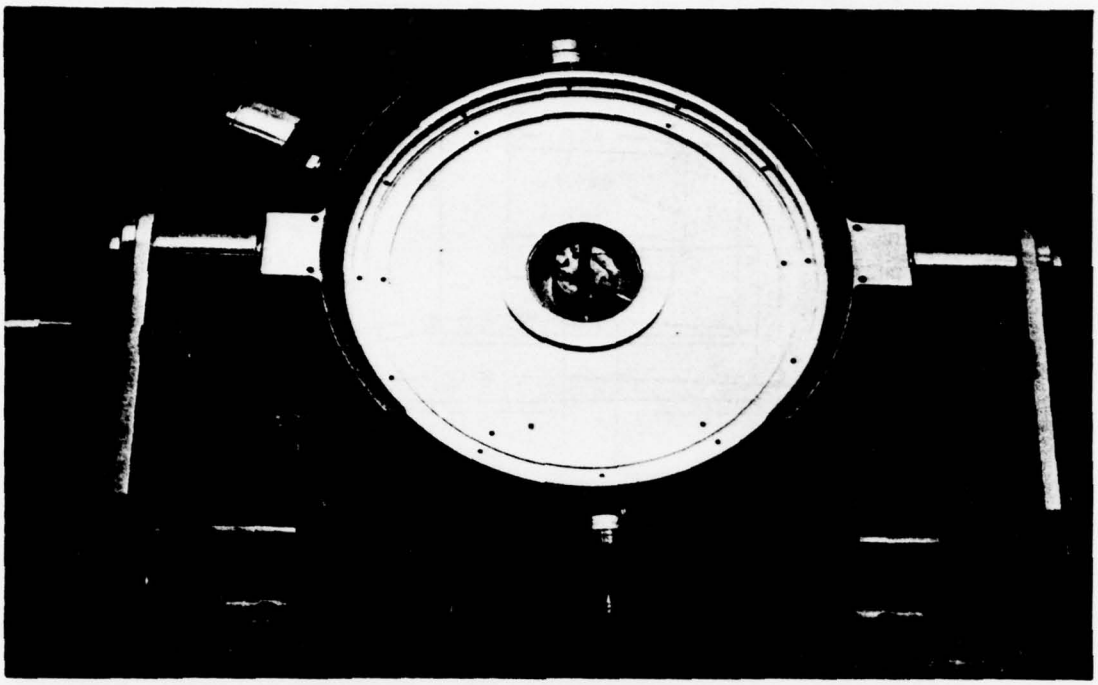

Figure 3-37. Top View of Main Baseplate and View of Holding Fixture

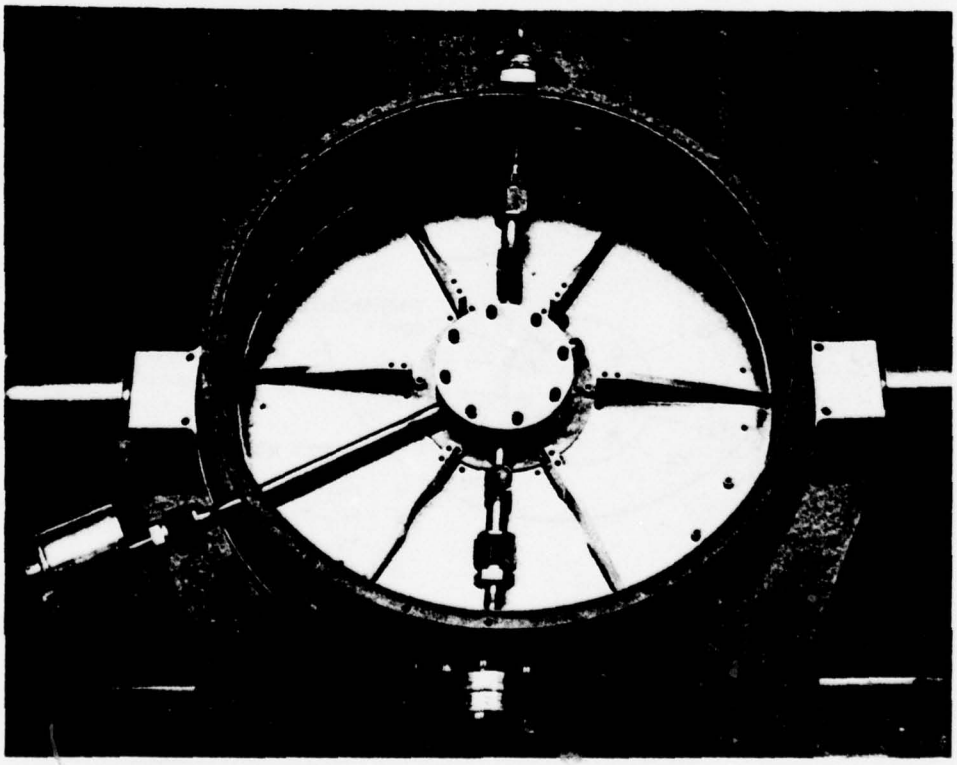

Figure 3-38. Bottom View of Main Baseplate and Mechanical Structure for State Selector, Output Plumbing Ports and Lower Assembly Cover Cylinder

is used where the mechanical structure is screwed to the main baseplate. This is a critical joint and the assembly must be leak-checked at this time. The intricate mechanical assembly includes a partition to divide the vacuum space in the clock into two chambers, two output ports for vacuum pumping the two isolated chambers and one port to extract electrical wiring from the interior of the clock. There are thirty (30) wires in all and the only other electrical wires to be extracted from the unit are those for the thermal sensors. The wires for the thermal sensors exit at the top plate of the vacuum enclosure. In the center of the picture, a solid flange is shown. This flange covers the hole where the state selector is placed. The dissociator assembly attaches to the unit in replacing the solid flange.

In Figure 3-37, which shows the top view of the main baseplate and part of the intricate mechanical assembly (center); a metal tube made from silicon bronze emerges from the mechanical structure. A thermal station which includes heater, sensor and thermocouple is located at the base of the silicon bronze tube.

4. The electrical wiring is placed in position and drawn through the plumging.

5. The lower assembly cover cylinder is attached to the main baseplate using screws (see Figure 3-38). The cylinder has three slots to accommodate the three output ports. In the flight model of the clock, the three output ports would terminate inside the cylinder and the slots would not be necessary. In the model for the spaceflight clock, an O'ring would be necessary at the interface between the main baseplate and the lower assembly cover cylinder.

6. Six plastic spacers made from Vespel are placed on the top face of the main baseplate (Figure 3-37). The lower cover of the third magnetic shield is placed on top of the plastic spacers.

7. The neck coil is threaded onto the silicon bronze tube and electrical connections are made to the coil.

8. Six metal spacers (aluminum) are placed on top of the third magnetic shield cover. The support ring of the lower outer oven sits on the spacers and is held to the main baseplate with plastic screws. The heater, sensor and thermocouple on the support ring was connected to wires and tested.

9. Six plastic spacers were placed on top of the lower oven support ring and the cover of the magnetic shield was positioned on top of the spacer.

10. The support ring of the inner lower oven was offset from the magnetic shield cover and held in place with 6 plastic screws. The heater, sensor and thermocouple on the oven were connected to wires and tested for operation. Figure 3-39 shows a picture of the assembly to this point.

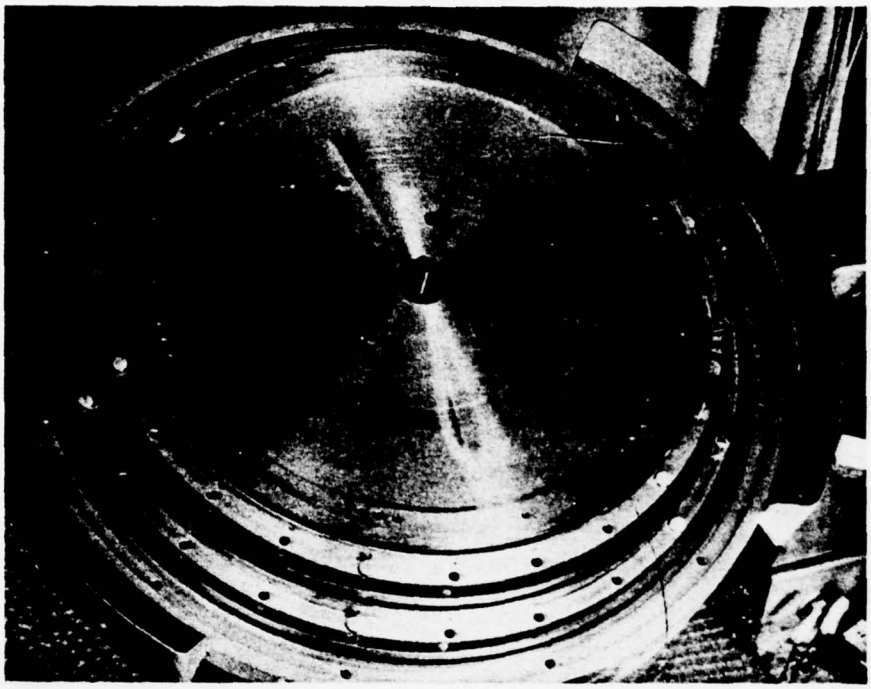

Figure 3-39. View of Partial Assembly; Baseplate; Cover of 3rd Magnetic Shield; Support Ring of Lower Outer Oven; Cover of 2nd Magnetic Shield; Support Ring of Lower Inner Oven (top)

11. The first (inner) magnetic shield cover is placed on the assembly offset from the oven by 6 plastic spacers.

12. The lower section of the degaussing circuit is attached on top of the inner magnetic shield (see Figure 3-40). The degaussing circuit consists of 6 gold-plated copper pieces which are designed to fit tightly against the inner surface of the aluminum cylinder holding the C-field coil; 6 copper wires (0.1143 cm diameter) and a copper structure which connects the 6 copper wires to the silicon bronze tube. The 6 gold-plated copper pieces sit on top of a beryllium oxide ceramic spacer. This spacer is a poor electrical conductor but a good thermal conductor. It is placed here to direct heat flow from the cavity and toward the inner lower oven.

13. A metal plate made from aluminum is attached to the assembly with 6 plastic screws (see Figure 3-41). This metal plate supports and positions the microwave cavity. The four holes around the outside of the plate permit room for the tuning rods protruding from the microwave cavity. In the center of the picture, a 0.0025 cm (.001 inch) thick Teflon sheet is placed between two flanges. This thin Teflon sheet permits the vacuum volume to be separated into two separate chambers. In addition, the thin plastic sheet thermally isolates the cavity from heat flow up the silicon bronze stem.

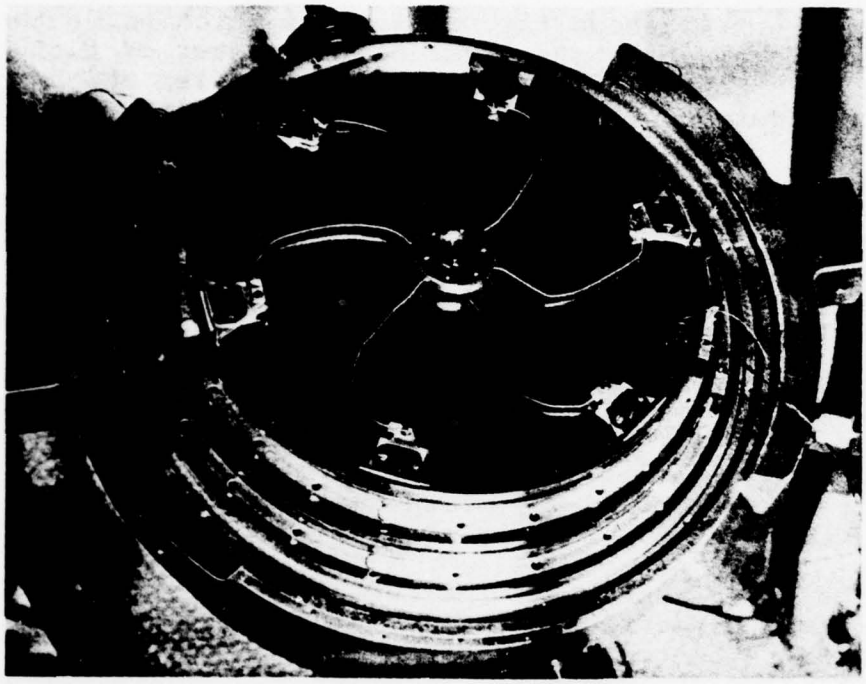

Figure 3-40. Cover of First Magnetic Shield and Lower Section of Degaussing Circuit Added to Assembly

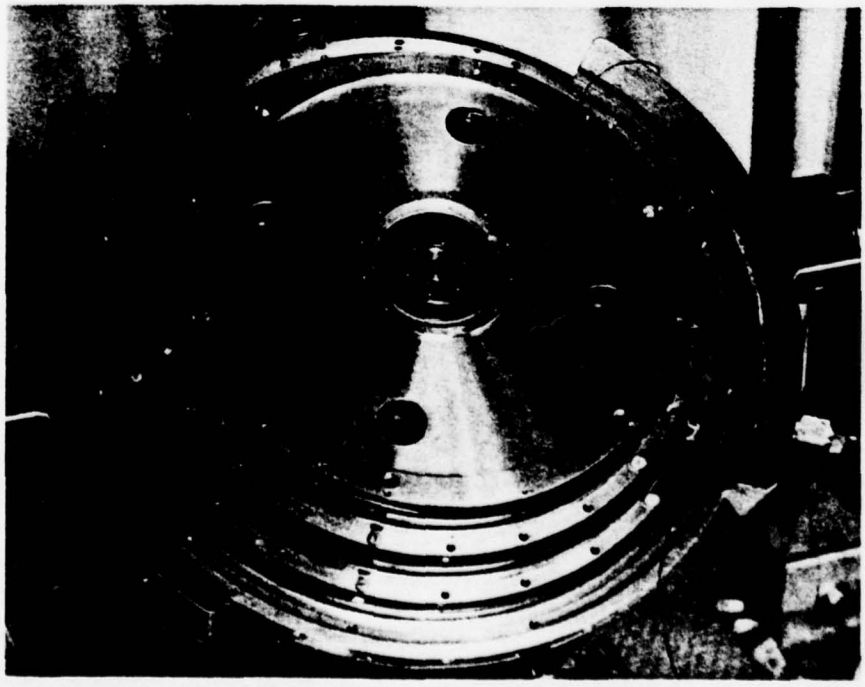

Figure 3-41. Flange for Holding Microwave Cavity and View (center) of Method of Partitioning into Two Vacuum Chambers

14. Figure 3-42 shows the metal plate which holds the Teflon film in place. Also the metal plate (center of picture) has a hole in its center to capture the Teflon stem which protrudes from the storage cell located inside the microwave cavity.

15. The microwave cavity assembly is placed in position and held to the metal flange by 12 metal screws (see Figures 3-43 and 3-44). The cavity assembly includes the film bulb, heaters, sensors, thermocouple, eight tuning rods and the RF output coaxial line. Two polished aluminum cylinders are placed over the cavity as thermal reflectors.

16. The C-field coil is placed over the microwave cavity (see Figure 3-45). The bottom of the C-field coil cylinder sits on the beryllium oxide spacers and fits snugly over the 6 gold-plated copper pieces of the lower section of the degaussing circuit (see Figure 3-40). The top of the C-field coil is positioned and held in place by three plastic spacers and screws.

17. The upper section of the degaussing circuit is placed on the assembly (see Figure 3-46). Figure 3-46 shows the thermal shield over the top of the cavity, the RF coaxial cable, a metal ring which is a part of the C-field coil cylinder, 4 tuning rods protruding from the cavity and a solid silicon bronze rod to complete the degaussing circuit.

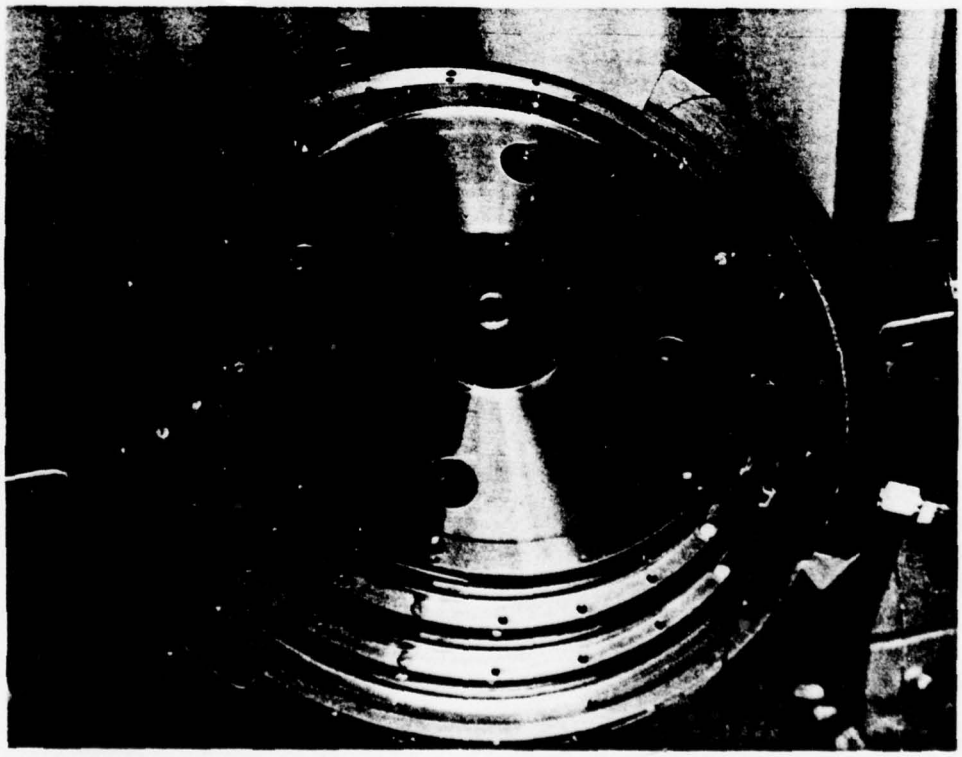

Figure 3-42. View of Assembly Before Addition of Microwave Cavity

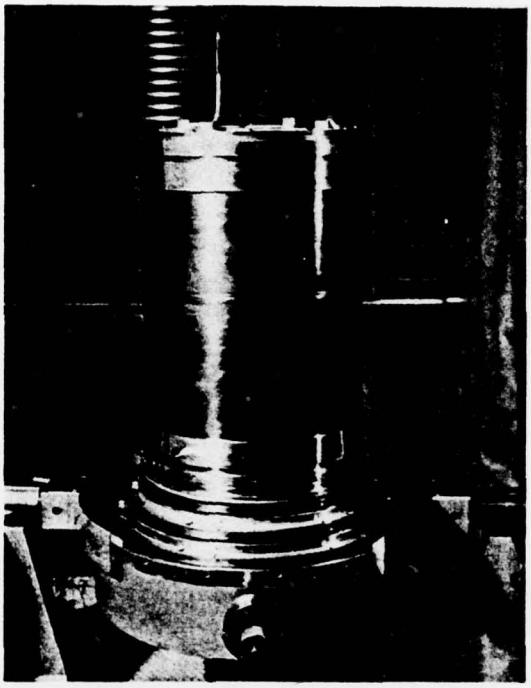

Figure 3-43. Microwave Cavity on Clock Assembly

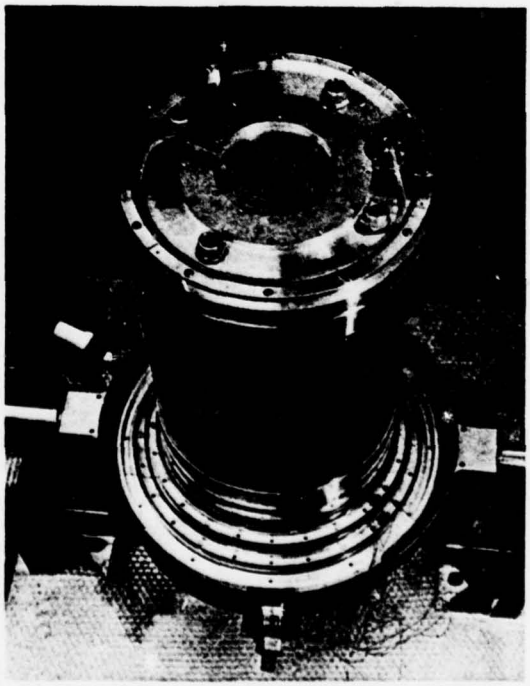

Figure 3-44. Top View of Microwave Cavity and Clock Assembly

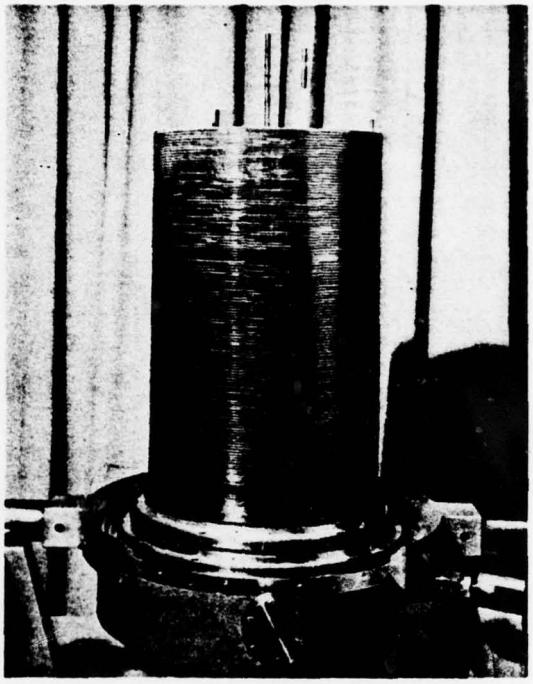

Figure 3-45. C-Field Coil Mounted on Clock Assembly

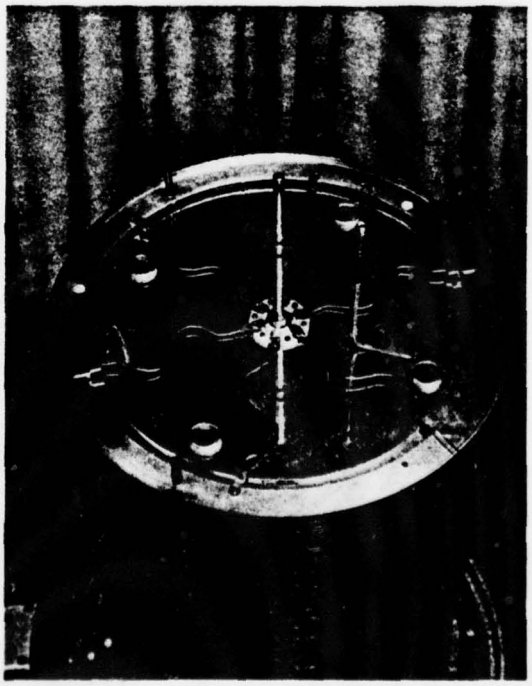

Figure 3-46. View of Upper Section of Degaussing Circuit Mounted on Assembly

18. The inner magnetic shield cylinder and top cover is assembled.

19. The inner oven assembly is completed by attaching the oven support cylinder, upper inner support ring and two thermal reflector plates (see Figure 3-47). Electrical connections are made and the oven is tested.

20. The second magnetic shield cylinder and top cover is put into position.

21. The outer oven assembly is completed by attaching the oven support cylinder, upper outer support ring and two thermal reflector plates (see Figure 3-48). Electrical connections are made and the oven is tested.

22. The vacuum feedthrough for the thermal sensors is attached to the outer oven support ring. The electrical leads from the 6 sensors are soldered to a terminal board (see Figure 3-48). All of the electrical wiring is checked at this point. A thermal reflector shield covers the top of the outer oven support ring.

23. The third magnetic shield cylinder and top cover is put into position.

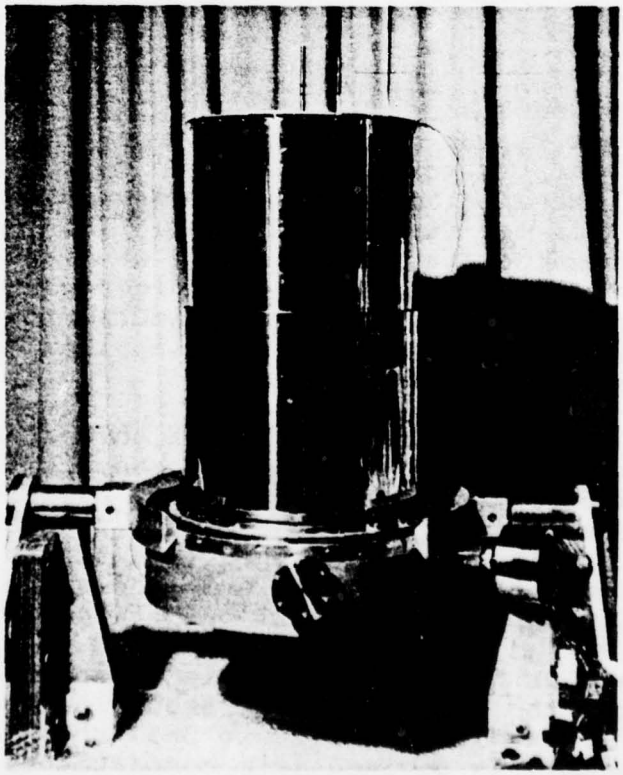

Figure 3-47. View of Assembly After Adding Inner Magnetic Shield and Inner Oven Assembly

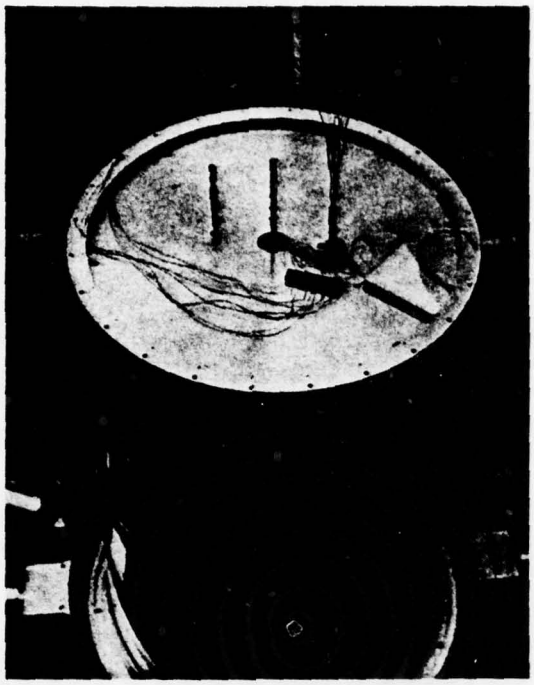

Figure 3-48. View of Assembly Upon Addition of Second Magnetic Shield, Outer Oven Assembly and Terminal Board and Output Port of Thermal Sensors

24. The vacuum enclosure cylinder and top plate are now placed on the unit (see Figure 3-49). The three vacuum feedthrough's protruding out of the top of the vacuum enclosure are screwed in position. The unit at this time undergoes one of its crucial tests and that is for vacuum tightness. The upper subassembly is now complete. Notice the top plate of the vacuum enclosure is partitioned into 9 chambers. (see Figure 3-50). These chambers are for housing the entire receiver electronics and the bridge circuits for the thermal sensors. This plate will be covered and held at a constant temperature.

25. To complete the lower assembly of the physics unit, the dissociator assembly on a test bed is seen in Figure 3-51 and it includes a pyrex bulb, RF oscillator, purifier, pressure control and optical monitor. To the bottom flange of the dissociator, the state selector is attached (see Figure 3-52). By the above arrangement, the center hole in the state selector can be externally aligned with the small output hole in the pyrex bulb.

26. The molecular hydrogen supply is attached and the electronics package for the purifier and pressure control is screwed in position (see Figure 3-53). Figure 3-53 shows how the space in the lower assembly is divided into compartments for various components. In the flight model of the clock, two vacuum pumps, power supply, molecular hydrogen supply, power amplifier module

for the heaters and the pressure control electronics would fit into these compartments.

27. The bottom cover is screwed in place and the outer-shield assembly is placed over the entire unit. This completes the assembly of the physics section of the clock.

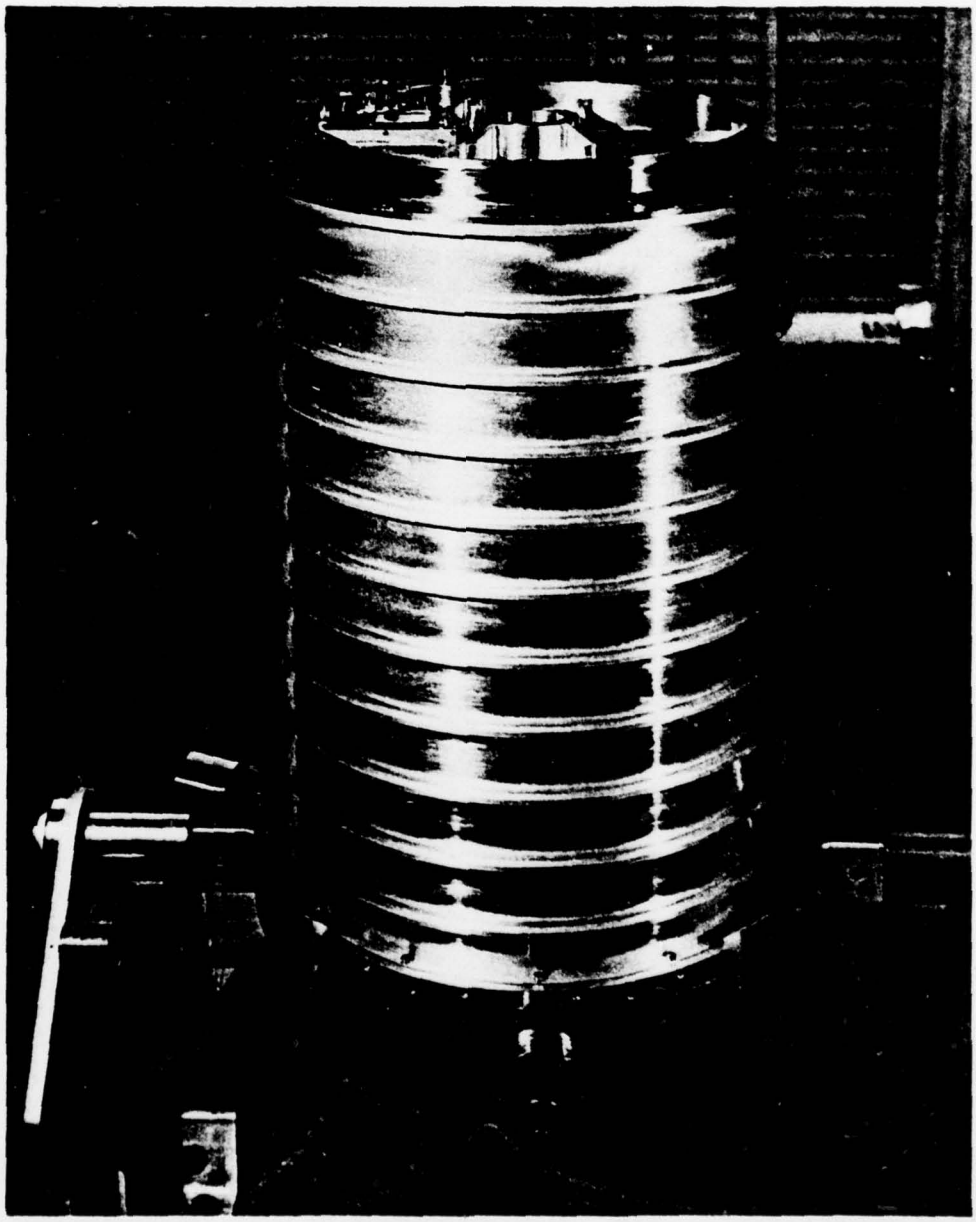

Figure 3-49. Vacuum Enclosure Cylinder and Top Plate Added to Assembly

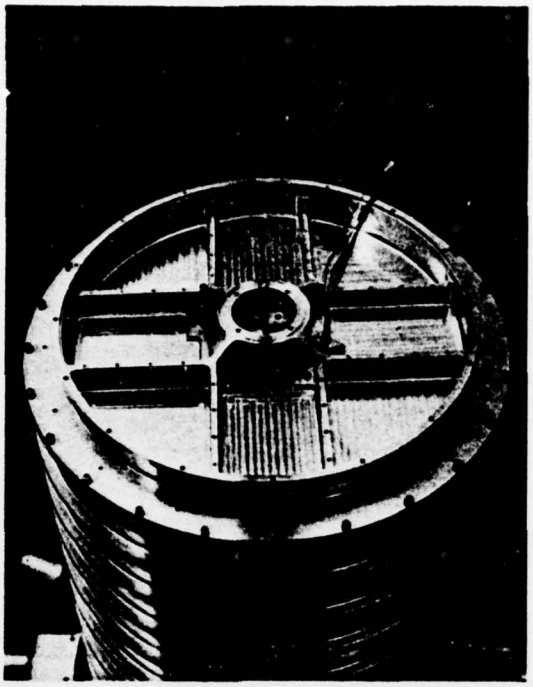

Figure 3-50. Top View of Top Plate of Vacuum Enclosure Showing Exit of Thermal Sensor Wires, Maser Output and Degaussing Terminal

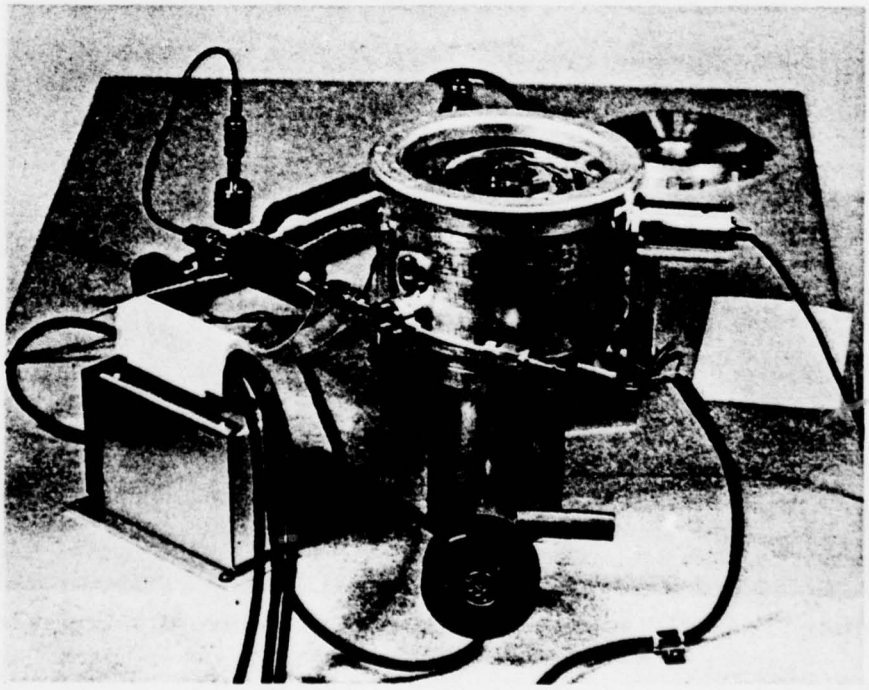

Figure 3-51. Dissociator Assembly Mounted on Test Fixture

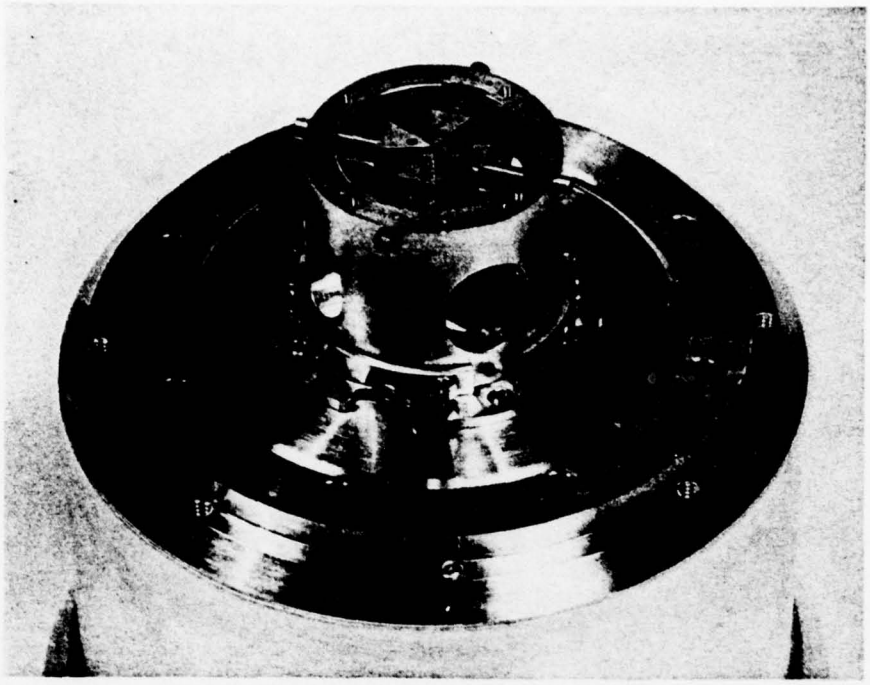

Figure 3-52. State Selector Attached to Flange of Dissociator Housing

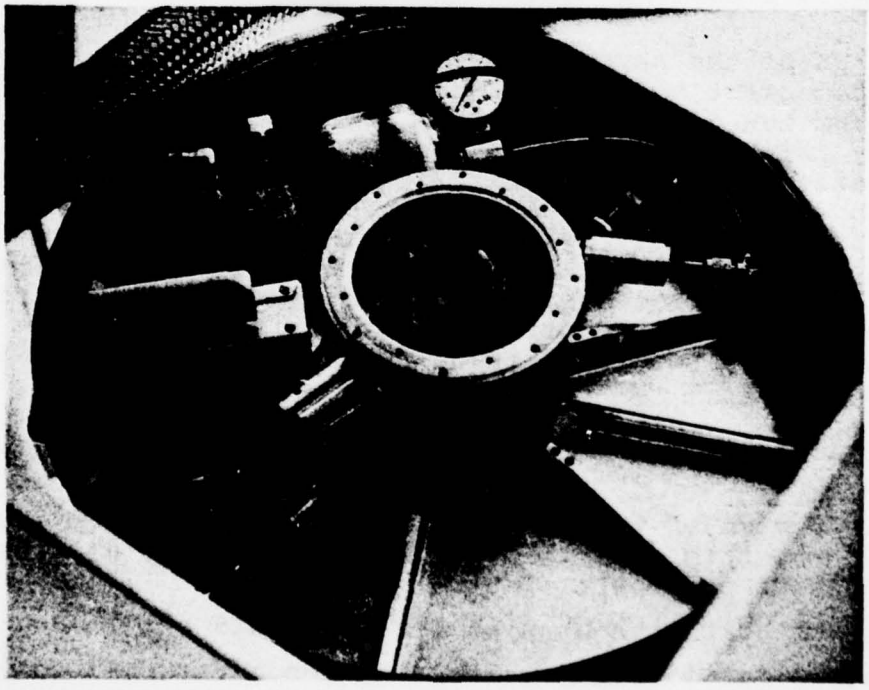

Figure 3-53. Bottom View of Lower Assembly Showing Dissociator Assembly, Purifier, Pressure Control, Pressure Control Electronics, Optical Monitor and Molecular Hydrogen Supply

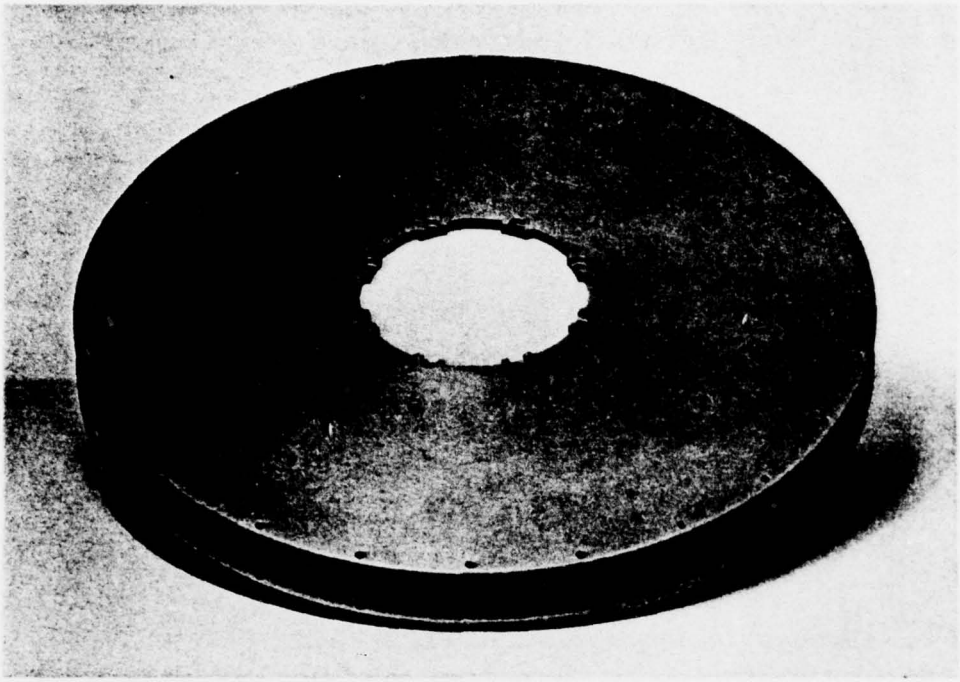

Figure 3-54. Bottom Cover of Lower Assembly

3.4 SUMMARY - PHYSICS UNIT

This design of the physics unit for the advanced development model of the spacecraft hydrogen clock system has a number of new components and new design features. Some of these innovations to be tested by this design will undoubtedly be incorporated in the final configuration of the spacecraft hydrogen clock. It was known from the beginning of this development program that the adoption of components from presently operating ground based clocks would not lead to a small reliable clock for use in space. It was necessary to be bold and inventive keeping in mind the overall objective of a small clock meeting the performance requirements of the system and the environmental constraints of space travel. The innovations of this design are:

(1) A quadrupole state selector which is small and weighs only 0.8 lb;

(2) The design of the hydrogen beam optics permits the entrance stem of the film bulb to be placed at only 7.0 cm from the exit of the state selector;

(3) A film bulb with a thickness of 0.0025 cm;

(4) An all metal cavity using molybdenum for cylinder;

(5) A vacuum envelope which encloses the cavity, field coil, 2 ovens and 3 nested magnetic shields;

(6) A new design for the neck assembly which in previous designs has been a major source of heat leakage to the cavity.

The small, lightweight state selector has obvious advantages. The reduction in the distance from the cavity to the state selector permits a reduction in the overall length of the clock. The film bulb has a number of advantages: small perturbation on cavity frequency, ease of fabrication, reproducibility and not susceptible to breakage. The all metal cavity is rugged, permits thermal fine-tuning, easy to copper plate and is relatively inexpensive. The vacuum enclosure makes the design simpler and helps in the thermal isolation of the cavity. The design for the neck assembly permits the volume in the vacuum space to be divided into two chambers without adding a major heat leak to the cavity.

This design has a diameter of 40.64 cm (16 inches) and the physics section is 69.8 cm (27.5 inches) in length with 6.35 cm (2.5 inches) added for electronics which makes the overall length 76 cm (30 inches). There is space for two vacuum pumps in the lower assembly but due to lack of time the vacuum pumps are connected outside the envelope of the clock.

With the testing of this model, the final configuration of the space flight model can be readily completed. This design uses a long length microwave cavity for the spacific purpose of reducing the cavity effects on the clock performance thereby permitting evaluation of other new components particularly the state selector and film bulb. The overall length of the clock can be substantially reduced from the present 76 cm (30 inches) to 50.8 cm (20 inches). This can be accomplished by a reduction in the cavity length from 40.64 cm (16 inches) to 20.3 cm (8 inches) and some minor changes in other places. The diameter of the clock which is presently 40.6 cm (16 inches) is difficult to reduce substantially. Depending on the data obtained from the present clock, it may be possible that the diameter could be reduced to 35.5 cm (14 inches). What about weight? There was not a serious attempt for weight reduction in the model and thus the weight of the model should be around 120 pounds. The space flight model as proposed in Figure 3-55 should be about 65 pounds. Since 25 pounds of this 65 pounds constitute the weight of the magnetic shields, it is difficult to reduce the weight much further without a new approach in the design of magnetic shielding.

From the extensive investigations on dissociators, a design of the dissociator bulb for the spacecraft clock is very evident. Our measurements have shown that a surface of either pyrex 7740 or quartz is difficult to improve from the view of hydrogen recombination. However, glass is fragile, not readily machinable and most of all has low thermal conductivity. To eliminate the disadvantages of glass, but to present a glass surface to the hydrogen, the dissociator bulb for the space clock should be constructed from beryllium oxide ceramic. On the inside surface of the BeO bulb a glass or quartz layer is deposited. A preliminary model of a glass coated BeO bulb was built and demonstrated to operate.

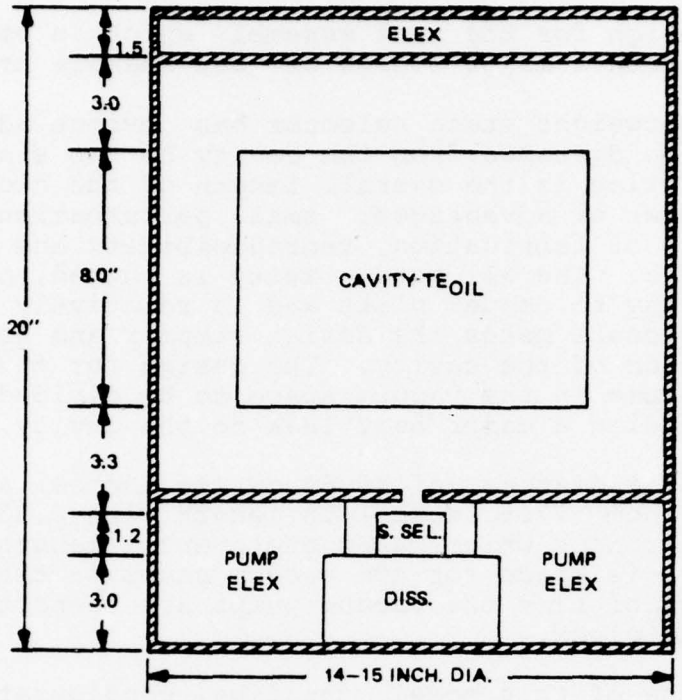

Figure 3-55. Sketch of Space Flight Clock

4.0 ELECTRONIC SYSTEMS

4.0 ELECTRONIC SYSTEMS

The electronic systems include those required to control the maser thermal and magnetic environments, to control the rate of flow of hydrogen, to convert molecular hydrogen to atomic hydrogen, and to provide an output signal at a useful frequency (20,000,000.00 Hz) which is a precise selectable submultiple of the oscillation frequency (1420405751.XXX Hz) of the hydrogen maser. An autotuner is also described in this section which may be used to automatically fine tune the resonant frequency of the microwave cavity precisely to the hydrogen line frequency.

4.1 BLOCK DIAGRAM RECEIVER SYNTHESIZER

The 1,420,405,751-Hz signal from the physics unit is processed by the Receiver/Synthesizer which produces an output signal of 20.00 MHz with essentially the frequency stability of the maser oscillation. A block diagram of the receiver/synthesizer is shown in Figure 4-1. The maser oscillator serves as the reference frequency in a phase-locked loop which is used to control the frequency of a voltage-controlled crystal oscillator from which the clock output frequency is derived. A triple conversion approach is used in the receiver to transform the maser output frequency to an audio frequency which is compared in a phase detector to a signal of the same frequency produced by the synthesizer. The error signal is filtered and amplified, and is used to control the VCXO. All local oscillator signals are derived from the VCXO by multiplication or division.

All components in the receiver/synthesizer are housed in a temperature-controlled section of the maser assembly in order to minimize the introduction of errors in time or frequency resulting from the effects of external temperature changes. Temperature control and care in the design of the preamplifier to ensure that it presents a constant load impedance for the maser eliminates the need for an isolator with its potentially harmful magnetic field.

The signal from the physics unit is amplified in a temperature-stabilized preamplifier whose output drives the first balanced mixer. A local oscillator signal, derived by multiplying the VCXO frequency by 70, is also introduced to the first mixer. The lower sideband signal at the output of the mixer is amplified in a 20.405 MHz IF amplifier. The output of this amplifier is fed to the second mixer which is supplied with a 20.00-MHz local oscillator signal. The lower sideband output signal is amplified in the 405 kHz IF amplifier whose output drives the third balanced mixer. The local oscillator input signal of 400 kHz is derived by dividing the 20.00-MHz VCXO frequency by 50 in a frequency divider. The lower sideband output of 5751 Hz is amplified in an active bandpass filter amplifier. The phase detector accepts one input from this 5751-Hz amplifier, and another from a programmable

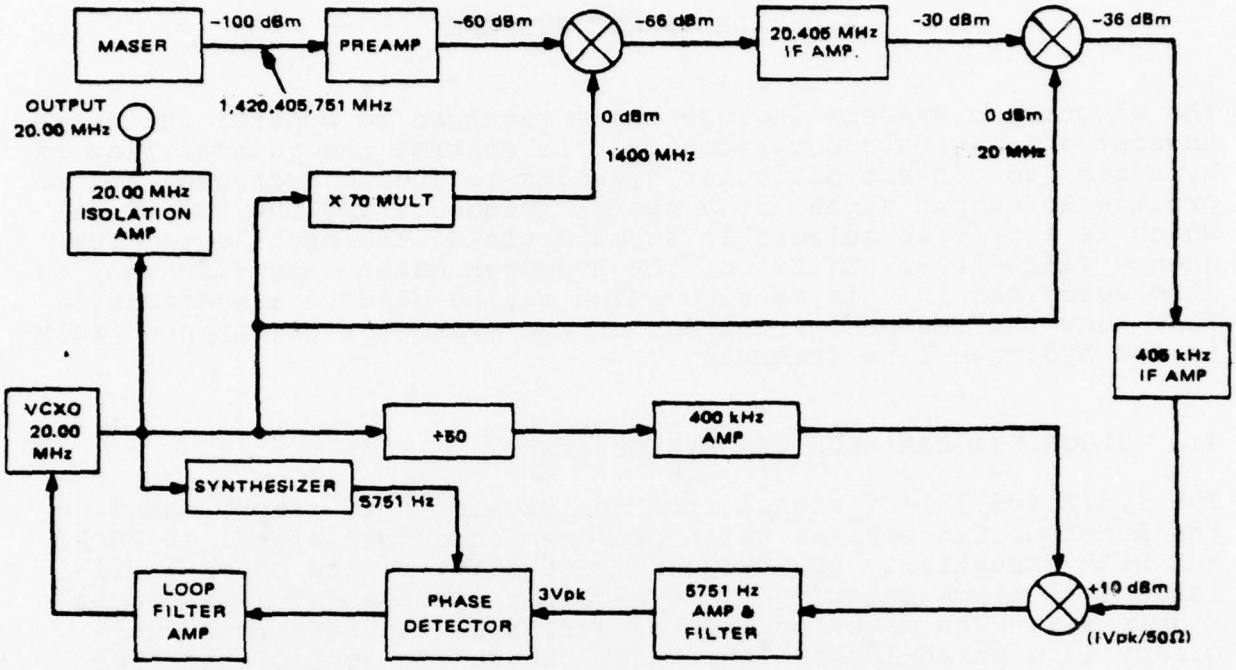

Figure 4-1. Receiver/Synthesizer Block Diagram

synthesizer whose reference is the 20.00-MHz VCXO frequency. The output of the phase detector is amplified and filtered in the loop filter whose output controls the VCXO frequency. The system forces the VCXO frequency to be such that the 5751-Hz frequency at the synthesizer output matches the 5751-Hz IF frequency when the loop is locked. A type of phase detector is used which provides an output logic level signal that is indicative of whether Input A is of a higher or lower frequency than Input B at the phase detector inputs. If both frequencies are equal, the output of the phase detector is a signal whose dc value is indicative of the phase difference. This type of phase detector provides a rapid and positive lock as long as the frequency pull range of the VCXO includes the lock-in frequency. The phase detector also provides a logic level lock signal which can be monitored.

The 20.00-MHz output is obtained from an isolation amplifier following the VCXO. The isolation amplifier serves as a buffer between the clock VCXO and other devices to which the clock is connected.

The receiver/synthesizer used in this maser has an advantage over others commonly used. The triple conversion allows the use of a simple synthesizer producing an output frequency in the audio range, and only one VCXO is required. The synthesizer, described in Section 4.1.1.4 is very simple and does not require any locked oscillators.

4.1.1 Receiver

The receiver consists of all the items shown in the block diagram of Figure 4-1, with the exception of the synthesizer. The various components are combined into three subassemblies which include:

(a) Preamplifier Module

(b) Local Oscillator Module

(c) Voltage-Controlled Crystal Oscillator (VCXO)

Each subassembly is described separately.

4.1.1.1 Preamplifier - The preamplifier contains the RF amplifier, 1st mixer, and 1st IF amplifier. The required operating characteristics are as listed in Table 4-1.

TABLE 4-1. OPERATING CHARACTERISTICS OF PREAMPLIFIER

Parameter	Value
RF Amplifier	
Frequency	1420.405 MHz
Gain	40 dB minimum
Noise Figure	3 dB maximum
Reverse Isolation	60 dB
DC Power	+5 Vdc @ 3mA
Input VSWR	1.5:1 nominal @ 1420.405 MHz 2:1 maximum
Mixer and IF Amplifier	
RF Frequency	1420.405 MHz
LO Frequency	1400 MHz
IF Frequency	20.405 MHz
LO Power	0 dBm nominal -10 dBm minimum
Conversion Gain	30 dB minimum
Noise Figure	8 dB
DC Power	+5 Vdc @ 18 mA
Mechanical	
Package Size	4 x 1.2 x 1.2 inches maximum, excluding connectors
Connectors	SMA

An amplifier-mixer assembly which satisfies the requirements was obtained as a vendor supplied item. Measurements made during breadboard testing on a unit supplied by FG Engineering, Phoenix, Arizona (Model FG 2552), show that in addition to meeting the basic requirements, the following sensitivities in phase shift were observed:

(a) Phase shift vs temperature = 0.19 degree/°C.

(b) Phase shift vs supply voltage = 0.003 degree/volt.

With temperature control of the preamplifier assembly, the above variations will not significantly affect clock stability.

4.1.1.2 Local Oscillator Module - The local oscillator module contains the second and third mixers and IF amplifiers, as well as the frequency multipliers and dividers required to produce the three local oscillator frequencies. A block diagram of the local oscillator module is shown in Figure 4-2, and a schematic is shown in Figure 4-3.

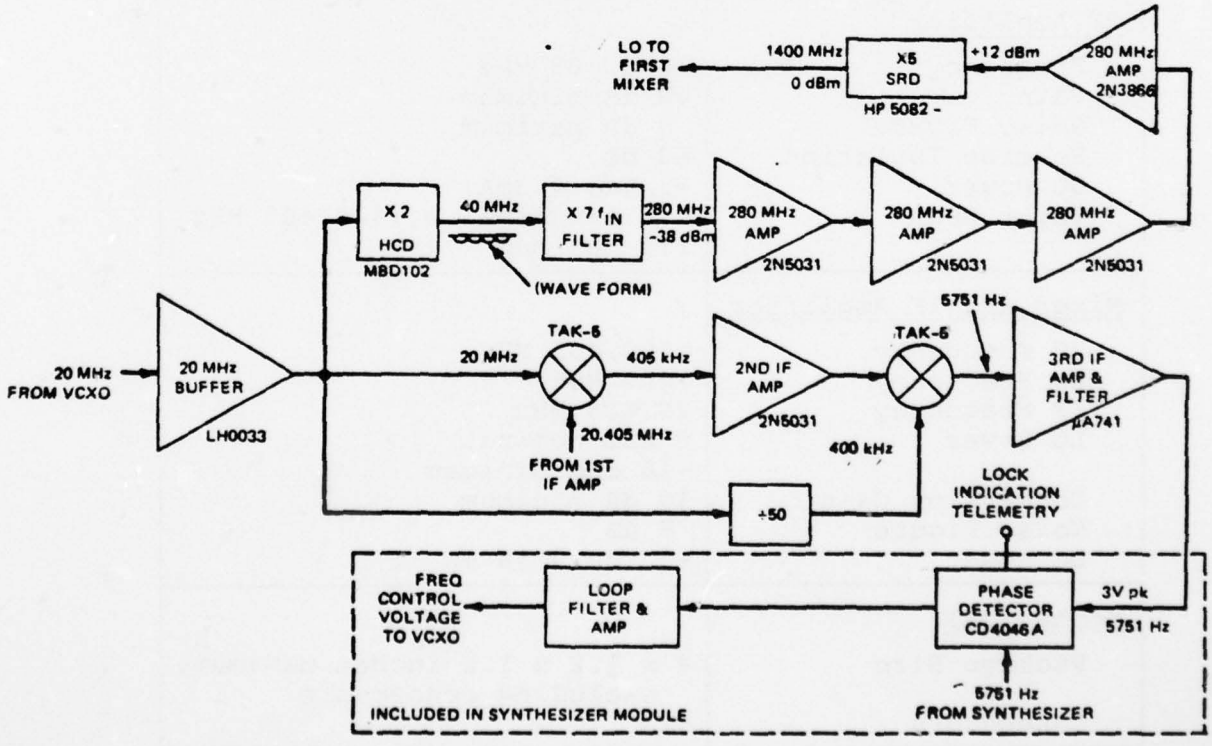

Figure 4-2. Local Oscillator Module Block Diagram

AD-A058 889 RCA ASTRO ELECTRONICS PRINCETON NJ F/G 22/2

SPACECRAFT HYDROGEN FREQUENCY STANDARD/CLOCK SYSTEM.(U)

APR 78 N00014-75-C-1148

UNCLASSIFIED AE-R-4258 NL

2 OF 2
ADA
058889

END
DATE
FILMED
11-78
DDC

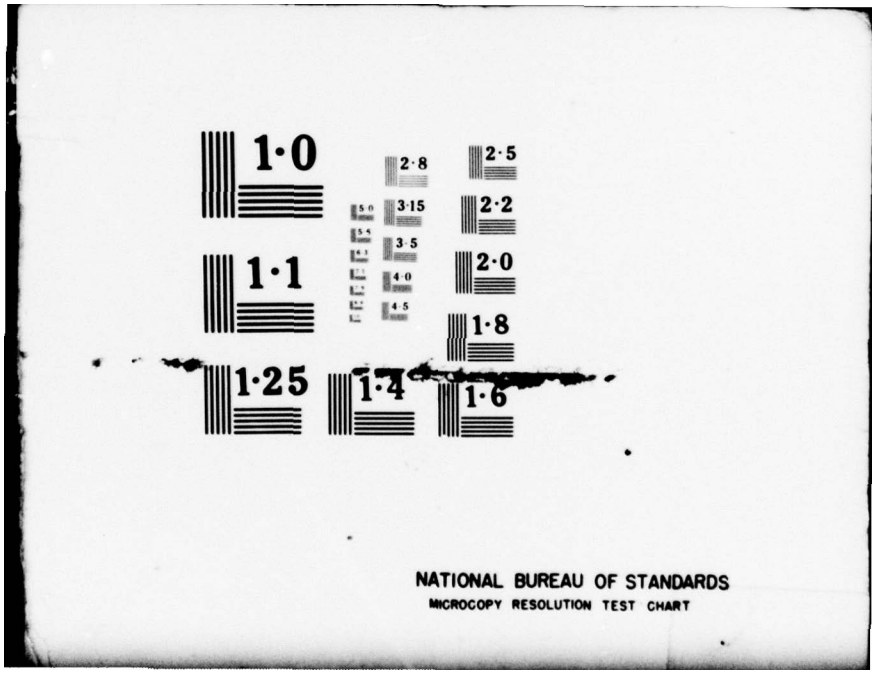
1·0
1·1
1·25
1·4
1·6
1·8
2·0
2·2
2·5
2·8
3·15
3·5
4·0
4·5
NATIONAL BUREAU OF STANDARDS
MICROCOPY RESOLUTION TEST CHART

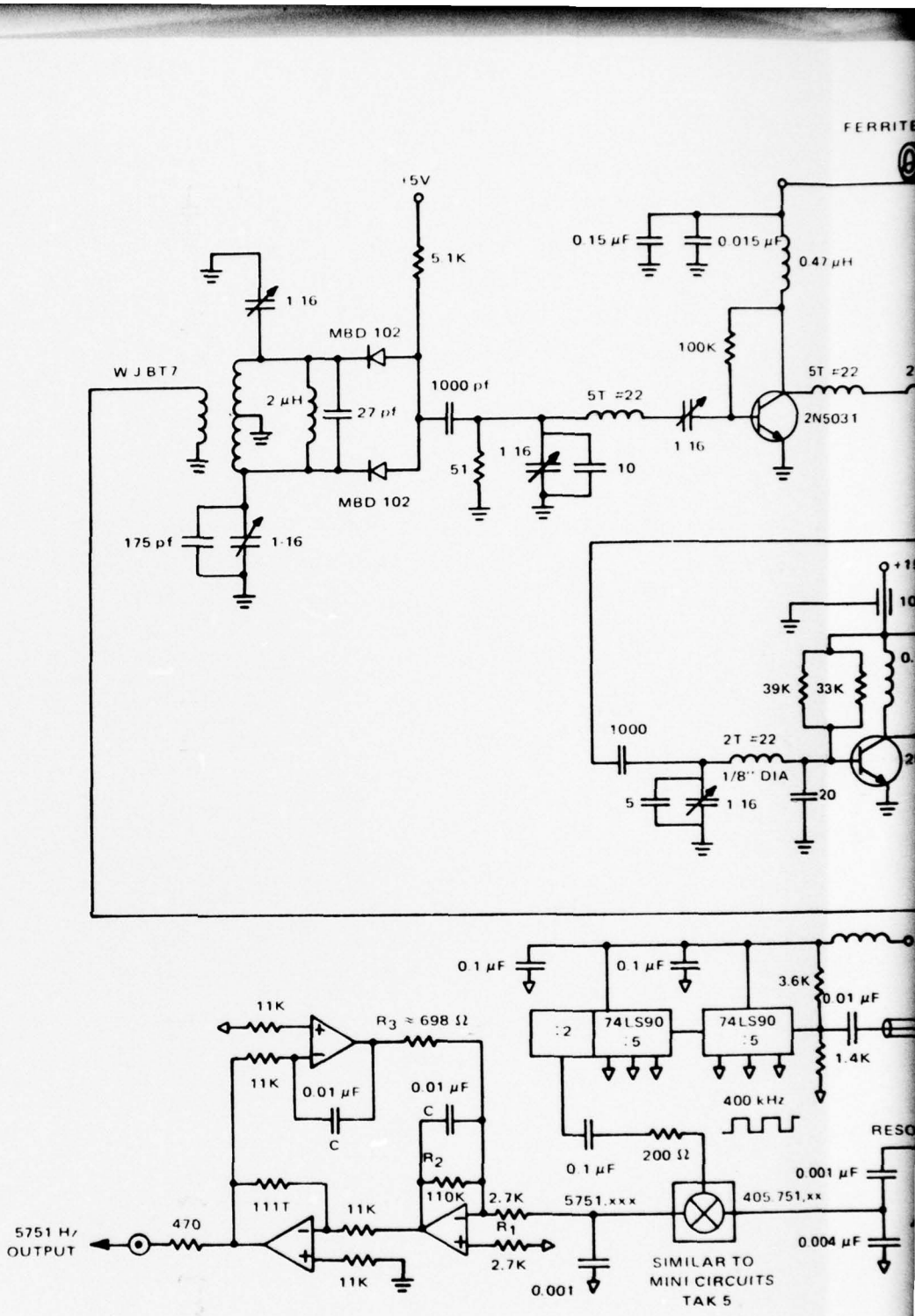

SELECT (METAL FILM RN60C)

R_1 FOR A ≈ 40

R_2 FOR GAIN ≈ 40

R_3 FOR F ≈ 5751.7 Hz

R_1 $Q/(K w_0 C)$

R_2 $Q/w_0 C$ KR_1

R_3 $1/(w^2 C^2 R_4)$

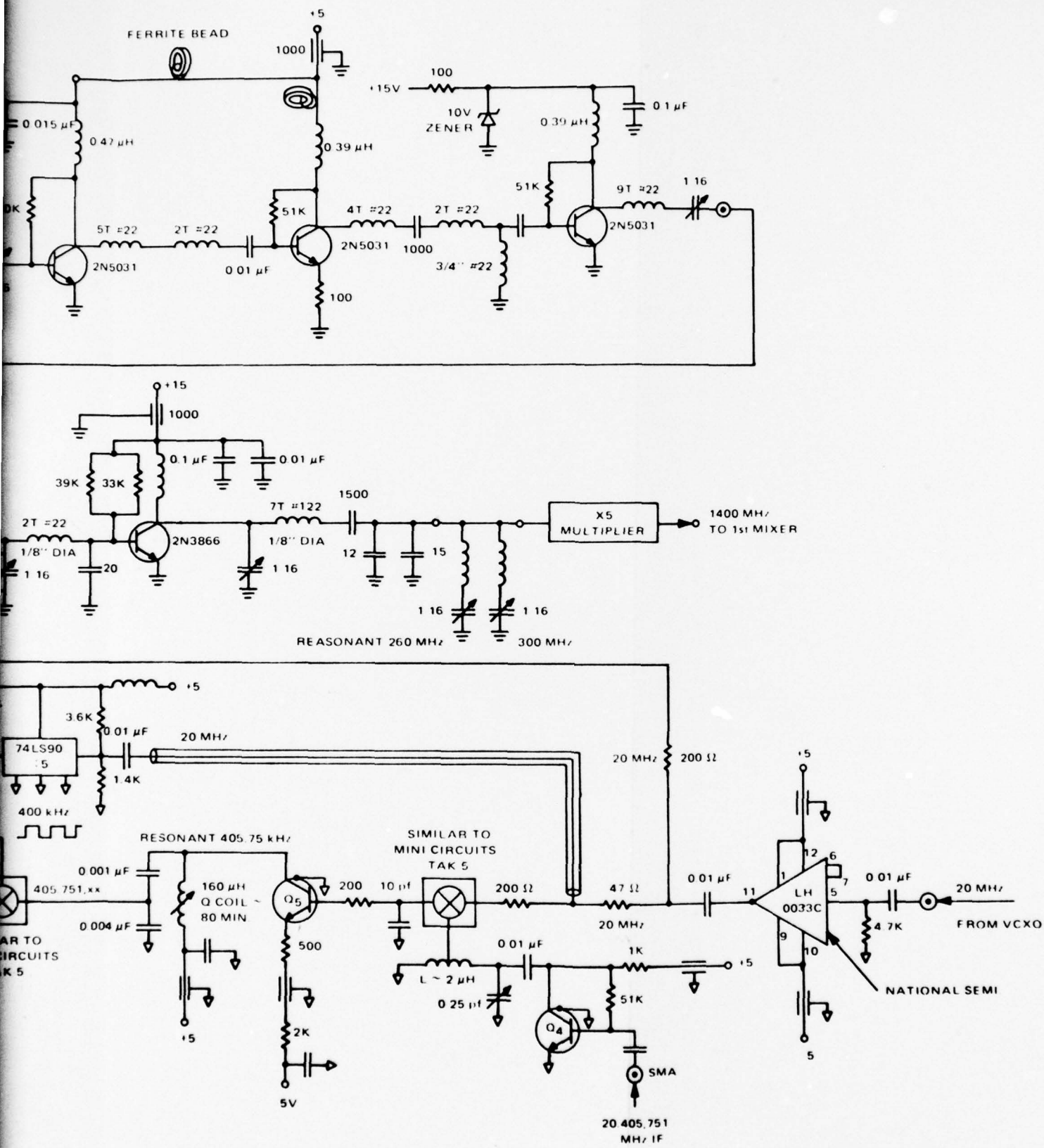

Figure 4-3. Schematic Local Oscillator Module

Temperature control of the location where the local oscillator module is mounted permits the use of simple circuit designs which do not require components with unusual or exotic temperature requirements. Circuit designs used in this module are based on approaches used successfully in several ground based masers.

All local oscillator frequencies are derived from the VCXO by frequency multiplication or division. The 1400-MHz signal for the first mixer is obtained by multiplying the VCXO frequency by 2 in a hot-carrier diode-balanced doubler, and filtering the seventh harmonic of the resulting waveform to produce a signal at 280 MHz which is amplified by 61 dB in a four-stage transistor amplifier. The output of the amplifier then drives a step-recovery diode x5 multiplier, producing an output at 1400.0 MHz with a nominal power of 0 dBm. The local oscillator signals for the second and third mixers are obtained by dividing the VCXO frequency by 1 and 50 respectively.

All amplifiers except the third IF are relatively broadband. The second IF amplifier is a single-tuned, single-stage transistor amplifier operating at 405 kHz. The third IF amplifier is an active filter with a center frequency of 5751 Hz which provides both gain and bandwidth restriction to minimize the effects of noise. Nominal gain in the third IF amplifier is 35 dB, with a 3-dB bandwidth of 200 Hz. The output of the third IF amplifier at a frequency of 5751 Hz serves as one input to the phase detector, with the second input provided by the synthesizer.

The phase detector is an RCA CD4046A. This type of phase detector provides an output logic level signal indicative of whether Input A is of a higher or lower frequency than Input B at the phase detector inputs. If both frequencies are equal, the output of the phase detector is a signal whose dc component is indicative of the phase difference. The phase detector output is filtered and applied to the VCXO as the frequency control voltage. The condition of the loop can be monitored by observing the lock indicator output of the phase detector. This output has been brought out as a test point. A high logic level output is provided at the lock indicator output when the loop is locked.

4.1.1.3 Voltage Controlled Crystal Oscillator (VCXO)

The VCXO is the source of the clock output frequency and all local oscillator signals. Since the VCXO is phase locked to the maser, the stability of the clock output is determined by the maser frequency stability for integration times greater than 1 second. The VCXO has the performance characteristics shown in Table 4-2

4.1.1.4 Synthesizer

Functional Description - The synthesizer is a unique design which employs pulse snatching techniques and frequency dividers to produce the audio signal which is applied to the phase detector for

for comparison with the signal derived from the maser oscillator. Phase-locked loops are not used in the synthesizer, and the VCXO signal serves as the reference.

TABLE 4-2. VCXO PERFORMANCE SPECIFICATION

Parameter	Value
Frequency	20.00 MHz
Power Supply	+15 Vdc @ 15mA
Output Type	TTL
Aging	$< 1 \times 10^{-9}$/day $< 5 \times 10^{-10}$day after 60 days
Temperature Stability	$\pm 5 \times 10^{-8}$ over 43°C ±0.5°C
Short-Term Stability	$< \pm 5 \times 10^{-10}$/second
Phase Noise	-120 dB/Hz @ 100 Hz -130 dB/Hz @ 1 kHz
Frequency Control Range	Sufficient to compensate for 8 years aging with 0-5 V control voltage range
Size	2 x 2 x 0.75 inches

An oscillator having these characteristics was obtained from Vectron Laboratories, Norwalk, Connecticut (Vectron Model 252-2986)

A functional block diagram of the synthesizer is shown in Figure 4-4. The 20.00-MHz VCXO output is divided by 2 to produce a 10.00 MHz signal (F_{IS}) which is applied to: (a) a programmable frequency divider which divides by a selected value N_1, and (b) a pulse snatcher consisting of a flip-flop and NOR gate. The output of the divider F_{IS}/N_1 serves as the second input to the pulse snatcher. The pulse snatcher removes pulses from F_{IS} at a rate given by F_{IS}/N_1 so that the frequency at the output of the pulse snatcher is $F_{IS}\ (1 - F_{IS}/N_1)$. This signal is then applied to a second pulse snatcher and a fixed frequency divider which divides by N_2. Pulses are removed at a rate given by $F_{IS}\ (\frac{1}{N_2} - \frac{1}{N_1 N_2})$ so that the output frequency from the pulse snatcher is $F_{IS}\left(1 - \frac{1}{N_1} - \frac{1}{N_2} + \frac{1}{N_1 N_2}\right)$. This signal is then divided by a factor N_3 so that the frequency at the output of the synthesizer is given by:

$$F_{OS} = \frac{F_{IS}}{N_3}\left(1 - \frac{1}{N_1} - \frac{1}{N_2} + \frac{1}{N_1 N_2}\right)$$

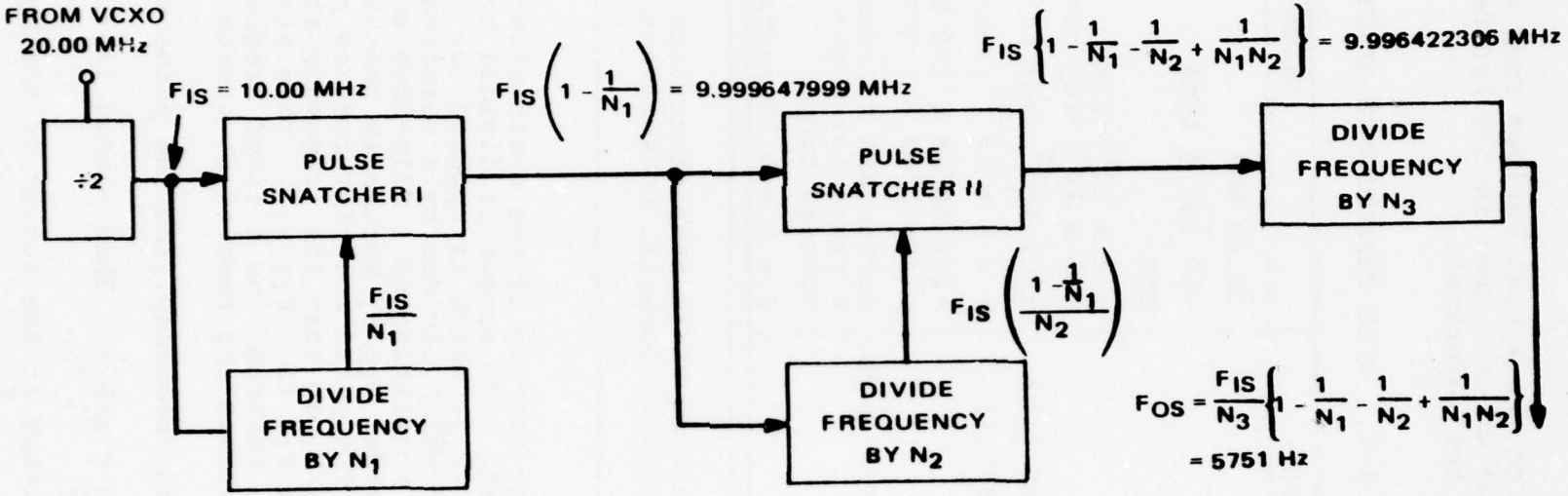

Figure 4-4. Synthesizer Block Diagram

In order to provide the clock output frequency of 20.00-MHz, the nominal value of the synthesixer output frequency should be 5751.68 Hz. To achieve this frequency, the divider values, N_X, are chosen to be:

$$N_1 = 28211,\ N_2 = 3100,\ \text{and}\ N_3 = 1738.$$

Divider N_1 is programmable over the range of 10,000 to 100,000 in order to provide a means for fine tuning the synthesizer output frequency. For the above range of values of N_1 and a VCXO frequency of 20.00 mHz, the synthesizer output frequency varies from 5751.308 Hz to 5751.826 Hz. This would allow the VCXO frequency to be set at exactly 20.00 mHz for a range of maser frequencies from 1420405751.308 Hz to 1420405751.826 Hz.

The values for N_2 and N_3 are fixed at 3100 and 1738 by design of the respective dividers, and the 20 MHz signal from the VCXO is divided by two before the first pulse snatcher in the feasibility test model clock. The value of N_1 is entered on twenty (20) small switches in a binary coded decimal format (five decades, four switches per decade). The programmable counter which divides by N_1 is organized such that a switch setting S, = 100,001-N_1 programs the counter to divide by N_1. An individual switch is set "OPEN" to produce a logic level 1. Table 4-3 illustrates the settings of the twenty individual switchs for N_1 = 28211, S_1 = 71790, which will lock the VCXO to exactly 20,000,000.00 Hz if the maser frequency is 1420405751.68 Hz.

TABLE 4-3. EXAMPLE OF SETTING SYNTHESIZER SWITCHES

	$x10^4$				$x10^2$				$x10^2$				$x10^1$				$x10^0$			
S	8	4	2	1	8	4	2	1	8	4	2	1	8	4	2	1	8	4	2	1
Switch No.	10	9	8	7	6	5	4	3	2	1	10	9	8	7	6	5	4	3	2	1
X-Switch "Open"		X	X	X				X		X	X	X	X			X				

S_1 = 71790

N_1 = 100,0001-S_1 = 28211

If f_m = 1420405751.68 Hz

f_o = 20,000,000.00 Hz

The sensitivity of the output frequency to changes in the value of N_1 is given by:

$$\frac{\Delta F_{OS}}{\Delta N_1} = \frac{F_{IS}}{N_1^2 N_3} \left(1 - \frac{1}{N_2}\right)$$

For the normal values of N_1, N_2 and N_3, $\Delta F_{OS}/\Delta N_1 = 7.229 \times 10^{-6}$ Hz/Unit of N_1. This translates to a change at the VCXO output of 1×10^{-7} Hz/Unit of N_1 or a sensitivity of 0.5×10^{-14}.

Divider N_3 is not, but could be made, programmable. Changes in N_3 then could produce offsets of several cycles in the clock output frequency which are necessary in some frequency and stability measuring schemes where a comparison is made between two frequency standards. For example, a change in N_3 from 1738 to 1717 produces a change in the VCXO frequency of approximately 1 Hz.

4.1.1.5 Circuit Description - A simplified schematic of the unique synthesizer is shown in Figure 4-5 and a more detailed schematic in Figure 4-6. Divider N_1 is a five section synchronous decade counter which is programmable to provide the capability of selecting any value for N_1 up to 100,000. To minimize

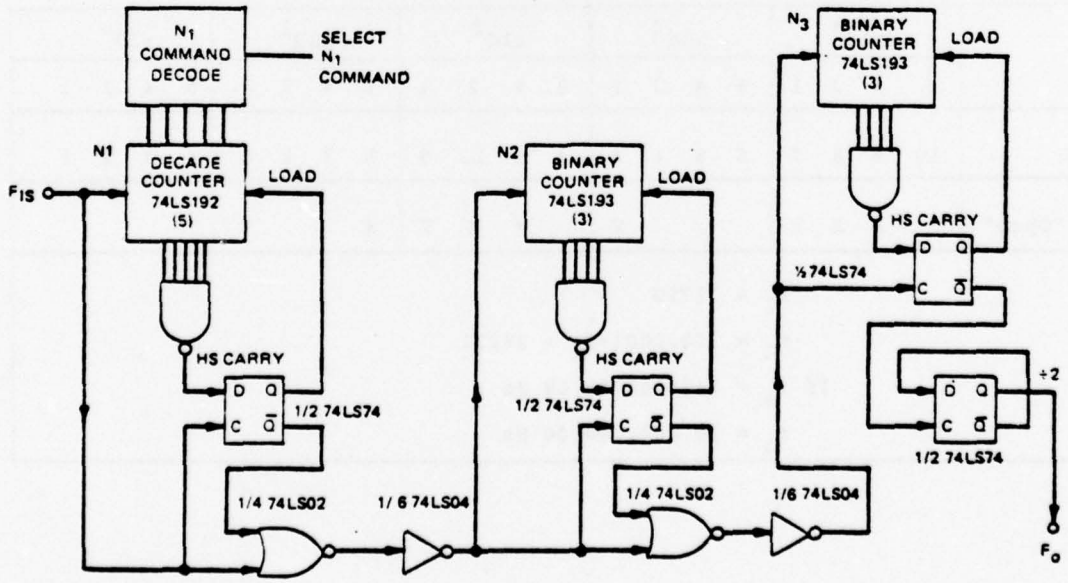

Figure 4-5. Synthesizer Simplified Schematic

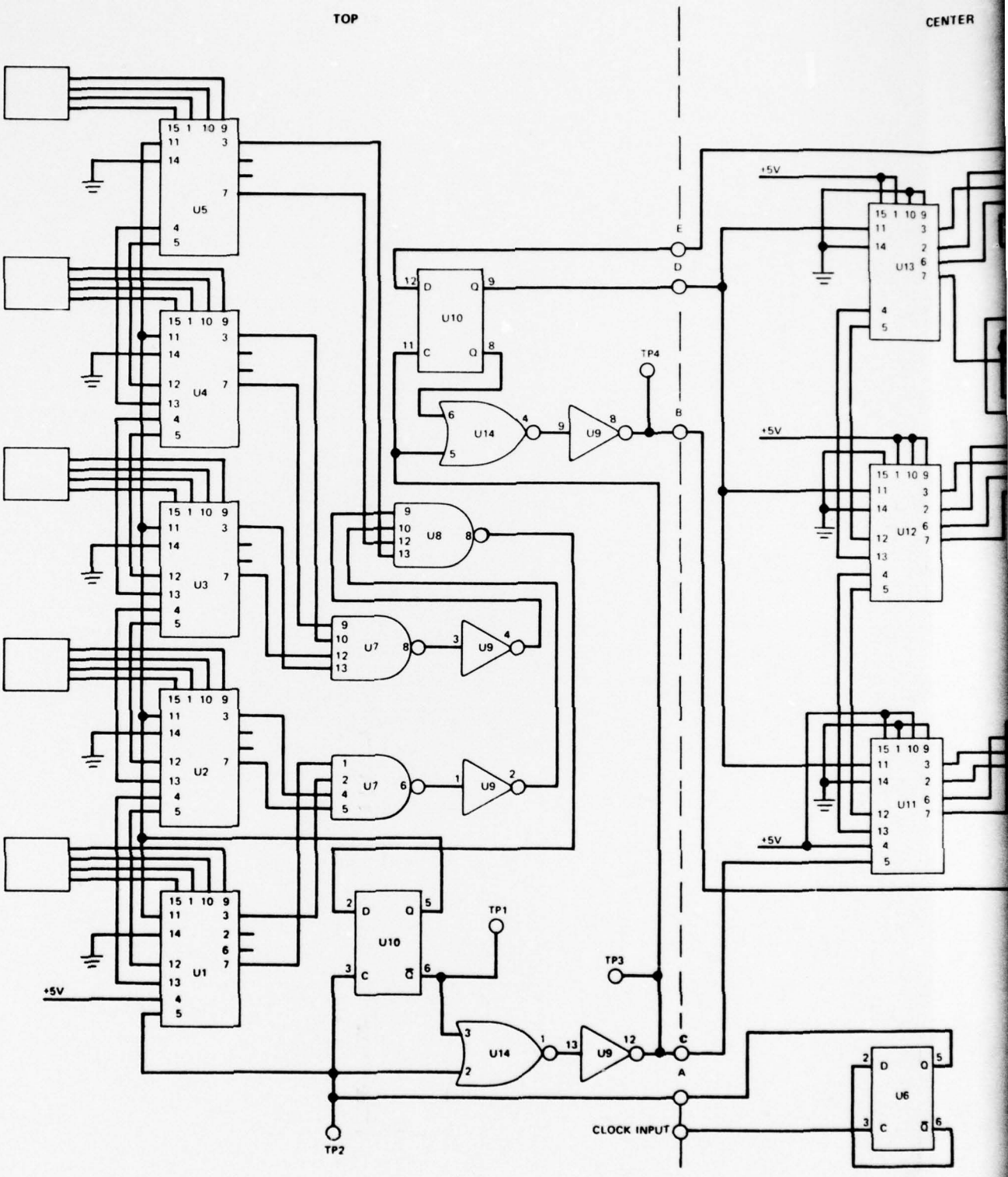
TOP
CENTER
U5
U4
U3
U2
U1
U10
U14
U9
U8
U7
U13
U12
U11
U6
+5V
TP1
TP2
TP3
TP4
CLOCK INPUT
A
B
C
D
E

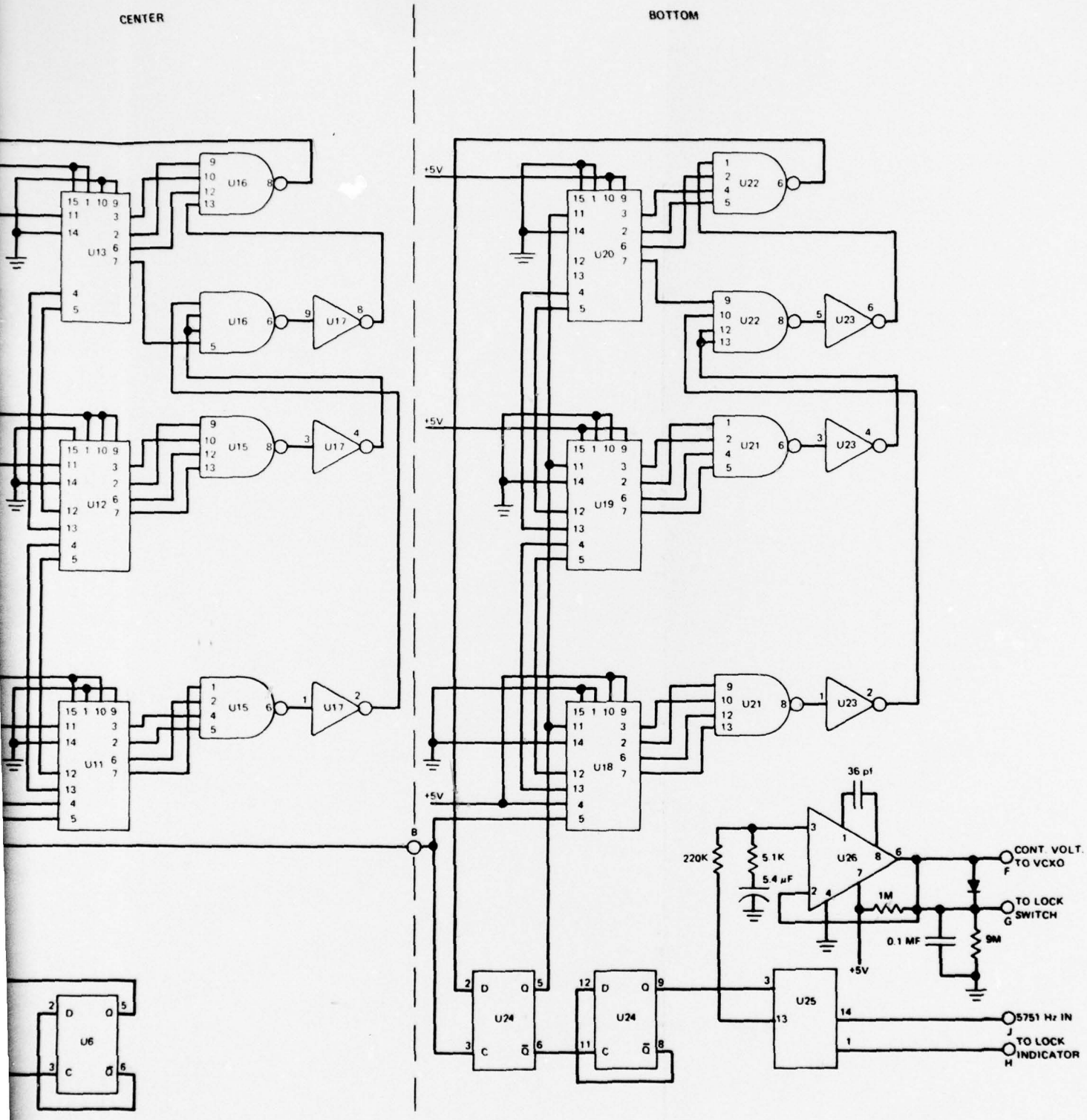

Figure 4-6. Synthesizer Schematic

2

delay through the counter chain caused by propagating the carry pulse ripple fashion from counter decade to counter decade, the outputs of the flip-flops of the individual counter chips are decoded and gated to provide the carry pulse when division by N_1 is completed. This function is indicated in the schematic by the NAND gate designated "HS Carry".

The carry pulse is applied to the D input of a D flip-flop. The D flip-flop along with the NOR gate forms the pulse snatcher. The presence of the carry pulse (low) at the D input causes the flip-flop to change state with the $\overline{Q}$ output going high and the Q output low. The low Q output loads the preset value required for division by N_1 into the counter.

The $\overline{Q}$ output serves as one input to a NOR gate. The other input to the NOR gate is the input signal to the synthesizer, F_{IS}. If $\overline{Q}$ is low, the output of the NOR gate is F_{IS} shifted in phase by 180°. When $\overline{Q}$ is high each time a carry pulse is generated, the output of the NOR gate remains low. This condition exists for one cycle of F_{IS} since the next positive going cycle of F_{IS} resets the flip-flop, returning Q to the low state and $\overline{Q}$ to the high state. Since a carry pulse is generated each time division of F_{IS} by N_1 is completed, pulses of F_{IS} are suppressed or "snatched" at a rate F_{IS}/N_1 so the frequency at the output of the pulse snatcher is $F_{IS}\ (1 - 1/N_1)$.

The process is repeated in a second pulse snatcher. The divider N_2 is a twelve stage synchronous binary counter (on three chips). The final divider is a programmable twelve stage synchronous binary counter (on three chips) which divides by $\frac{N_3}{2}$ followed by a flip-flop configured as a ÷2 circuit in order to produce a symmetrical output waveform. The net result is division by N_3.

Low power Schottky logic is used in order to minimize power drain. The maximum dc power required for the synthesizer is 2 watts.

4.1.1.6 Receiver/Synthesizer Interface Circuits

Several miscellaneous circuits used in the receiver/synthesizer designated as interface circuits appear in Figure 4-7.

The 5751 Hz Amplifier is inserted between the 5751 Hz output of the 5751 Hz active filter of the local oscillator module and the 5751 Hz input terminal to the phase detector. It consists of a µA741 OP Amp in a configuration producing a gain of 11, non-inverting.

The 20 MHz DC level shifter is inserted between the output of the VCXO and the 20 MHz input to the synthesizer. This circuit insures that the 20 MHz signal be at the proper DC level for interfacing with the TTL logic in the synthesizer.

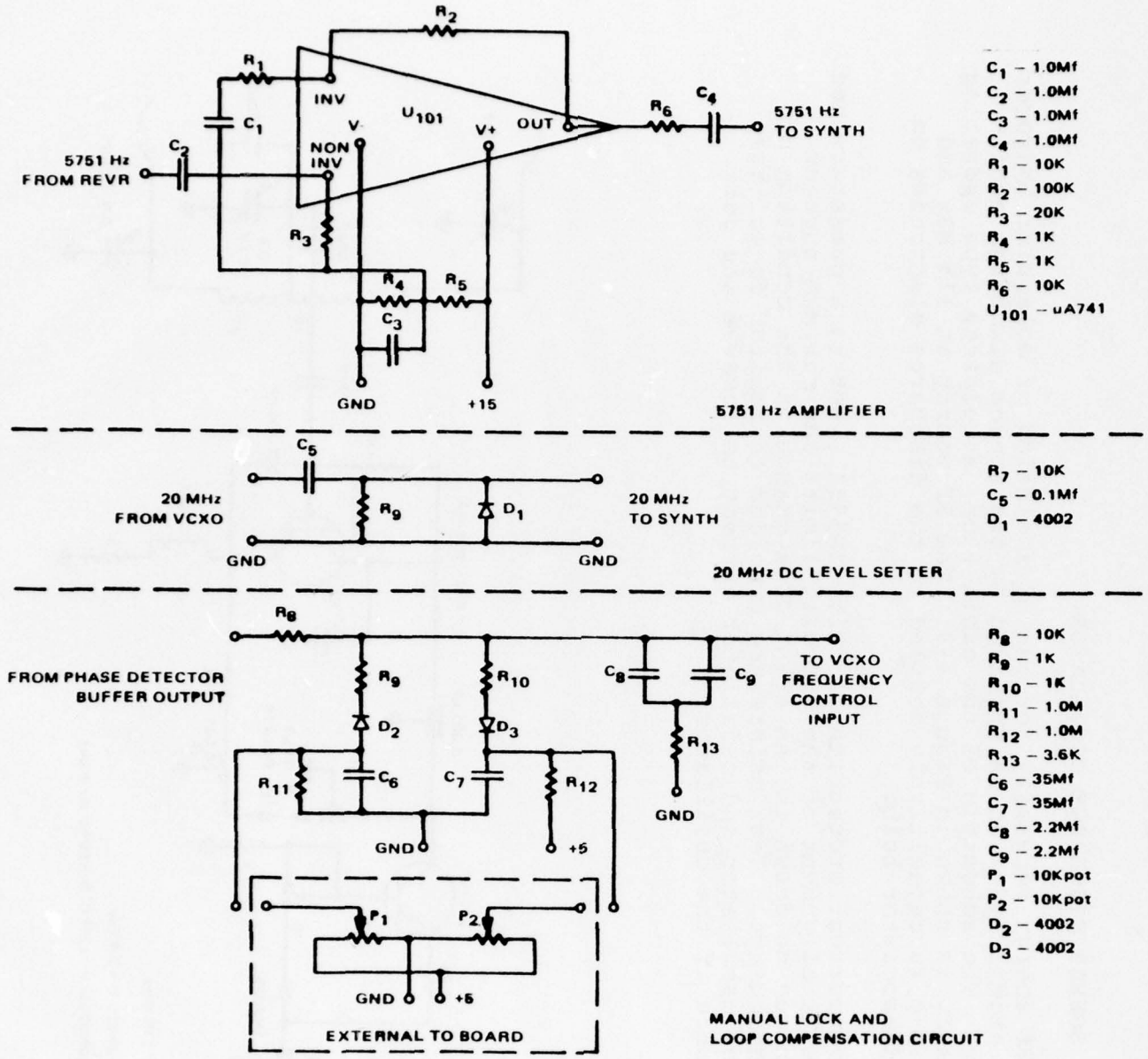

Figure 4-7. Receiver/Synthesizer Interface Board

The manual lock and loop compensation circuit is inserted between the DC signal output from the phase detector buffer output, and the VCXO frequency control input terminal. It provides additional loop compensation, and a means for manually setting the DC input (through the two potentiometers) to the VCXO in a range which will allow the loop to achieve "lock".

4.2 SOURCE DISCHARGE OSCILLATOR

The RF energy necessary for the dissociation of molecular hydrogen into atomic hydrogen is provided by the source discharge oscillator. The schematic of the oscillator, a Colpitts type operating Class C, is shown in Figure 4-8. The RF energy at 115 MHz and 300 Vp-p is capacitively coupled to the discharge electrodes on the dissociator bulb.

An overcurrent protection circuit (2N5955), set to a predetermined value at alignment of the circuit, limits the maximum current which can be drawn in the event of a change in the condition of the discharge. Test points are provided to monitor dc voltage to the oscillator and oscillator current to observe the performance of the oscillator.

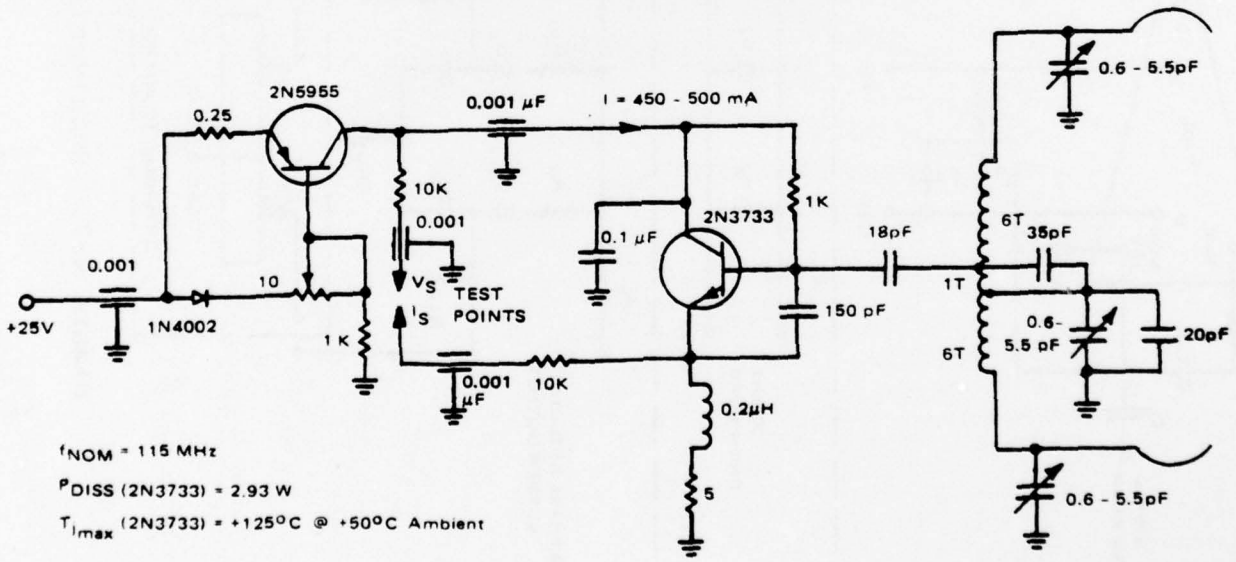

Figure 4-8. Source Discharge Oscillator

The quality of the discharge in the dissociator will be monitored by observing with an optical detector the amount of atomic hydrogen being generated. The optical detector consists of a filter tuned to the hydrogen Balmer α-line, a photo-detector (e.g., Bell & Howell type 509-50), and associated amplifier.

4.3 PRESSURE CONTROL CIRCUIT

Pressure control of the hydrogen entering the dissociator is accomplished by using a Pirani gauge as an element in a bridge circuit where the bridge voltage is amplified and used to control the temperature of the Pd-Ag purifier which regulates the hydrogen flow. Pressure is set by the pressure set voltage applied to the resistor bridge as shown.

The pressure control circuit has a thermal controller for maintaining the temperature of the Pirani gauge assembly at a constant temperature in order to prevent changes in pressure from being introduced by external temperature variations. A pulse width modulation scheme is used to provide the heater voltages at maximum efficiency.

4.4 TEMPERATURE CONTROL CIRCUITS

Thermal controllers accurately maintain the temperature of the following assemblies:

(a) Cavity

(b) Upper and lower inner ovens

(c) Upper and lower outer ovens

(d) Electronics package.

In order to maintain the required accuracy, the temperature control circuits have been designed with the following features:

(a) Use of resistors with low temperature coefficients in critical applications such as bridge resistors, and use of low drift operational amplifiers as preamplifiers to sense the resistance changes in the thermistor sensors.

(b) Physical separation of the resistance bridge and preamplifier from the power amplifier portion of the circuits which is used to drive the heater element in order to isolate sensitive components from heat sources.

(c) Mounting of the resistance bridge and preamplifier circuit in a temperature-controlled portion of the maser assembly.

(d) Use of pulse width modulated techniques to improve the efficiency and reduce dissipation in the oven control circuits.

A schematic diagram typical of the various temperature control circuits is presented in Figure 4-10.

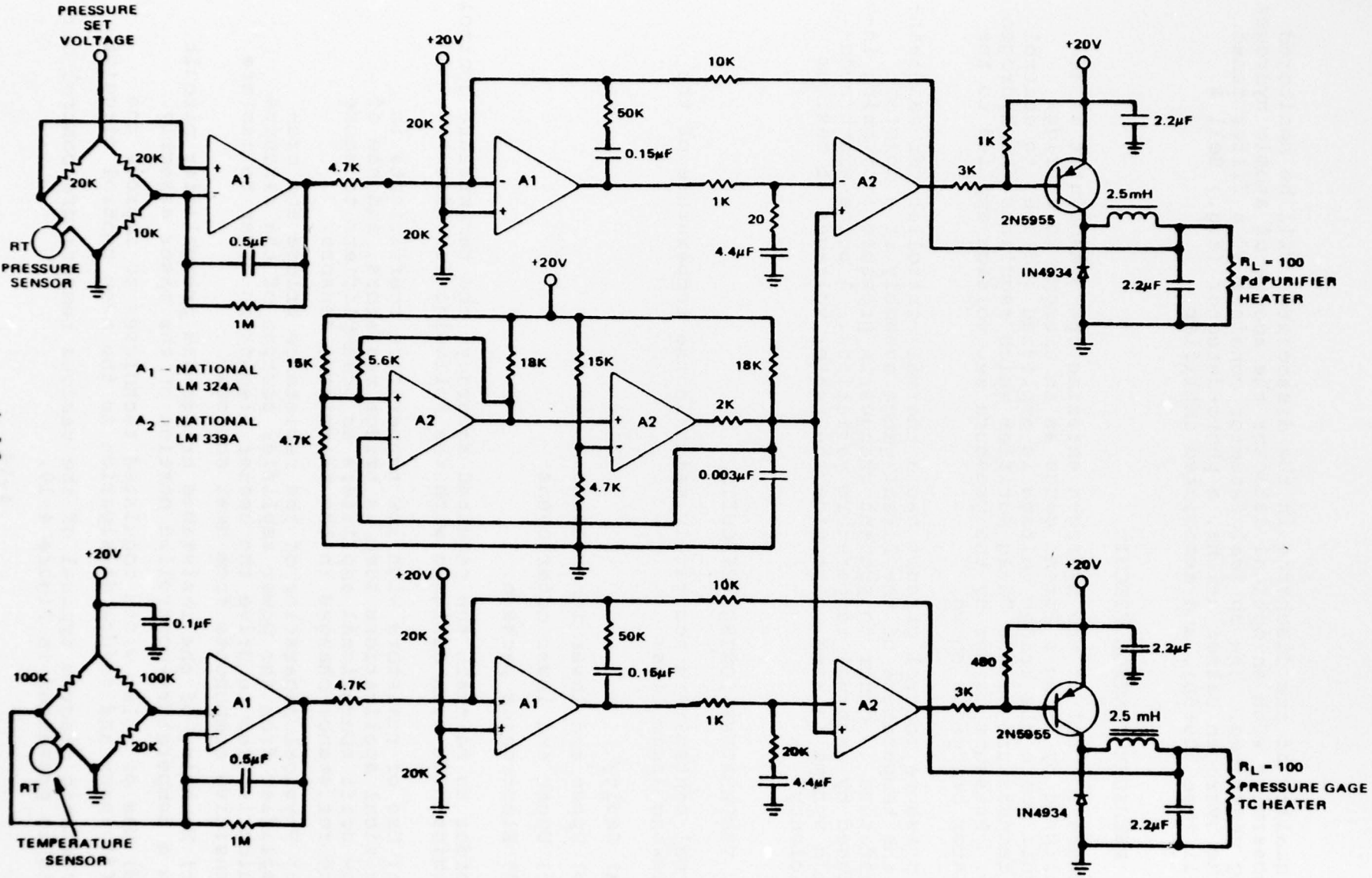

Figure 4-9. Pressure Control Circuit

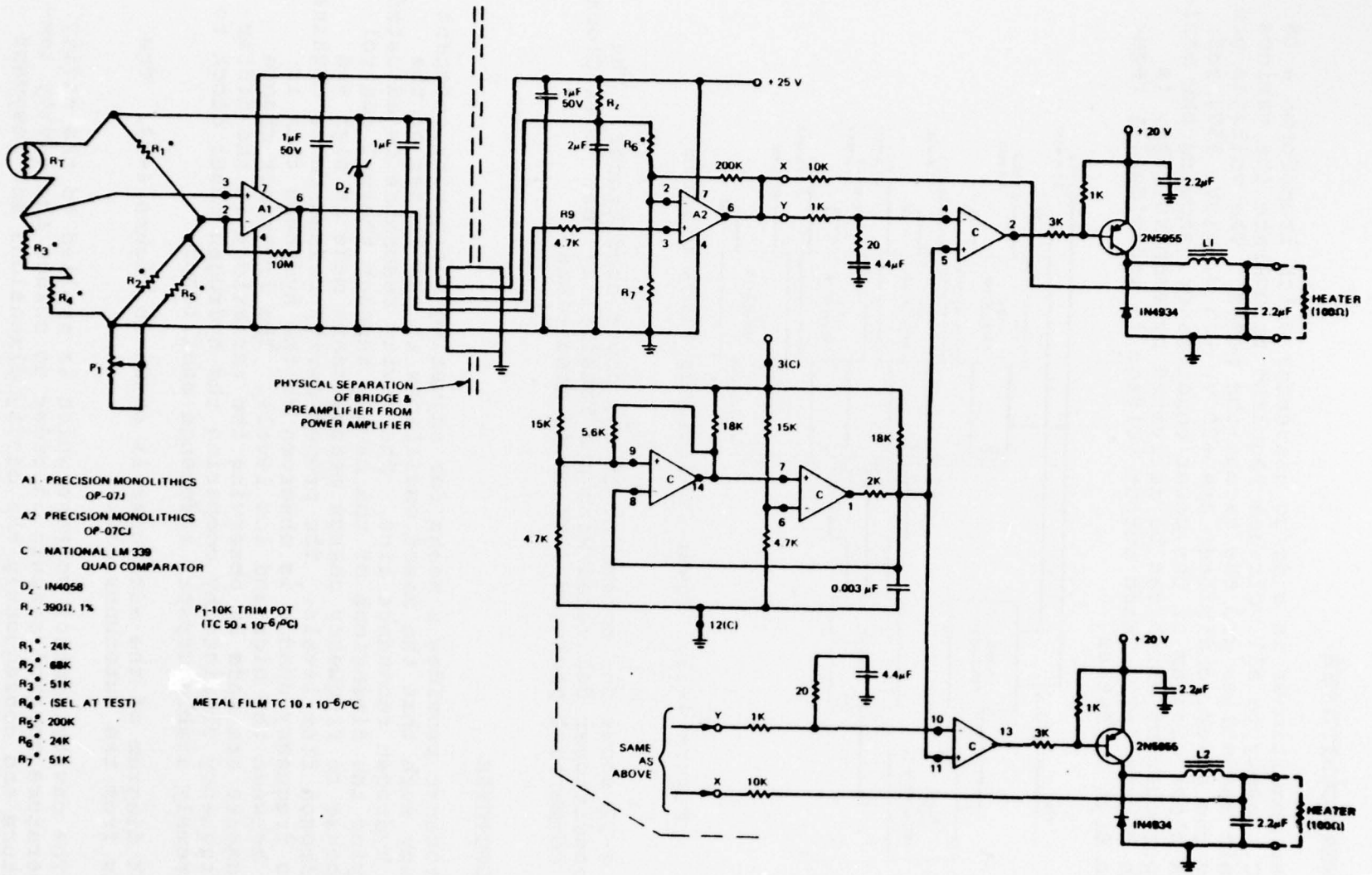

Figure 4-10. Typical Temperature Control Circuit

4.5 POWER CONDITIONER

The power conditioner is a dc/dc converter which transforms a 28 volt D.C. supply to all voltages required to operate the various electronic assemblies and the vacuum-ion pumps. The voltages provided by the power conditioner are +20 V, +25 V, ±15V, ±5V, and 3 kV. A block diagram of the power conditioner, showing the maximum output current which can be delivered by each voltage, is shown in Figure 4-11. Each output voltage is individually regulated to 0.1% or better.

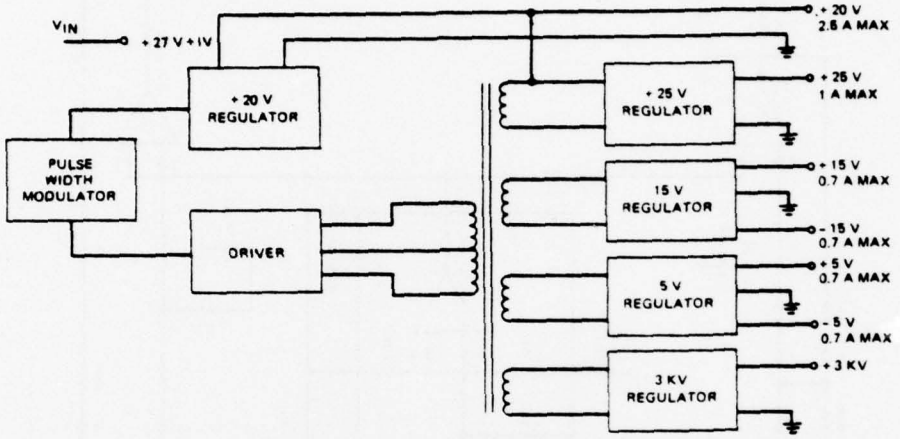

Figure 4-11. Power Conditioner Block Diagram

Figure 4-12 shows the schematic of the power conditioner. The power conditioner delivered with the Feasibility Test Model Clock uses a commercial packaged 3-kV power conditioner.

4.6 AUTOTUNER

The autotuner provides a means for adjusting the cavity resonant frequency such that the maser oscillates at the center of the atomic hydrogen resonance line. The cavity resonance is adjusted by varying the dimensions of the cavity through thermal control in response to frequency change measurements made at high and low hydrogen flux levels. The proper cavity resonance is obtained when no frequency change is observed as the hydrogen flux is varied between the high and low levels. The frequency change measurements are made by observing the variations in the difference frequency obtained by comparing the hydrogen maser clock to an extremely stable crystal reference oscillator.

A block diagram of the autotuner is shown in Figure 4-13. The outputs from the autotuner are:

(a) The cavity control voltage which is applied to the cavity temperature control circuit in order to change the cavity temperature and consequently the cavity dimensions and resonant frequency.

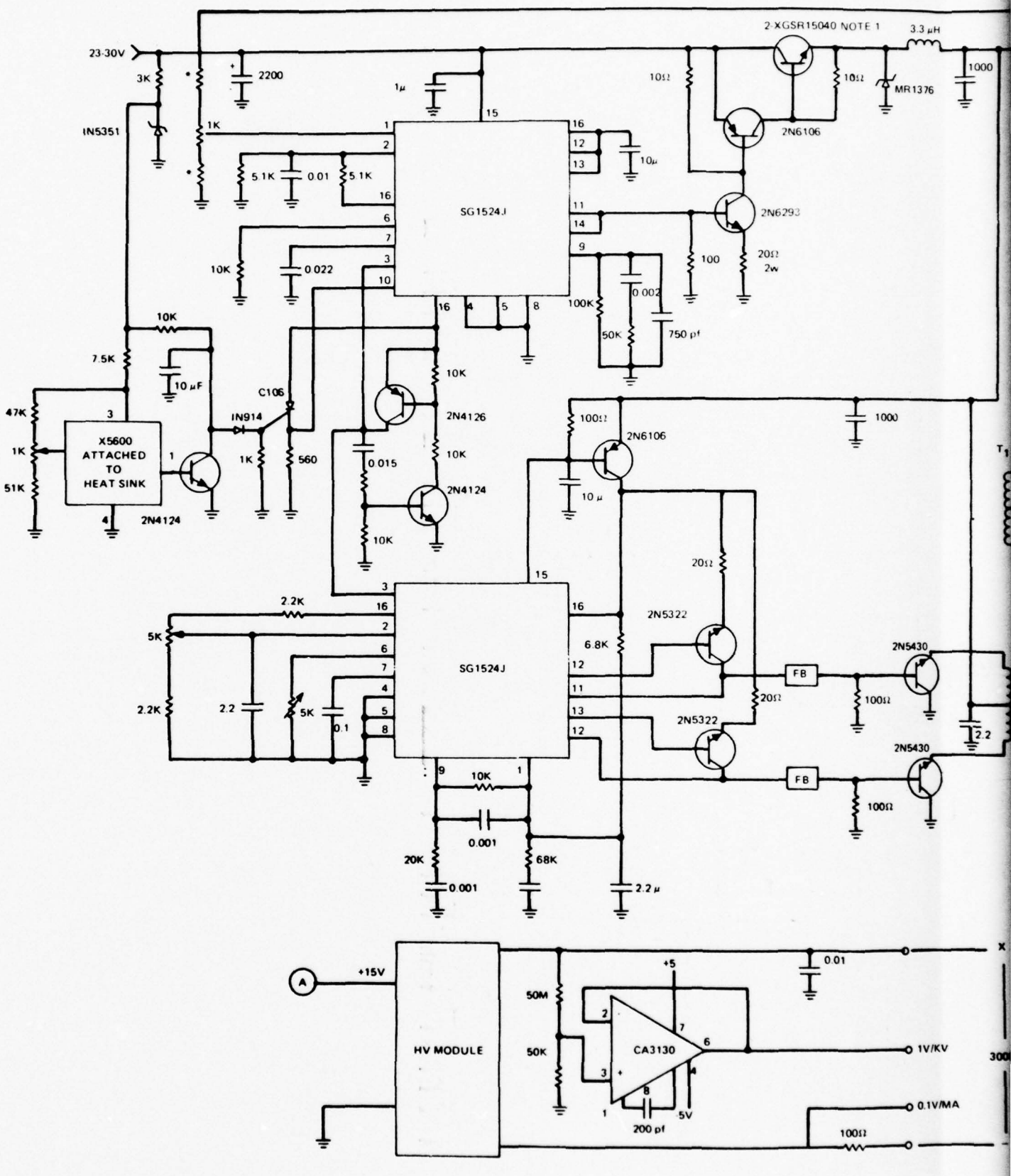
23-30V
3K
IN5351
2200
1K
5.1K
0.01
5.1K
1μ
SG1524J
10K
0.022
10K
7.5K
10 μF
47K
1K
51K
X5600
ATTACHED
TO
HEAT SINK
2N4124
IN914
C106
1K
560
2N4126
10K
0.015
2N4124
10K
2.2K
5K
2.2K
2.2
5K
0.1
10K
0.001
20K
0.001
68K
2.2 μ
2-XGSR15040 NOTE 1
3.3 μH
10Ω
10Ω
MR1376
1000
2N6106
10μ
2N6293
100
20Ω
2w
0.002
100K
50K
750 pf
100Ω
2N6106
10 μ
1000
20Ω
2N5322
6.8K
2N5322
20Ω
FB
2N5430
100Ω
2.2
FB
2N5430
100Ω
A
+15V
HV MODULE
50M
50K
CA3130
+5
-5V
200 pf
0.01
1V/KV
0.1V/MA
100Ω

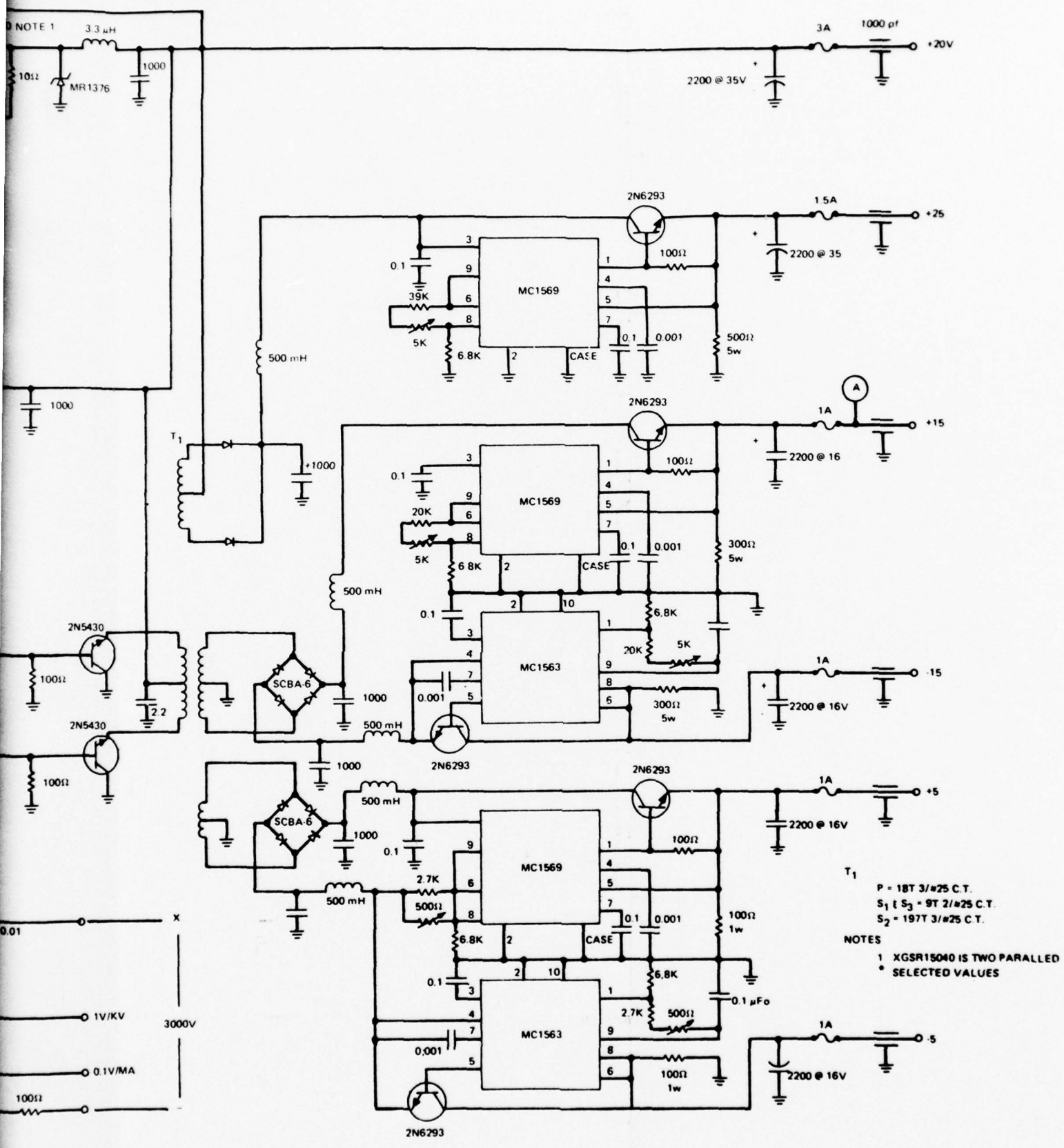

Figure 4-12. Power Conditioner Schematic

(b) The beam shutter control voltage which causes the beam shutter to vary the hydrogen flux density between the high and low levels.

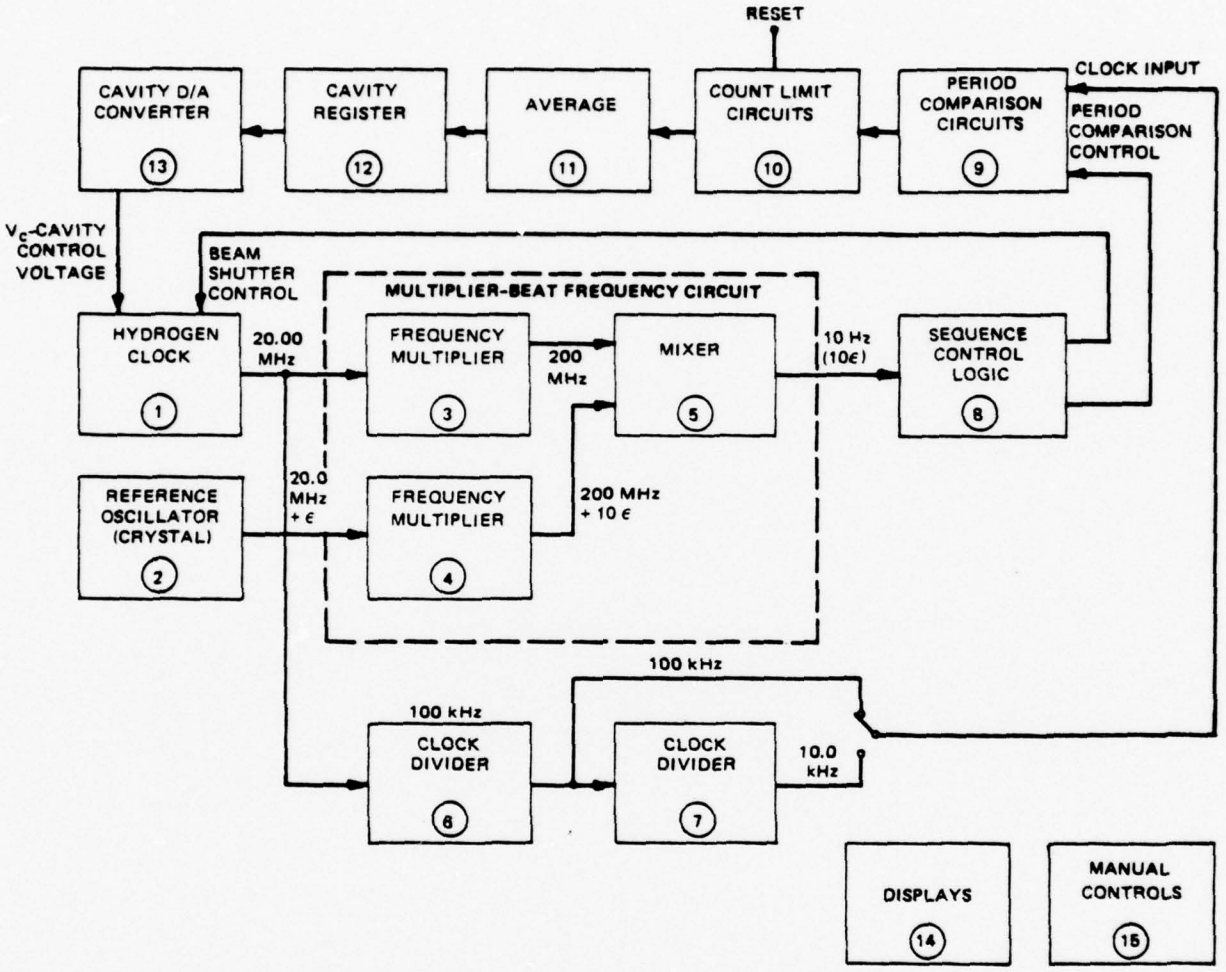

Figure 4-13. Autotuner Block Diagram

In the following discussion, the numbers in parentheses refer to the corresponding blocks in Figure 4-13. A 10-Hz beat frequency is derived in the multiplier-beat frequency circuit (3, 4, 5) by comparing the hydrogen clock (1) and a reference oscillator (2) frequency which has been offset from the nominal clock frequency by 1 Hz. As the hydrogen flux is varied between the high and low values, the beat frequency will change.

The period comparison circuit (9) measures the period of the beat frequency at each flux level, and periodically provides a series of pulses representing the difference between the period measurements. Each difference measurement or comparison cycle will take 120 seconds. The count limit circuit (10) allows a maximum of 10 counts

representing period measurement differences between high flux and low flux or low flux and high flux to pass into the averager circuit in each comparison cycle. It is then reset for the next cycle.

The averager (11) integrates the counts received from the count limit circuit (10), and increments the cavity register (12) by plus one count for each plus 100 integrated counts or minus one count for each minus 100 integrated counts. It is then reset and produces the next plus one or minus one output count after the next plus 100 or minus 100 integrated counts are accumulated. The cavity register (12) controls the cavity temperature (and resonant frequency) through the cavity D/A converter (13). The cavity register may be manually set or automatically set by the autotuner. If a high or low limit is reached on the cavity register, the autotuning function is automatically stopped and a warning signal is generated.

Clock pulses, at rates of 100.0 kHz or 10.0 kHz, are provided for the period comparison circuits (9) by the clock dividers (6, 7). Either rate can be selected by external command. The sequence control logic (8) provides signals for controlling the beam shutter and period comparison circuits.

The schematic of the circuits which implement the functions indicated in the autotune block diagram is shown in Figure 4-14. Provisions have been made for displaying the numbers in the period comparison register, averager register, and cavity register. Manual controls will be provided for setting the cavity register for manual tuning, for initial value for autotuning, and for resetting the sequence control circuits for autotuning.

4.7 MAGNETIC FIELD CONTROL

The current in the cavity field coil must be maintained to within 0.01% of the nominal value in order to meet the clock stability requirements. To satisfy this condition, current for the cavity field coil is supplied from a highly regulated source. Fine control is obtained through use of multi-turn potentiometers. Provisions are made for adjusting currents in the three sections of the C-field coil to three different values as necessary to produce a homogenous field. The schematic of the field coil control circuit is shown in Figure 4-15.

4.8 DEGAUSSING

Degaussing is accomplished by passing an alternating current of initially a high value (100 to 300 amperes) axial through the C-field coil form and then decreasing this current gradually to zero in the feasibility demonstration model.

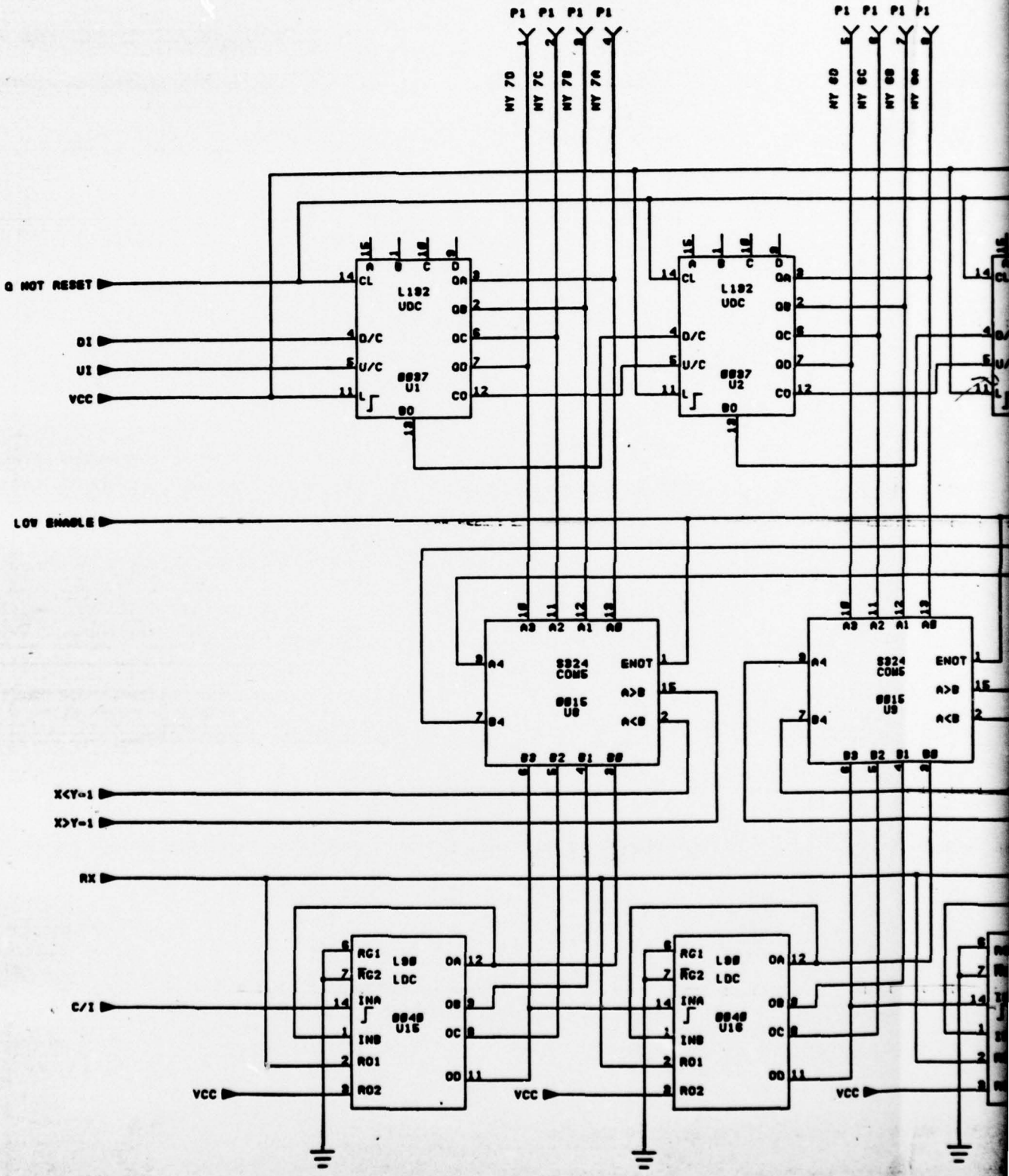
P1 P1 P1 P1
NY 7D
NY 7C
NY 7B
NY 7A
P1 P1 P1 P1
NY 8D
NY 8C
NY 8B
NY 8A
Q NOT RESET
DI
UI
VCC
L192
UDC
8897
U1
8897
U2
LOW ENABLE
8824
COMS
8816
U8
8824
COMS
8816
U9
X<Y=1
X>Y=1
RX
C/I
L98
LDC
8848
U16
L98
LDC
8848
U16
VCC
VCC
VCC

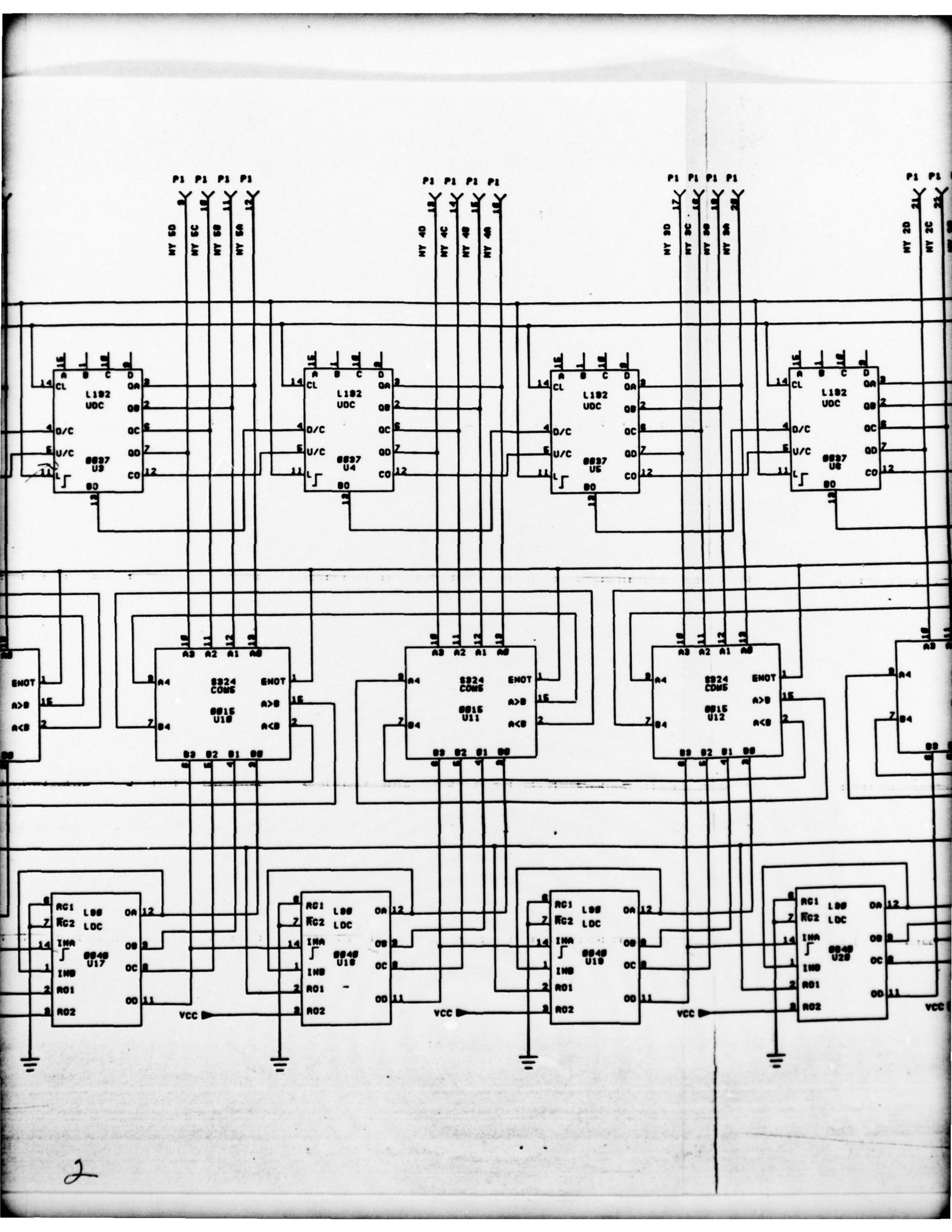
P1
NY 5D
NY 5C
NY 5B
NY 5A
NY 4D
NY 4C
NY 4B
NY 4A
NY 3D
NY 3C
NY 3B
NY 3A
NY 2D
NY 2C
L192
UDC
8897
U3
8897
U4
8897
U5
8897
U6
S324
COMS
8815
U10
8815
U11
8815
U12
ENOT
A>B
A<B
L98
LDC
8940
U17
8940
U18
8940
U19
8940
U20
VCC

2

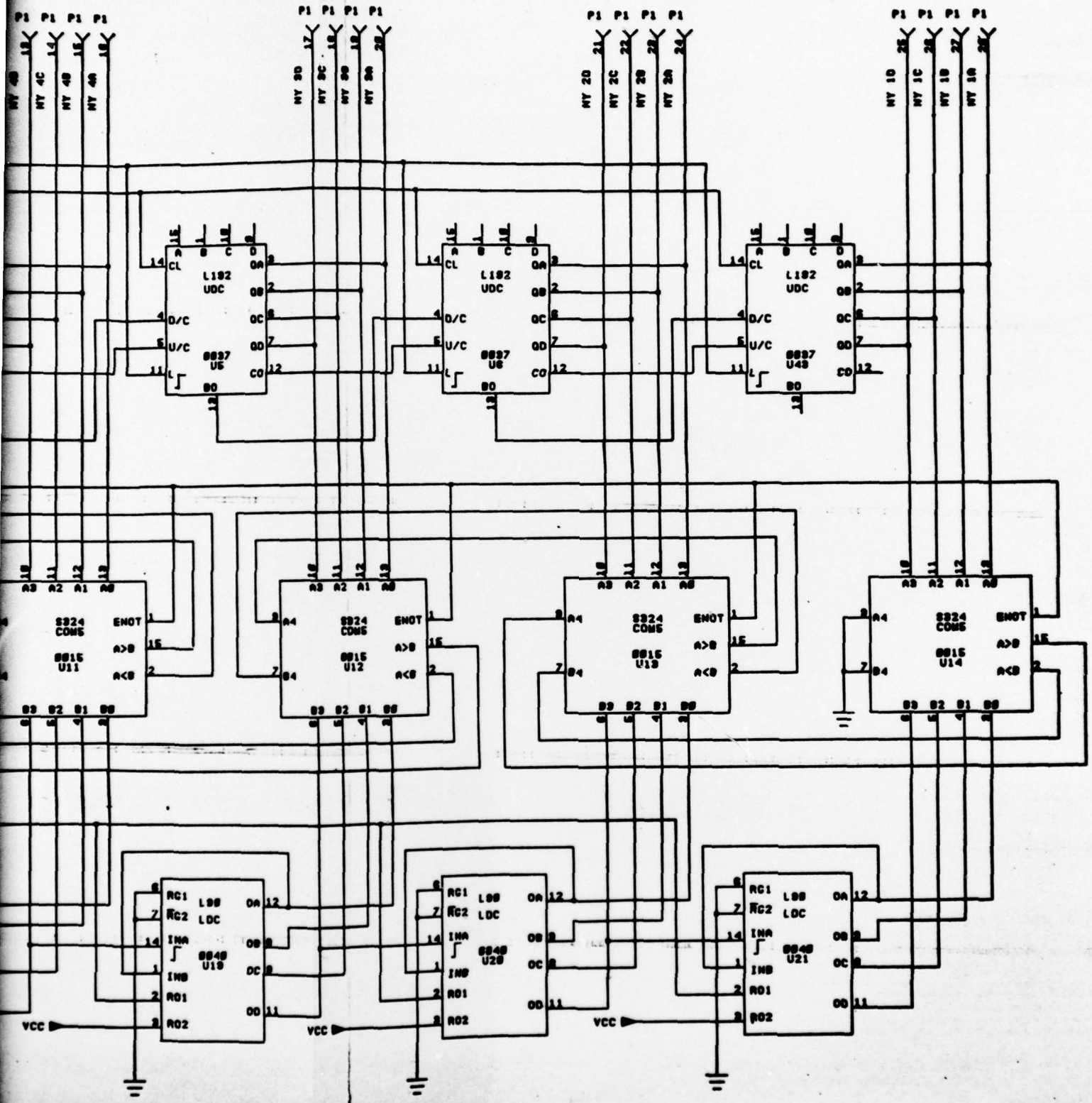

Figure 4-14. Autotuner Logic Diagram (Sheet 1 of 3)

3

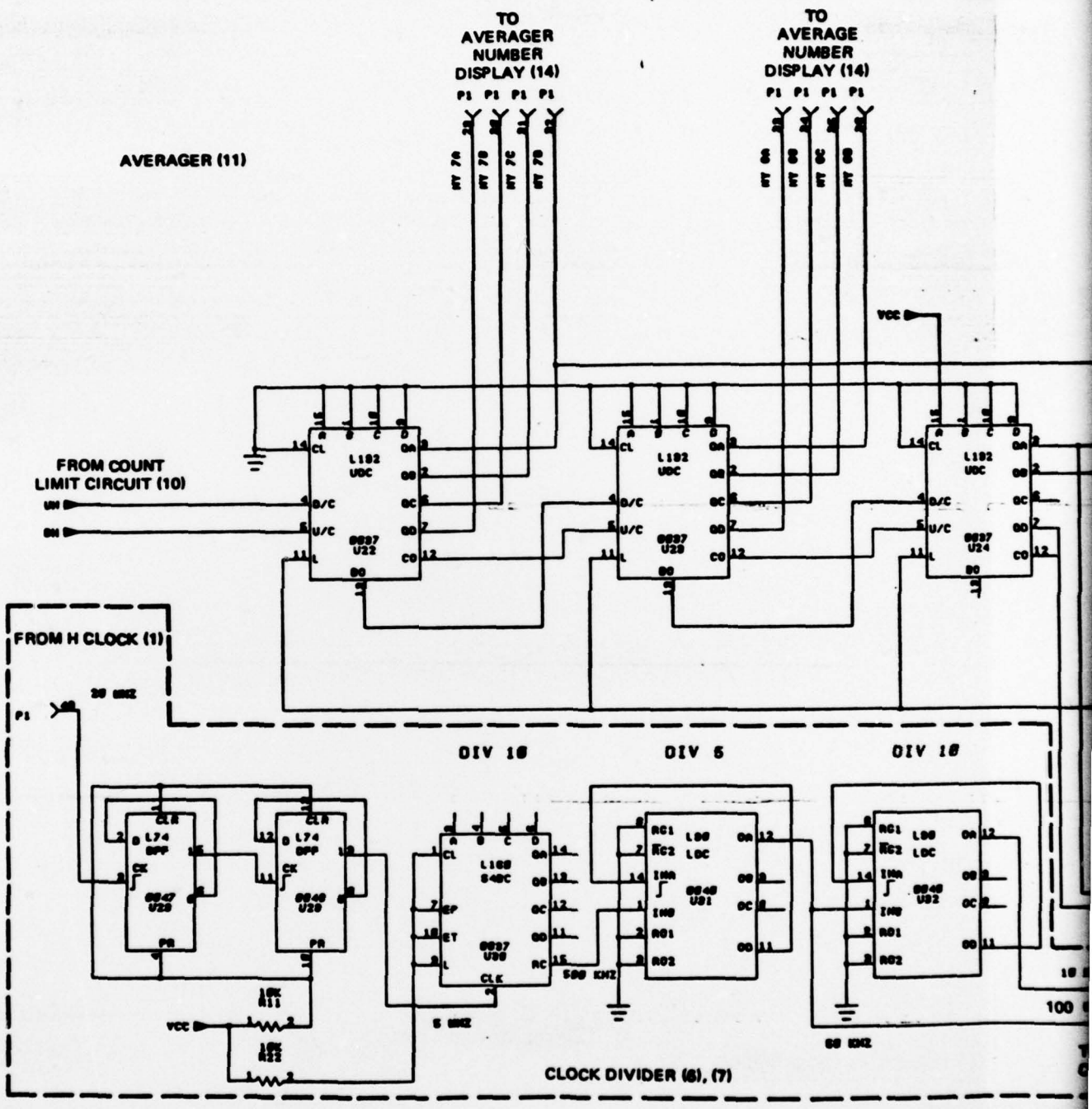
TO AVERAGER NUMBER DISPLAY (14)
TO AVERAGE NUMBER DISPLAY (14)
AVERAGER (11)
FROM COUNT LIMIT CIRCUIT (10)
FROM H CLOCK (1)
DIV 10
DIV 5
DIV 10
CLOCK DIVIDER (6), (7)

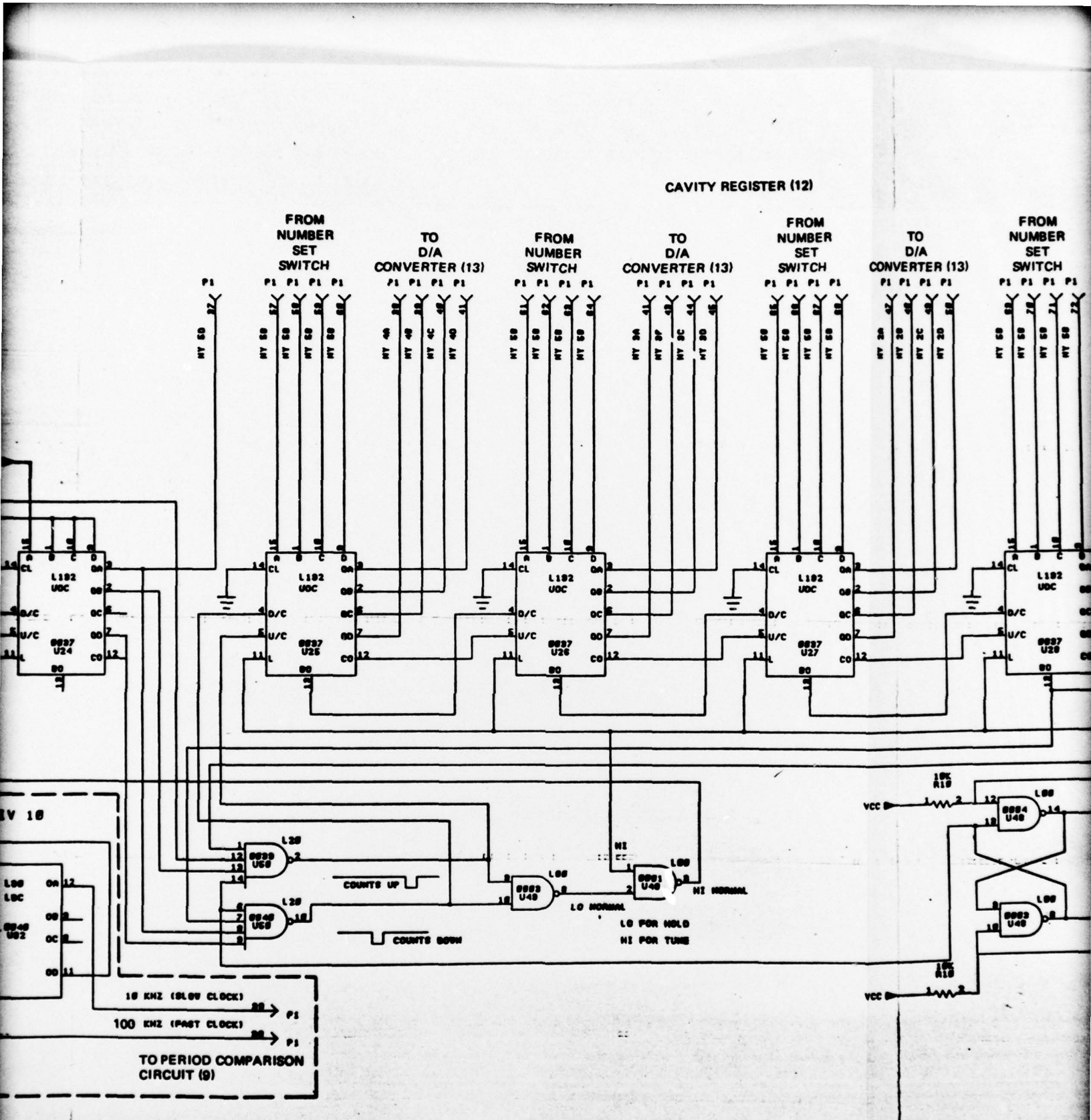
CAVITY REGISTER (12)
FROM NUMBER SET SWITCH
TO D/A CONVERTER (13)
FROM NUMBER SWITCH
TO D/A CONVERTER (13)
FROM NUMBER SET SWITCH
TO D/A CONVERTER (13)
FROM NUMBER SET SWITCH
L192 U0C
8897 U24
8897 U25
8897 U26
8897 U27
8897 U28
8939 U68
8949 U68
8883 U49
8881 U48
8884 U48
COUNTS UP
COUNTS DOWN
LO NORMAL
HI NORMAL
LO FOR HOLD
HI FOR TUNE
10K R18
VCC
10 KHZ (SLOW CLOCK)
100 KHZ (FAST CLOCK)
TO PERIOD COMPARISON CIRCUIT (9)

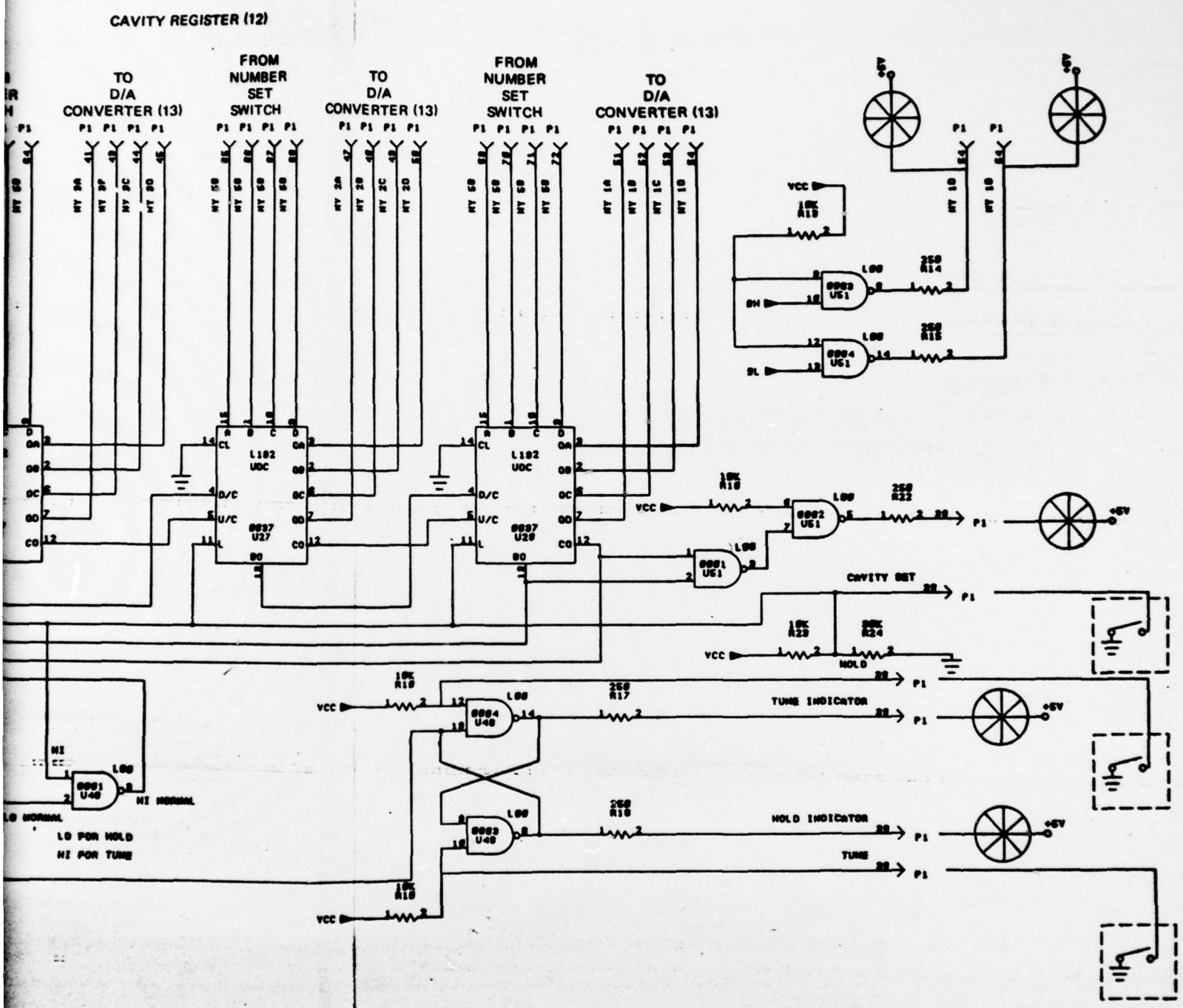

Figure 4-14. Autotuner Logic Diagram (Sheet 2 of 3)

3

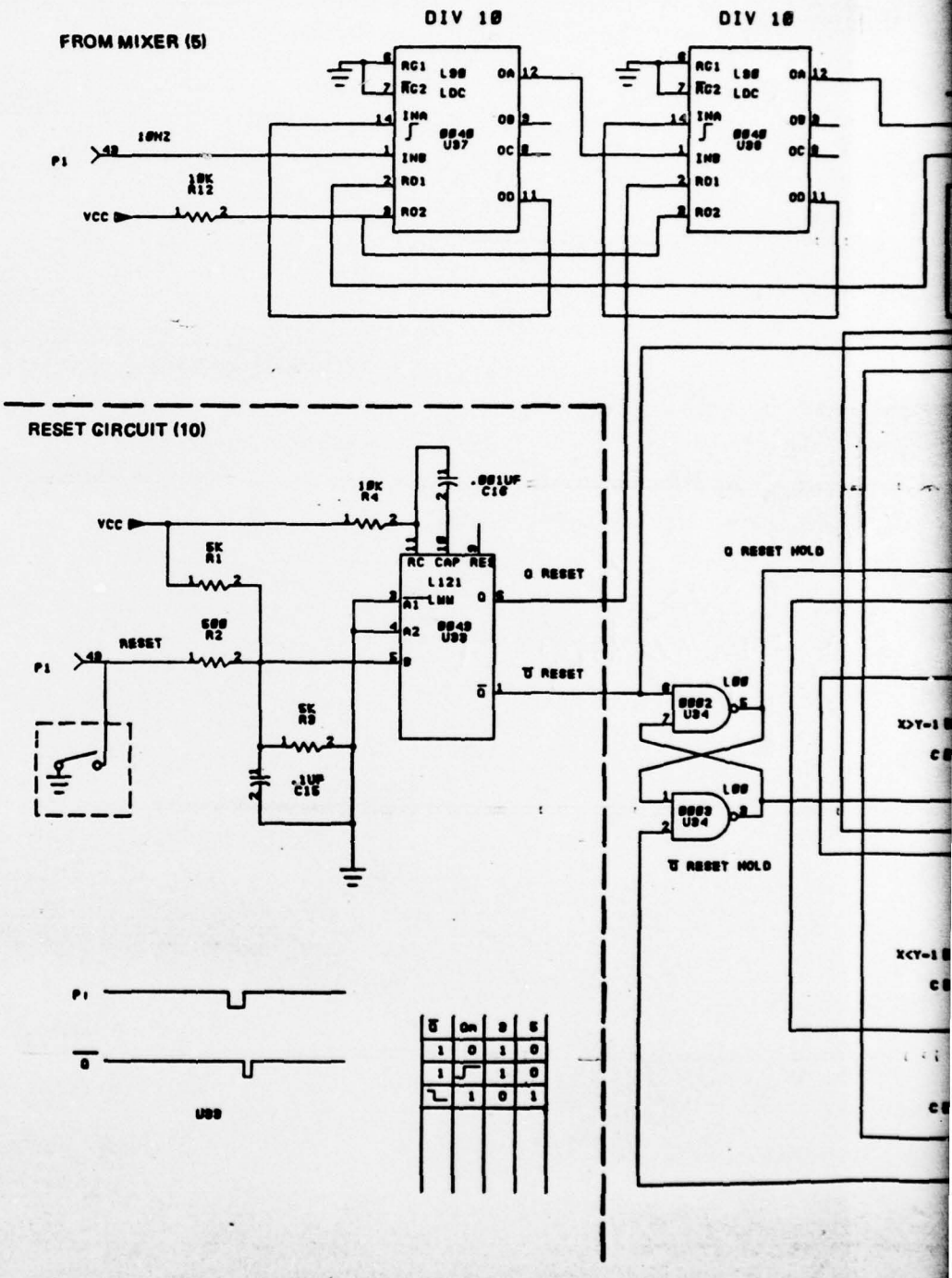
FROM MIXER (5)
DIV 10
DIV 10
P1
10K2
10K
A12
VCC
RESET CIRCUIT (10)
10K
R4
.001UF
C10
VCC
5K
R1
RESET
680
R2
P1
5K
R9
.1UF
C16
Q RESET
Q RESET HOLD
Q RESET
Q RESET HOLD
P1
Q
U59

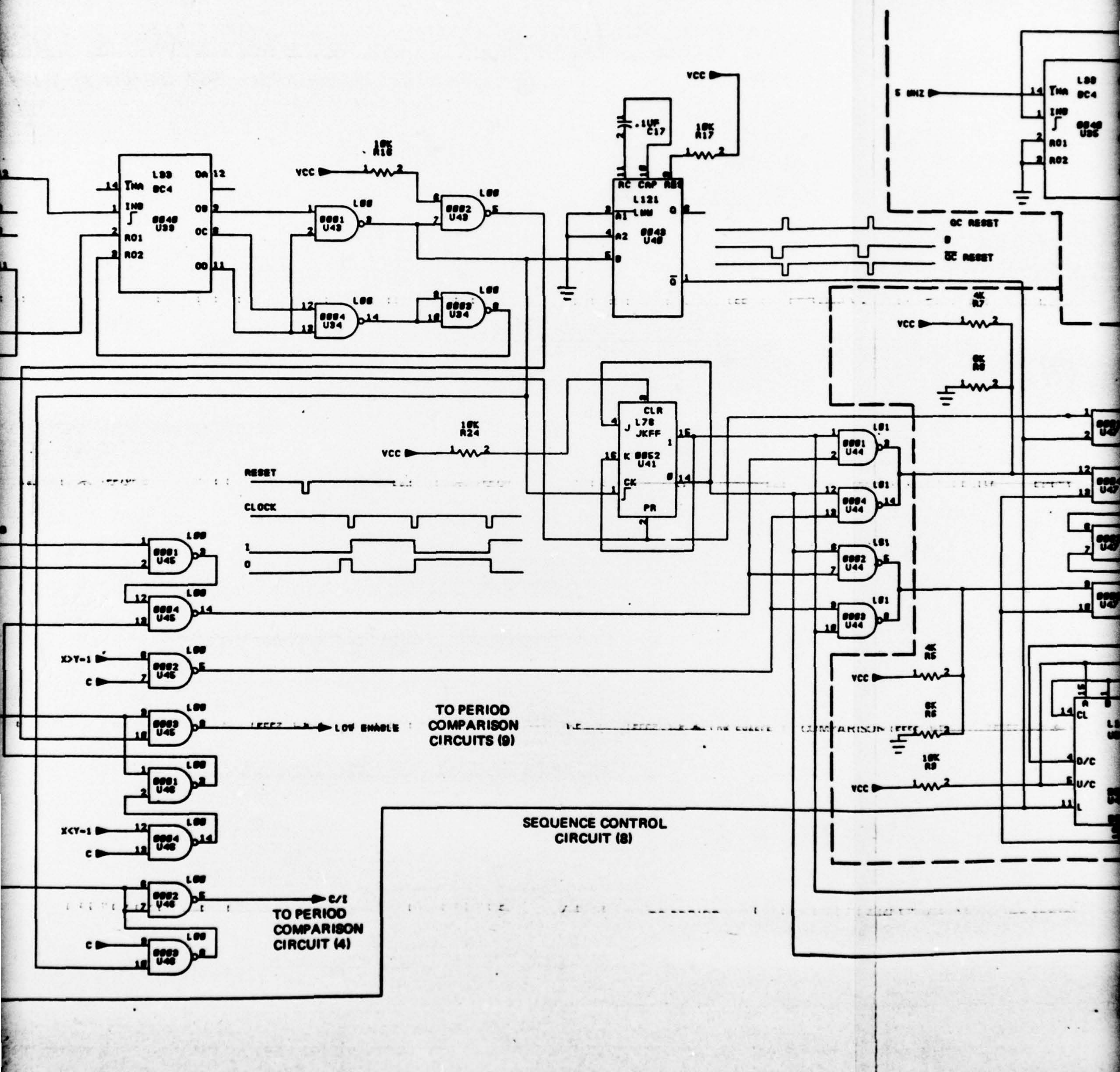
TO PERIOD COMPARISON CIRCUITS (9)
SEQUENCE CONTROL CIRCUIT (8)
TO PERIOD COMPARISON CIRCUIT (4)
RESET
CLOCK
VCC
5 MHZ
QC RESET
LOW ENABLE

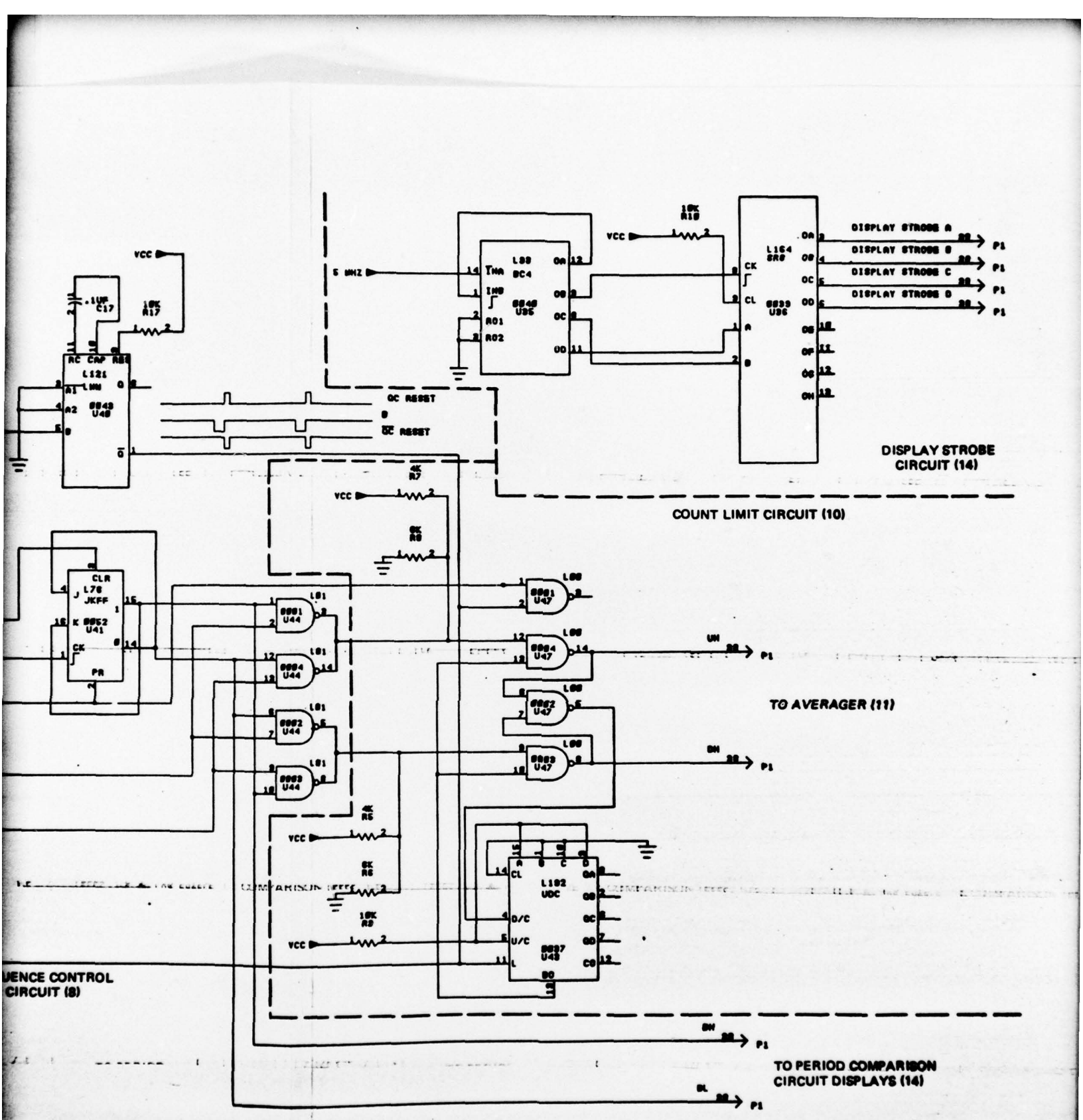

Figure 4-14. Autotuner Logic Diagram (Sheet 3 of 3)

3

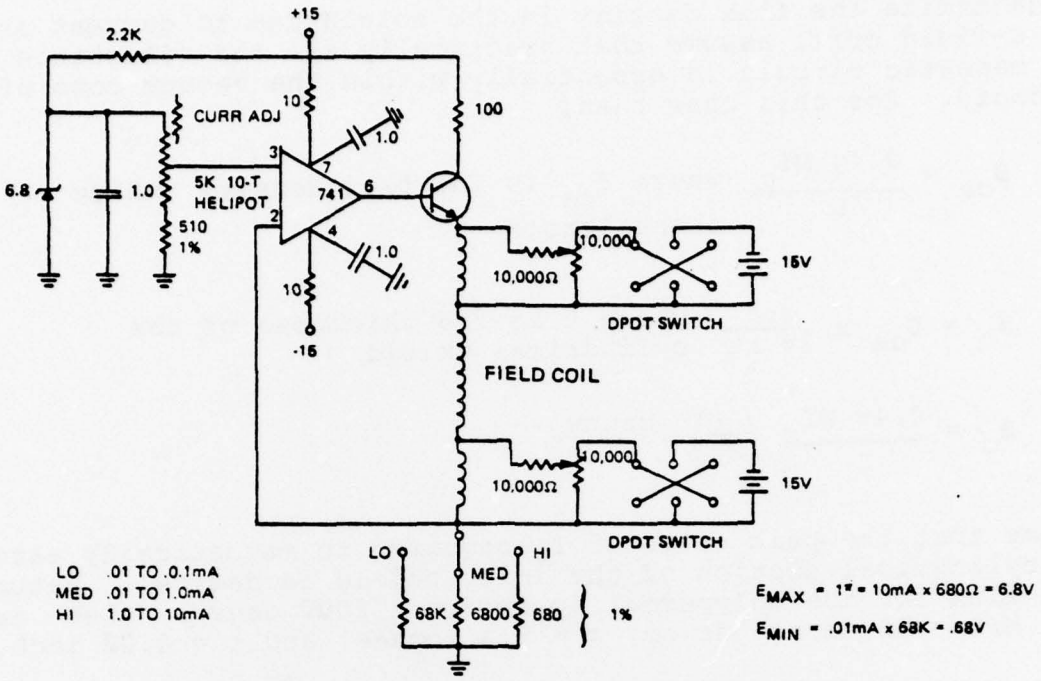

Figure 4-15. Field Coil Control Circuit

This method of degaussing is not attractive for degaussing in orbit because: (1) the magnitude of current requires a very high-current capability of the degaussing electronics (a rather large current transformer); (2) a low-resistance electrical connection to the C-field coil form complicates the thermal isolation problem within the inner oven and inner magnetic shield, from the external environment; and (3) the magnetic domains are "shaken" at right angles to the optimum shaking direction to achieve optimum axial field-component degaussing.

For the flight clocks, it is suggested that degaussing be accomplished by passing an alternating current of about 1 ampere maximum and decreasing the current gradually to zero over a short period of time through the C-field coil and coils wound around the outsides of each of the three inner shields. This method is attractive because: (1) the current required is modest and requires simple lightweight electronics; (2) the magnetic domains are "shaken" in the optimum axial direction for degaussing the axial field component; and (3) it does not affect the thermal isolation from the external environment within the inner oven and inner magnetic shield, since the existing C-field coil is used in conjunction with the coils wound around the shields. Since this method has not been previously used or evaluated, it should be tested for effectiveness on the feasibility demonstration model using only the C-field coil which would degauss the inner shield, and other shields pending adequacy of leakage flux when the inner shield becomes saturated. Preliminary analysis indicates that it should be effective.

To determine the flux density in the shield due to current in the C-field coil, assume that practically all the reluctance of the magnetic circuit is essentially within the vacuum cone of the solenoid. For this case then,

$$B_{ca} = \frac{0.4\pi\ NI_c}{L}$$ where B_{ca} is the flux density inside the solenoid

$$B_c = B_{ca} \times \frac{\pi r^2}{2\pi\ rt}$$ where t is the thickness of the cylindrical shield

$$B_c = \frac{0.4\pi\ NI_c}{L} \left(\frac{r}{2t}\right) \text{ gauss}$$

Assume that the peak value of I_c required to magnetically saturate the cylindrical section of the inner shield is desired. Saturation flux for the molypermalloy is about 8000 gauss. Also, assume that M/L = 10 turns per cm, r = 5.5 inches, and t = 0.02 inch.

$$I_c = \frac{B_c}{0.4\pi} \left(\frac{L}{N}\right) \left(\frac{2t}{r}\right)$$

$$I_c = \frac{8000}{0.4\pi} \left(\frac{1}{10}\right) \left(\frac{2 \times 0.2 \times 2.54}{5.5 \times 2.54}\right)$$

$$I_c = 4.62 \text{ amperes}$$

Figure 4-16 is a diagram illustrating additional coils wound around the outside of each of the three inner shields and the flux paths due to degaussing currents which would be passed through these coils for positively degaussing the outer three shields in the event that tests yet to be made indicate that current through the C-field coil alone is not adequate. Note that the currents through the degaussing coils alternate in direction, i.e., the current through C_2 is opposite to that of C_1, C_3 current is opposite to C_2 current, and C_4 current is opposite to C_3 current.

Let,

L_1, L_2, L_3, L_4 = lengths of respective shield cylinders

r_1, r_2, r_3, r_4 = radius of respective shield cylinders

n_1, n_2, n_3, n_4 = turns in coils 1, 2, 3 and 4 respectively

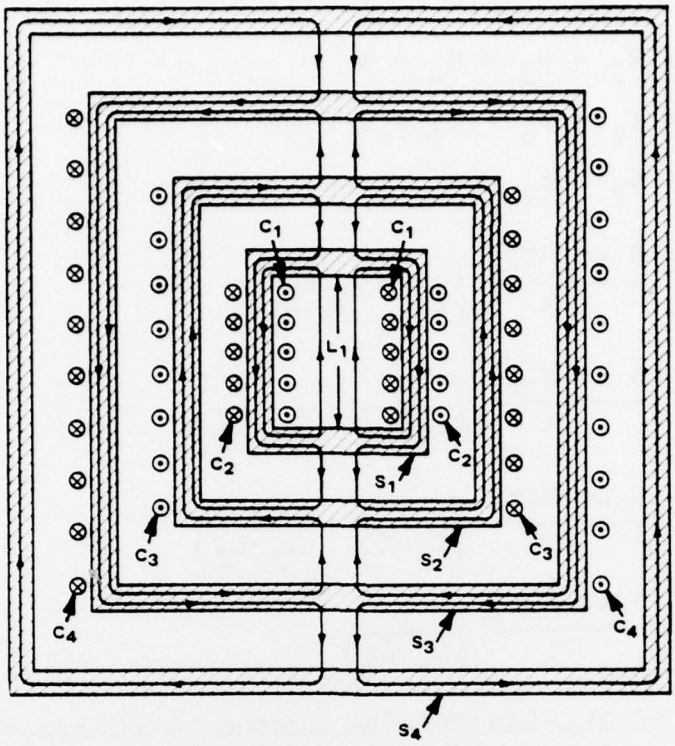

Figure 4-16. Proposed Degaussing Coil Configuration for Flight Clocks

t_1, t_2, t_3, t_4 = thickness of each shield respectively

B_1, B_2, B_3, B_4 = flux density in each cylinderical shield

I_1, I_2, I_3, I_4 = current in each coil

Assuming that the reluctance of the magnetic circuits in the air gaps is very large compared to the reluctances through the shields,

$$B_1 = \frac{0.4\pi\ N_1\ I_1}{L_1}\left(\frac{r_1}{2t_1}\right) + \frac{0.4\pi\ N_2\ I_2}{L_2-L_1}\left(\frac{r_1}{2t_1}\right)$$

$$B_2 = \frac{0.4\pi\ N_1\ I_2}{L_2-L_1}\left(\frac{r_2}{2t_2}\right) + \frac{0.4\pi\ N_2\ I_3}{L_3-L_2}\left(\frac{r_2}{2t_2}\right)$$

$$B_3 = \frac{0.4\pi\ N_3\ I_3}{L_3-L_2}\left(\frac{r_3}{2t_3}\right) + \frac{0.4\pi\ N_4\ I_4}{L_4-L_3}\left(\frac{r_3}{2t_3}\right)$$

$$B_4 = \frac{0.4\pi\ N_4\ I_4}{L_4-L_3}\left(\frac{r_4}{2t_4}\right)$$

If $N_1 = N_2 = N_3 = N_4 = N$

$I_1 = I_2 = I_3 = I_4 = I$

$t_1 = t_2 = t_3 = t_4$

$$B_1 = \frac{0.4\pi\ NIr_1}{2t}\left(\frac{1}{L_1} + \frac{1}{L_2-L_1}\right)$$

$$B_2 = \frac{0.4\pi\ NIr_2}{2t}\left(\frac{1}{L_2-L_1} + \frac{1}{L_3-L_2}\right)$$

$$B_3 = \frac{0.4\pi\ NIr_3}{2t}\left(\frac{1}{L_3-L_2} + \frac{1}{L_3-L_2}\right)$$

$$B_4 = \frac{0.4\pi\ NIr_4}{2t}\left(\frac{1}{L_4-L_3}\right)$$

Using dimensions of shields for the design being proposed, the values of flux densities which will be produced in the magnetic shields follow.

L_1 = 12.5 inches or 31.75 cm

L_2-L_1 = 1.5 inches or 3.81 cm

L_3-L_2 = 1.0 inches of 2.54 cm

L_4-L_3 = 8.5 inches or 21.59 cm

r_1 = 5.8 inches or 14.73 cm

r_2 = 6.4 inches or 16.26 cm

r_3 = 6.9 inches or 17.53 cm

r_4 = 7.5 inches or 19.05 cm

N = 12.5 x 25 or 312 turns per coil

t = 0.020 inch or 0.0506 cm

I = 1 ampere

$$B_1 = \frac{0.4\pi \times 312 \times 1 \times 14.73}{2 \times 0.0506}\left(\frac{1}{31.75} + \frac{1}{3.81}\right)$$

$$B_1 = 3874 \times 14.75\left(\frac{1}{31.75} + \frac{1}{3.81}\right) = 16{,}798 \text{ gauss}$$

$$B_2 = 3874 \times 16.26 \left(\frac{1}{3.81} + \frac{1}{2.54}\right) = 41332 \text{ gauss}$$

$$B_3 = 3874 \times 17.53 \left(\frac{1}{2.54} + \frac{1}{21.59}\right) = 29882 \text{ gauss}$$

$$B_4 = 3874 \times 19.05 \left(\frac{1}{21.59}\right) = 3418 \text{ gauss}$$

The above typical calculations show that with a modest current (1 ampere) in practical coils (25 turns per inch of #24AWG) it is possible to exceed saturation flux values (approximately 8000 gauss) by several times for the three inner shields which would more than adequately degauss them. To saturate the outer shield will require a larger current through the outer coil; however, effective degaussing probably does not require shaking the domains to saturation levels, only shaking them enough to successively reverse the direction of net magnetization.

This technique is attractive since: (1) reasonable values of degaussing ac currents are required, which can readily be produced by spacecraft compatible electronics; and (2) the thermal isolation between the various thermally controlled volumes of the maser, and in particular, the volume enclosing the cavity, is minimally disturbed by thermal conductivity of the small wires entering the volume.